Chem Soc Rev

Macro-/Micro-environment-sensitive Chemo-sensing and Biological Imaging

Journal:	*Chemical Society Reviews*
Manuscript ID:	CS-REV-01-2014-000051.R1
Article Type:	Review Article
Date Submitted by the Author:	13-Mar-2014
Complete List of Authors:	Kim, Jong Seung; Korea University, Chemistry Peng, Xiaojun; State Key Laboratory of Fine Chemicals, Dalian University of Technology, Dalian University of Technology Yang, Zhigang; Korea University, Chemistry Cao, Jianfang; Dalian University of Technology, State Key Laboratory of Fine Chemicals Dalian He, Yanxia; Korea University, Chemistry Yang, Jung Ho; Korea University, Chemistry Kim, Taeyoung; Korea University, Chemistry

Macro-/Micro-environment-sensitive Chemo-sensing and Biological Imaging

Zhigang Yang, [1,2] Jianfang Cao,[3] Yanxia He,[1,2] Jung Ho Yang,[1] Tae Young Kim,[1] Xiaojun Peng,[3]* and Jong Seung Kim[1]*

[1]Department of Chemistry, Korea University, Seoul 136-701, Korea

[2]Key Laboratory of Sensor Analysis of Tumor Marker Ministry of Education, College of Chemistry and Molecular Engineering, Qingdao University of Science and Technology, Qingdao 266042, China

[3]State Key Laboratory of Fine Chemicals, Dalian University of Technology, Dalian 116024, China

Abstract

Environment-related parameters, including viscosity, polarity, temperature, hypoxia, and pH, play pivotal roles in controlling the physical or chemical behaviors of local molecules. In particular, in a biological environment, such factors predominantly determine the biological properties of the local environment or reflect corresponding status alterations. Abnormal changes in these factors would cause the cell malfunctions or become a hallmark to indicate the occurrence of severe diseases. Therefore, in recent years, they have increasingly attracted research interest from the fields of chemistry and biological chemistry. With the emergence of fluorescence sensing and imaging technology, several fluorescent chemosensors have been designed to respond to such parameters and to further map their distributions and variations *in vitro*/*in vivo*. In this work, we reviewed a number of various environment-responsive chemosensors related to fluorescent recognition of viscosity, polarity, temperature, hypoxia, and pH that have been reported thus far.

1. Introduction

The local environment (microenvironment) is an extremely significant factor in the determination of the physical or chemical behaviors of surrounding molecules.

Several factors collectively define the properties of a specific location, including the local viscosity, polarity, temperature, redox and acidic-basic status. They play a crucial role in controlling diffusion, transportation, and intermolecular interactions. For a large volume of homogeneous fluid, it is feasible to determine all parameters using various well-developed tools, e.g. viscometer, thermometer, pH meter, and so on. However, for a micro-scale volume of liquid, as seen inside a single cell, the tools mentioned above are unable to satisfy the requirements. More importantly, intracellular micro-environments are heterogeneous with different compositions in varying locations, e.g. in the cytosol, sub-organelles, or the membrane systems, and the micro-environment in each location plays an essential role in various biological processes, such as the intracellular transportation of mass and energy, transduction of various signals, interactions between biomacromolecules (proteins), activity of enzymes, and rates of cellular metabolism.

First, viscosity, as a crucial factor relating to diffusion-controlled processes, plays an essential role in different biological activities, as well as in chemistry and other fields, and typically governs the rates of mass transport of reagents. Obvious diffusion events generally occur in the interface region of heterogeneous fluid systems. In particular, in biological systems, viscosity plays a major role in determining various biological activities at the organismal and cell levels.[1-2] For example, viscosity within cells is critical in manipulating transportations of nutrients and metabolic wastes, transduction of intra/intercellular signals, and interactions between biomacromolecules. Furthermore, at the sub-organelle levels, microviscosity in mitochondria greatly impact on the respiratory state and tricarboxylic cycles through the molecular influence of mechanical or osmotic inducing mitochondrial network changes in organization, which indicates that mitochondrial matrix viscosity changes may largely interfere with mitochondrial metabolism.[3-5] Abnormal variations of viscosity have been considered a vital contributor or indicator for various severe diseases, such as atherosclerosis, diabetes, Alzheimer's disease, and even cell malignancy.[6-10]

Polarity (hydrophilicity/hydrophobicity) is another significant environmental factor that charges cellular functional proteins (e.g. activation of proteins by separation from their inhibitors) and initiates signal transduction processes[11] and membrane systems, due to the predominance of hydrophobic interactions in biological processes.[12-15] Most cellular behaviors are controlled by the transient activation of different proteins in specific regions, such as the signal transducing pathway, enzyme-based catalysis, nascent protein maturation etc. Thus, the investigation of protein activity in the natural state or post-translational modification is extremely significant for understanding protein function. On the other hand, the structure and function of the cellular membrane is largely controlled by their lipid composition and particularly by cholesterol, which interacts firmly with phospholipids and other lipids within cell membranes (e.g. sphingomyelin). Therefore, the development of effective tools to monitor protein activities and membrane functions in living cells is urgently required.

It is well-known that temperature determines many biological processes inside cells, which are responsible for cellular functions occurring at specific locations, such as the nucleus, mitochondria etc.[16-20] Therefore, temperature variations within cellular organelles or between different cell types demonstrates the thermodynamics and main functions of intracellular components.[21] In medical researches, the pathogenesis of diseases at cell level such as cancers, viral infection, inflammation etc, is characterized by excessive heat generation.[22] The visualization of intracellular temperature would provide a better understanding of cellular events in order to develop new strategies for diagnoses and therapy. In spite of the increasing demand in the fields of life science in recent years, micro-environmental temperature distributions within living cells have not yet been fully understood, because conventional methods have limitations in spatial and temperature resolution and are unable to exert their functions within cells.

Hypoxia, resulted from insufficient oxygen supply, is a significant feature of a variety of diseases, including solid tumors, cardiac ischemia, and inflammatory diseases.[23-25] The hypoxic status in solid tumors is thought to be a typical hallmark of

adverse prognosis, under which tumors are ready to progress to a malignant phenotype with enhanced metastatic ability, and exhibit increased resistance to various treatments.[26] Consequently, hypoxic status of cells usually facilitate a cancer-specific targeting strategy for diagnosis and therapy. It is of great importance to develop new approaches for hypoxia targeting and detection.

Furthermore, all biological activities within live cells always occur normally under proper acid-base conditions.[27-31] Different acid-base conditions are seen in different intracellular locations, with different pH values in cellular compartments.[33-34] Intracellular pH status regulates several cellular behaviors involved in cell proliferation and apoptosis, as well as enzyme activity and protein degradation. In a normal mammalian cell, the pH inside cells is variable, ranging from ca. 4.5 (lysosome) to 8.0 (mitochondria). A disruptive pH shift probably causes organelle dysfunction. Therefore, abnormal pH or pH variations can be generally considered as a hallmark of various diseases, including cancer, stroke, Alzheimer's disease, and inflammation. Accurately detecting pH changes within live cells is thus very important for studying cellular metabolic situations and obtaining insights into physiological and pathological processes.

Together with environmental considerations, abnormal changes in these factors would finally result in dysfunction of the body with various diseases, or would become a hallmark of certain severe diseases, e.g. Parkinson's disease, Alzheimer's disease, prion diseases, malignant tumors, or severe inflammation. Therefore, it is of great significance to measure such micro-environmental properties at the cellular level. Chemosensing has recently emerged as an ideal tool for the investigation of single molecule interactions or micro-environmental properties, and is very sensitive to the surrounding environment. In recent years, with the emergence of fluorescence-based detection, environment-sensitive chemosensing and biological imaging have also been the focus of tremendous research interest in the chemistry and biochemistry fields. Furthermore, many active studies on the development of chemosensors responsible for such environmental parameters have been published. The numbers of research

studies in related fields have increased significantly during the last several years. Our laboratory has introduced some microenvironment-sensitive chemosensors. To the best of our knowledge, no comprehensive review papers on environment-based chemosensors have been published. Here, we summarize recent developments in fluorescent chemosensing and biological imaging of the macro-/micro-environment.

2. Viscosity-based fluorescent chemosensing and biological imaging

2.1. Fluorescence intensity-based viscosity chemosensors

Viscosity predominantly determines diffusion-controlled processes. Various viscometers for the measurement of large volumes of liquid have been well-developed in recent years, such as the falling ball viscometer, falling piston viscometer, and rotational viscometer. However, microviscosity measurements in biological systems remain a problem. The local viscosity inside a single cell significantly influences multiple intracellular processes. Abnormal changes in the local viscosity in a single cell would probably cause cellular malfunction or severe disease. Powerful tools for the measurement of microviscosity are greatly in demand.

In recent years, with the application of fluorescence technology, microviscosity-targeted fluorescent sensors, termed “molecular rotors”, have gradually emerged. In terms of chemical structure, they are composed of a fluorophore with a rotationally conjugating moiety that is capable of rotation relative to the whole molecule. In non-viscous environments, the faster rotation relaxes the excitation energy resulting in significant quenching of fluorescence or shortening of the fluorescence lifetime, whereas in viscous medium, rotation is gradually inhibited, thereby reducing the possibility of non-radiating pathways, and enhancing fluorescence intensity or markedly lengthening the fluorescence lifetime.

In 1982, R. O. Loutfy et al.[35] first described a group of fluorescent molecular rotors as microscopic fluorescent probes (**1–3**) (Fig. 1) for the measurement of the torsional rigidity of the local media. These probes are fluorescent dyes with a charge donor and a charge acceptor. The fluorescence of these dyes is quenched in non-viscous solution

and is also a function of temperature. Furthermore, the singlet-excited-state lifetimes of **1–3** are as short as 3–10 ps, and the rapid deactivation of the excited state was ascribed to fast internal torsional relaxation. The authors of this study further revealed that the environmental factors inhibiting the intramolecular rotation of the fluorescent dyes could lead to an evident increase in fluorescence quantum yields and the lifetime of first-excited-state.

Subsequently, Loutfy and coworkers[36] studied both the static and dynamic changes in free volume of polymers as a function of polymerization reaction parameters, molecular weight, crosslinking, stereoregularity, polymer chain relaxation, and flexibility by molecular rotors (**1–3**). Because of the dependence of fluorescence on the media polarity, the probe location in the polymer matrix could be continuously monitored simultaneously. Furthermore, Reed et al.[37] employed molecular rotor **3** to investigate the microviscosity of some artificial bilayers, e.g. sodium dodecyl sulfate (SDS) micelles and small dipalmitoylphosphatidylcholine (DPPC) vesicles. Upon correlating the fluorescence quantum yields with viscosity, the effective microviscosity was measured with the free volume concept for the solvents with medium- to high-viscosity (712 cP). And effective microviscosities in DPPC vesicles were measured ranging from 70 to 120 cP with the temperature between 60 and 10°C. It exhibited a transition temperature at 34°C by comparing the activated energies of solvent, hydrocarbon chain mobility, and the rotational dynamics of **3**. Compound **3** mainly located in the interior of the hydrocarbon core with a microenvironmental dielectric constant of 17.9. At 25°C in SDS micelles, the dye reported a more polar interface environment ($\varepsilon = 41.6$) with a lower effective microviscosity (6.9 cP).

The molecular rotor **3** has been used to monitor local environmental changes. Harriman and coworkers found that **3** was adequate to discriminate between viscosity and polarity effects.[38] It underwent slow internal rotation and had activation energy of ca. 35 kJ/mol in solution, as confirmed by ^{1}H NMR. The absorption and fluorescence spectra were both fairly insensitive to variations in solvent polarity. Quantum chemical calculation on **3** demonstrated rapid rotation around the dicyanovinyl double

bond, resulting in mainly non-radiative deactivation. However, intramolecular charge transfer played a relatively minor role in the overall photophysics.

A group of 9-(dicyanovinyl)-julolidine derivatives of **4** were synthesized by Theodorakis et al.[39] In these molecules, different lengths of hydrocarbon chains were attached to the rotors to control cell membrane compatibility. A derivative of **4** that preferentially attaches to the cell membrane showed higher sensitivity to changes in cell membrane viscosity. Another analogue of molecular rotor **5** exhibited an even higher sensitivity (more than 20-fold) than **4** when mapping membrane viscosity changes. However, it did not fully exclude migration into the cell interior. These authors further reported another new family of phospholipid-bound molecular rotors **6**.[40] These molecular rotors were attached *via* a polymethylene linker to the hydrophobic or hydrophilic end of a phospholipid structure. This kind of modification did not affect the sensitivity of the rotor to viscosity and allowed adequate accumulation into artificial bilayers as well as complete localization in the plasma membrane of living cells. Compound **6** and its derivatives with the non-polar end of the phospholipid displayed the characteristic property of viscosity-dependent fluorescence quantum yield of a fluorescent rotor.

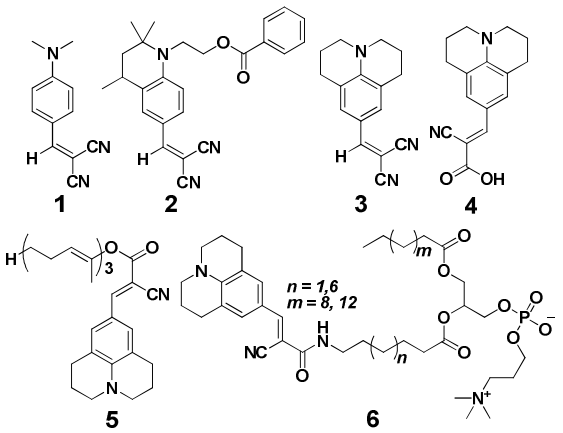

Fig. 1 Chemical structures of molecular rotors (**1–6**).

Haidekker et al.[41] investigated the structure-property relationships of a series of *N, N*-dialkylaniline containing molecular rotors (**7–11**) (Fig. 2) with regard to fluorescence emission wavelength, intensity and sensitivity to microviscosity. The

extension of the conjugation between the donor moiety and the acceptor unit was found to dramatically influence the fluorescence wavelength and evidently increase the Stokes' shift. The nitrogen of alkyl side chains had no evident contribution to the excitation and emission wavelengths. Changes in the molecular structure caused different background fluorescence quantum yields and demonstrated different sensitivities in viscosity measurement. The alteration of chemical structure was favorable in the rational design of molecular rotors that were optimized for a specific application.

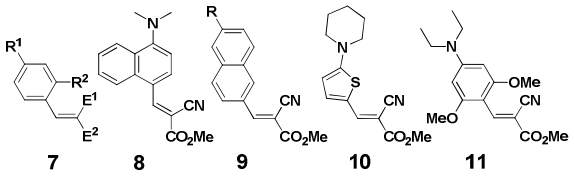

Fig. 2 Chemical structures of molecules (**7–11**).

A series of new fluorescent molecular rotors (**12–19**) (Fig. 3) for viscosity measurements were synthesized by Zhao and coworkers.[42] They studied the relationship between the sensitivity of the rotors toward solvent viscosity and polarity through different methods, such as UV/Vis absorption, fluorescence emission spectra, and DFT/TD-DFT theoretical calculations. These new rotors showed a large red-shift in emission wavelengths at 620 nm, Stokes' shifts of 170 nm, and 40-fold enhancement in fluorescence intensity with increasing solvent viscosity, than those observed with reported molecular rotors. In different solvents, the molecular rotors displayed various fluorescent responses, e.g. the rotors worked as non-fluorescent molecular rotors in solvents with high viscosity but low polarity, such as PEG400 or dimethyl silicone oil, whereas they showed fluorescent molecular rotor properties with ethylene glycol/glycerol. Compounds **18–19** showed both obvious solvent effects in fluorescence emission and fluorescent molecular rotor properties. Furthermore, the results of trifluoroacetic acid titration and DFT/TD-DFT calculations demonstrated that the emissive excited states of the rotors corresponded to locally excited (LE) states, and twisted intramolecular charge-transfer (TICT) states were believed to be dark states, indicating that the internal rotation about the C=C double bonds

(dicyanovinyl group) in the S_1 state, but not that about C–C single bonds, was the main non-radiative deactivation channel. Additionally, the extension of the π conjugation of the rotors created the more difficult rotation barrier about the C=C double bond in the S_1 state, resulting in the blocking of non-radiative channels and a higher fluorescence quantum for the new rotors.

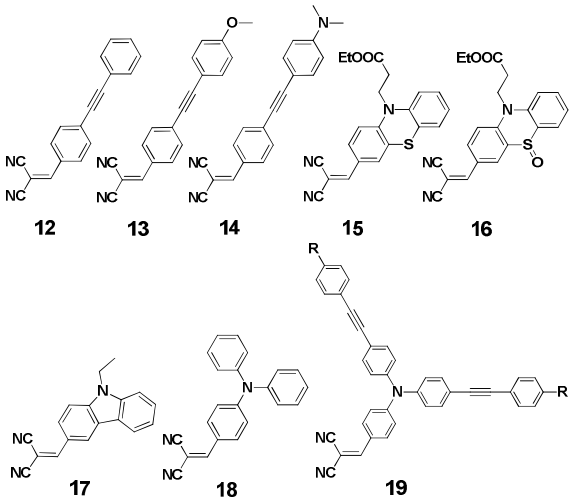

Fig. 3 Chemical structures of compounds (**12–19**).

As the absorption and fluorescence emission of **1–3** mainly locates in the region of 350**–**500 nm, it is not suitable for real-time viscosity measurement *in vivo*. Benniston and Harriman et al.[43] reported a prototype consisting of two remote BODIPY fluorophores conjugated by a long flexible spacer (**20**) (Fig. 4), and studied its ability to monitor local viscosity changes. This probe avoided TICT interference while possessing more amenable absorption and emission wavelengths. The *meso*-phenylene ring rotation of the BODIPY moiety and the accompanying distortion of the dipyrrin backbone generated the main non-deactivation route of the excited state, resulting in the extraordinary sensitivity to viscosity.

The BODIPY-based fluorophore possessed a *meso*-phenyl group (**21**) as the rotor attached to a long flexible chain; this made it easy to incorporate into biological media and evaluate the viscosity of the surrounding medium. The size of the rotary phenyl group significantly affected the barrier height for ring rotation and local viscosity sensitivity. Another BODIPY dye bearing a *meso*-phenanthrene unit (**22**) was designed and studied by Harriman.[44] The larger phenanthryl moiety cannot rotate

freely around the C–C linker, but can only oscillate over a dihedral angle. The oscillation had little effect on the photophysical properties of BODIPY, making **22** a poor probe with low sensitivity to viscosity.

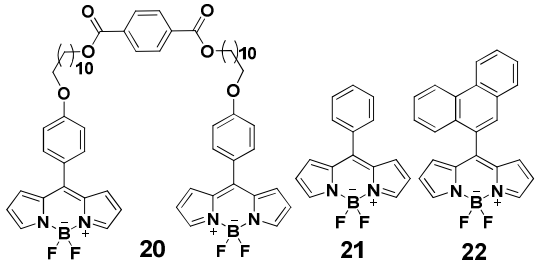

Fig. 4 Chemical structures of molecular rotors (**20–22**).

Zhu and coworkers[45] synthesized two ferrocene-BODIPY molecules (**23–24**) (Fig. 5), with the typical D–A mode. Compared with **24**, compound **23**, with a long rigid bridge, was able to work as a molecular rotor with good viscosity responses, the emission of which increased drastically as the viscosity increased, especially in a low-viscosity solution. This is a potential candidate for a viscosity probe for the detection of diseases in biological systems.

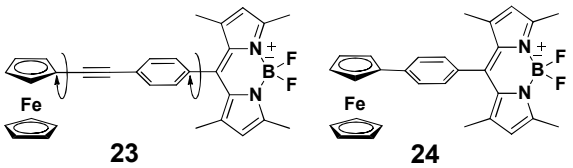

Fig. 5 Chemical structures of target compounds (**23–24**).

2.2. Fluorescent ratiometry- and lifetime-based viscosity chemosensors and biological imaging

Fluorescence intensity-based viscosity sensors are unable to quantitatively determine intracellular microviscosity or its variations due to their spatial variations in the concentration and the heterogeneity of intracellular media. Therefore, new molecular rotors capable of quantifying viscosity in heterogeneous phase or in living cells are indeed in demand. Both ratiometric and fluorescence lifetime imaging approaches have been suggested to overcome these problems, which can be used to accurately measure biological viscosity.

In 1993, Luby-Phelps and colleagues[46] developed a ratio pair for the fluorometric

determination of solvent viscosity. This ratiometric fluorescent pair was composed of a Cy3 dye and a Cy5 dye together tethered to inert carrier macromolecules. When the environmental viscosity was varied, the fluorescence intensity ratio (I_{Cy3}/I_{Cy5}) in a mixture of the macromolecules in solution was found to be dependent on the solvent viscosity and independent of other solvent parameters such as polarity, temperature, and hydrogen bonding. The ratio values (I_{Cy3}/I_{Cy5}) were also insensitive to biomacromolecules (proteins). After the macromolecular material labeled with Cy3 and Cy5 was injected into the cytoplasm of living cells (nonmotile interphase CV1 and PtK1 cells), ratio imaging revealed that the viscosity of the cytoplasm was not significantly different from that of water and showed no spatial variation.

Wandelt and coworkers[47] studied the microviscosity for single cell in rat thoracic smooth muscle through ratiometric imaging using compound (**25**) (Fig. 6) as a membrane-permeable probe. When excited at 469 or 360 nm, this probe showed dual emissions in aqueous solution, both producing an emission band around 600 nm. The ratio of the two bands (I_{469}/I_{360}) was well responsive to local microviscosity. The intracellular fluorescence ratio of the dye could be conducive to special processes or chemomechanical responses for cell biology studies. Fluorescence emission at ca. 600 nm exhibited the possibility of simple microscopic observations, avoiding influences from cell or biological tissue autofluorescence.

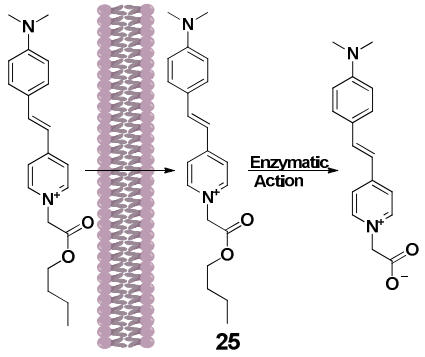

Fig. 6 Proposed chemical reactions for molecule **25** during passing through cell membranes.

In 2006, Haidekker et al.[48-49] reported the first fluorescent ratiometric sensor for viscosity measurement (**26**) (Fig. 7). The rational design was based on the covalent

conjugation of two distinct fluorescent dyes, in which motif was conjugated to a 7-methoxycoumarin-3-carboxylic acid (MCCA) and a CCVJ fluorophore. The MCCA moiety as the energy donor was viscosity-insensitive; and the CCVJ part, as the energy acceptor, was highly viscosity-dependent. MCCA acted as the internal reference and energy donor, exciting the CMAM motif to show a viscosity-sensitive fluorescence quantum yield. The covalently linking between the dyes achieved energy transfer from MCCA to the acceptor together with measurable donor emission. This ratiometric system was capable of eliminating the effects of medium refraction and heterogeneous distribution of dye molecules, allowing fast and exact measurements of fluid viscosity.

Following this, this group[50] developed another ratiometric molecular rotor (**27**) with the ability of self-calibration to overcome local concentration gradients. It was incorporated into a dilauroylphosphatidylcholine (DLPC) liposome model when exposed to a membrane-fluidizing agent of propanol. Self-calibrating dyes can be utilized in real-time viscosity monitoring in liposome, and have advantages over lifetime measurement, with low cost steady-state instrumentation.

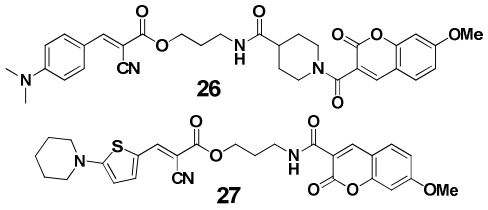

Fig. 7 Chemical composition of sensors **26–27**.

Kuimova and coworkers[51] designed a type of ratiometric molecular rotor (**28**) (Fig. 8) for quantifying and imaging intracellular viscosity in single cell and simultaneously inspecting cell viscosity changes, which was constructed as a conjugated porphyrin dimer. The spectral properties of a butadiyne-linked porphyrin dimer was assigned to be in two conformations (710 and 780 nm), in which an emission maximum at 710 nm corresponded to the twisted conformation (porphyrin monomer) and that at 780 nm was assigned to the coplanar conformation (porphyrin dimer). Because of the relative rotation of the two porphyrin moieties to an angle, the monomer's emission

was mainly observed at high viscosity. On the other hand, the conjugated dimer was also a sensitizer for photodynamic therapy (PDT) of cancer. When the dimer of porphyrin was exposed to light irradiation, it was easy to generate short-lived cytotoxic agents ($^1O_2$) that would change the cellular viscosity. The molecular rotor (**28**) could inspect viscosity changes by ratiometric fluorescence imaging.

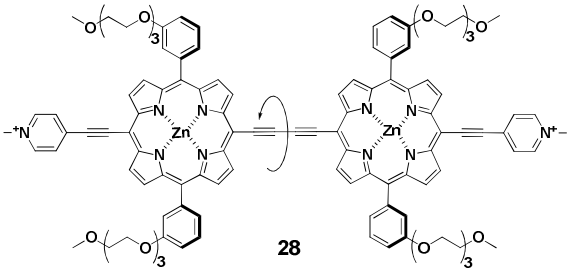

Fig. 8 Chemical structure of molecular rotor **28**.

Additionally, fluorescence lifetime imaging (FLIM) is another method in cellular viscosity investigation. In contrast to fluorescence intensity, the fluorescence lifetime is independent of fluorophore concentration and other factors, and can be used to detect dynamic excited state quenching or aggregation. In recent years, it has received wide research interest as a powerful tool in the fields of chemistry and biological chemistry.

In 2008, Kuimova and Suhling[52] devised a molecular rotor to map local microviscosity using FLIM. After comparing of the fluorescence properties of a series of BODIPY-based fluorescent dyes, they selected compound **29** (Fig. 9), a long-tail phenyl-substituted BODIPY without tetramethyl groups, as the ideal molecular rotor candidate. Fluorescence lifetime imaging is sensitive to local microviscosity. The fluorescence lifetime was found to increase from 0.7 ± 0.05 to 3.8 ± 0.1 ns with an increase in the surrounding viscosity from 28 to 950 cP. FLIM was further used to map the viscosity distribution in living cells by incubation with the molecule rotor. *Meso*-substituted BODIPY can be used in FLIM and polarization-resolved fluorescence decay measurements. Suhling and coworkers[53] synthesized another BODIPY dye with long, hydrophobic tails to target non-aqueous intracellular membrane regions (**30**). Compared with **29**, the molecular rotor **30** can report on spatial variations in the viscosity of biological environments through FLIM.

Fluorescence lifetimes of the two dyes were measured across a wide range of viscosities, ranging from 100 ps to 4 ns, and imaged with FLIM.

Very recently, Kuimova et al.[54] determined heterogeneous viscosity distributions in a microbubble coating by recording FLIM images of the viscosity-sensitive dye **29**. They found that compound **29** could be seamlessly incorporated into a microbubble with a surfactant encapsulated and surrounded by a phospholipid layer. Ahead of FLIM measurements, they investigated the preparation of microbubble in detail, including the effect of the preparing method, encapsulating composition, and size on the magnitude and spatial distribution of the effective surface viscosity of individual bubbles. The results confirmed that the microbubbles were sufficiently stable in the presence of laser irradiation at low powers to obtain FLIM images, and exhibited a large change in viscosity across the microbubble population. This proved a comprehensive method with a unique tool to help understand the structures and physical properties of microbubble coatings at the microscopic scale.

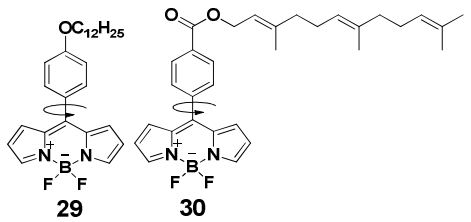

Fig. 9 Chemical structures of BODIPY-based fluorescent molecular rotors (**29–30**).

The concept of a dual-mode viscosity probe was first raised by Peng and coworkers,[55] in which a Cy5 based fluorescent viscosity sensor **31** (Fig. 10) with an aldehyde group (-CH=O) at the central position of the polymethine chain was prepared as a molecular rotor to show intracellular viscosity responses. The Cy5 rotor was the first case capable of bimodal fluorescence imaging of cellular viscosity, including ratiometry imaging and FLIM. The restriction of rotation of the aldehyde group in viscous or low-temperature environments resulted in marked fluorescence increase (6-fold enhancement) and the fluorescence lifetime lengthening (from 200 to ca. 1450 ps). In the meanwhile, this fluorescent rotor possessed two groups of absorption (λ_{abs} 400 and 613 nm in ethanol) and emission (λ_{em} 456 nm [blue] and 650

nm [red] in ethanol), exhibiting a ratiometric response (12-fold) and a large pseudo-Stokes' shift (ca. 250 nm). The use of two imaging approaches provided the possibility of viscosity measurement with more accurate and reliable results.

Two-photon microscopy (TPM) has been widely applied in fluorescence sensing and biological imaging. Peng's group subsequently[56] reported a carbazole-based ratiometric fluorescent probe **32** to image cellular and tissue viscosity with good two-photon absorption properties. The target compound was obtained by linking a carbazole aldehyde with a 2,3,3-trimethylindolenium salt. It displayed maximal absorption at 380 nm and two emission bands located at 485 and 580 nm, respectively. A dramatic fluorescence enhancement of **32** was observed with increasing solvent viscosity, with the red emission at 580 nm increasing much faster than that of the blue band. This sensor was able to map cellular viscosity, and furthermore, to image viscosity in tissue.

Min[57] devised a hybrid genetic-chemical molecular rotor (**33**) in Fig. 10 to measure protein-specific local environmental viscosity in live cells using FLIM. A trimethoprim was attached to a Cy3 dye, which was selected as viscosity-sensitive reporter because of the rotation of the backbone. A trimethoprim (TMP) was employed as specific targeting ligand towards dihydrofolate reductase (eDHFR) with nano-molar affinity. The fluorescence lifetime of **33** was independent of the concentration of the fluorophore. This was a promising tool to obtain valuable information about protein functions in the complicated and constantly changing microenvironment with high specificity and good spatial-temporal resolution.

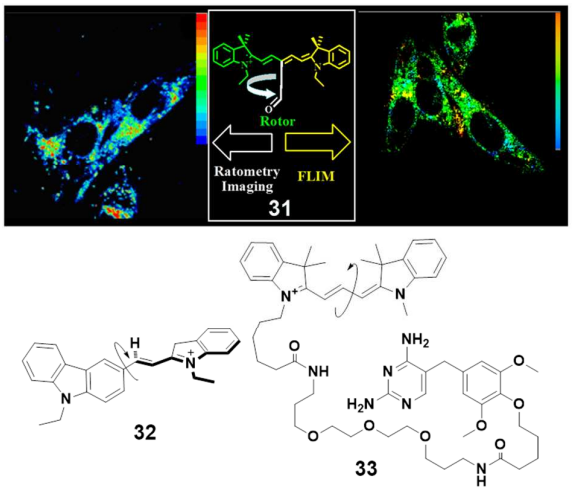

Fig. 10 Cyanine dye-based fluorescent molecular rotors (**31–33**) and dual mode cell imaging (**31**). Adapted with permission from ref. 55 (**31**) ©2011 American Chemical Society.

Xiao et al.[58] reported the first BODIPY-based fluorescent probe for lysosomal viscosity imaging (**34**) (Fig. 11). The molecular rotor possessed a morpholine moiety as the lysosome guiding group. The fluorescence intensity of **34** exhibited fluorescence sensitivity to both pH and viscosity. The fluorescence lifetime of **34** was responsive only to viscosity and was independent of pH changes and polarity. The sensor showed great potency in real-time monitoring of dynamic changes in lysosomal viscosity in live cells through the FLIM technique.

Changes in mitochondrial matrix viscosity may play a crucial role in modulating metabolite diffusion and mitochondrial metabolism. Kim and coworkers[59] designed a smart self-calibrating bipartite viscosity sensor (**35–36**) to measure mitochondrial viscosity with dual modalities. It was composed of a coumarin moiety and a BODIPY unit, connecting through a rigid phenyl spacer to construct a through bond energy transfer (TBET) system, and triphenylphosphonium as the mitochondria-targeting unit. This system showed an advantage over Fo□rster resonant energy transfer (FRET) molecular pairs in avoiding the uncertainties caused by the variable distance and dipole orientation of the two fluorophores. Linear relationships were observed between fluorescence ratio, fluorescence lifetime, and viscosity, suggesting the suitability of this system for mitochondrial viscosity imaging. The rotor was also

capable of determining viscosity changes upon mitochondrial apoptosis induced by treatment with monensin and nystatin: the viscosity increased from ca. 60 to 110 cP, which approached known results reported by others.

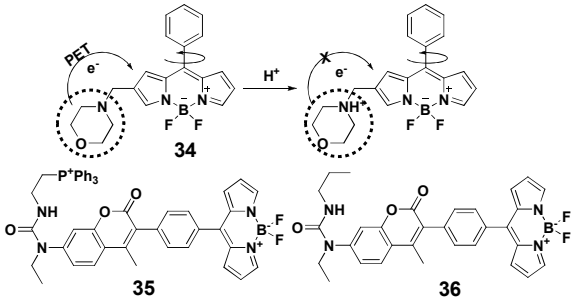

Fig. 11 Organelle-targeted fluorescent molecular rotors (**34–36**).

3. Polarity-sensitive fluorophores and chemosensing

Besides viscosity, environmental polarity is another significant factor controlling the physical and chemical properties of the surrounding molecules. Several organic or inorganic processes are markedly dependent on the surrounding polarities, which greatly control the reaction processes. In biological systems, especially at the cellular level, the polarity determines the interaction activities of a large number of proteins or reflects the permeability of membrane compartments. Specific recognition and interaction between proteins (e.g. enzymes) mainly depend on their hydrophobic interactions. Polarity-sensitive fluorescent probes are considered ideal candidates to sense polarity or changes thereof. These probes mainly include environment-sensitive chromophores composed of an intramolecular electron donor (e.g. amino groups), a conjugating spacer, and an electron receptor to construct a typical intramolecular charge transfer (ICT) system. When the surrounding polarity changes, they usually exhibit marked blue/red shifting in the maximal emission peak or large fluorescence quantum yield changes, and sometimes display dual fluorescence emission (local excited (LE) fluorescence and ICT fluorescence). (Fig. 12)

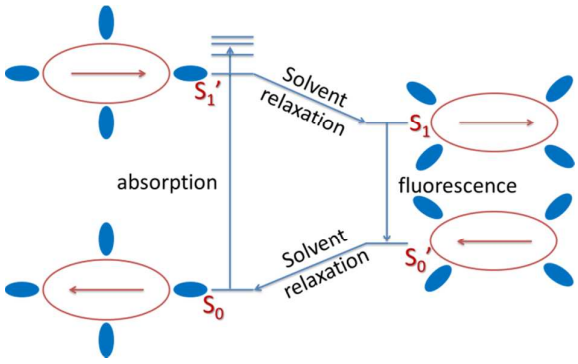

Fig. 12 Proposed solvent effects on fluorescence decay process.

Aminonaphthalene-sulfonic acid (**37**) derivatives are one of the first solvatochromic fluorescent dyes with maximal emission below 500 nm, and still remain powerful tools for protein labeling and biological membrane imaging. Slavik[60] first studied the fluorescent actions of **37** in solutions of various polarities. Its fluorescence was strongly quenched in aqueous solution, but could be largely increased upon binding to hydrophobic pockets in proteins, and the maximal emission exhibited an obvious shift.

The analog fluorophore (dansyl amide) (**38**) (as shown in Fig. 13) is one of the first used in protein labeling, and is obtained from the reaction of active dansyl chloride with corresponding amines. It shows very similar fluorescence intensity and the emission maximum changes between polar and nonpolar environments; it is able to covalently label various proteins with the excessive amino groups. Schultz et al.[61] developed a strategy to selectively and efficiently incorporate a small fluorophore into proteins at assigned sites through biological synthetic methods. A fluorescent amino acid (**39**) was genetically expressed in *Saccharomyces cerevisiae* by an amber nonsense codon and an orthogonal tRNA/aminoacyl-tRNA synthetase pair. The environment-sensitive dansyl amide was introduced into human superoxide dismutase to monitor the unfolding of the protein when exposed to guanidinium chloride. This can facilitate studies of protein structure and function.

Weber and coworkers[62] reported 6-propionyl-2-(dimethylamino) naphthalene (PRODAN) fluorophore that is relatively small in size. It can emit fluorescence ranging from 400 nm (in cyclohexane) to ca. 530 nm (in water) in various solvents,

which have subsequently received significant research interest as protein labeling agents, because they are very small in size and are unlikely to interfere with the biological activity of proteins. Subsequently, Potter et al.[63] synthesized another polarity-sensitive fluorophore 6-acryloyl-2-methylaminonaphthalene (ACRYLODAN) (**40**), in which the acryloyl group is capable of reacting with free thiols in proteins. Upon labeling proteins with ACRYLODAN, fluorescence quantum yields could be largely enhanced. This is a powerful tool in the study of the hydrophobic domains of biological macromolecules.

In order to reduce interference from auto-fluorescence of cells or tissues, Barrio and colleagues[64] extended the emission of the dye to a larger region (470–610 nm in hydrophobic and viscous environments) by stretching the conjugation moiety (dicyanoethylene group) (**41**). They found that the fluorescence of the obtained fluorophore was sensitive to both polarity and viscosity, because of the intramolecular rotational relaxation. The fluorescence quantum yield was rather low, due to the facile alteration from the lipid- or protein-bound state to aqueous media.

To obtain a consistent view of nucleotide-induced conformational changes around Cys697 (SH2) and Cys707 (SH1) in skeletal myosin subfragment-1 (S-1), Hiratsuka and coworkers mainly employed two thiol-reactive prodan fluorophores, ACRYLODAN (**42**) and 6-bromoacetyl-2-dimethylaminonaphthalene (**43**), to mark the above proteins.[65] After reacting with SH1 or SH2, the same fluorophores were obtained from **42** and **43**. As **42** was a very useful fluorescent reagent that readily reacted with only SH2 of S-1, it was employed to investigate the nucleotide-induced changes in ADS- 1 and BD-S-1. A different environment can be observed during ATP hydrolysis through the fluorescence spectral changes of compound **42**. It was found that the former has hydrophobic and closed characteristics, whereas the latter has hydrophilic and open ones.

To study the sensitivity of the 6-acetyl-2-dimethylaminonaphthalene derivative to the surrounding polarity, Parasassi et al. made a comparison of the steady-state and dynamic fluorescence spectra of 2-dimethylamino-6-lauroylnaphthalene (LAURDAN)

(**44**) and some other naphthalene analogues.[66] In both polar environments and phospholipid liquid-crystalline phase, the sensor displayed a marked red shift in the emission maxima, rationalized by solvent molecule dipolar relaxation. In phospholipid, in addition to the intramolecular relative reorientation of different moieties, such as the dimethylamino, carbonyl groups or the whole fluorescent moiety, the solvent dipolar relaxation observed for LAURDAN and PRODAN in phospholipid bilayers resulted from a small amount of water molecules present at the membrane interface.

In order to investigate the electrostatic effect on virtually all protein structure and activity, McAnaney and Park et al.[67] reported a fluorescent amino acid ALADAN (**45**, **46**) that was able to detect the electrostatic status of a protein at multiple sites. Compounds **45** and **46** are very sensitive to local polarity and can be selectively modified to buried and exposed sites in both soluble and membrane proteins. Steady-state and time-resolved fluorescent results of **45–46** residues at different buried and exposed sites in the B1 domain of protein G demonstrated its polar and heterogeneous interior.

Monitoring the structures and dynamics of DNA and their surroundings is a significant step for understanding various biological events accompanying biomolecular interactions. Okamoto and Saito at al.[68] developed novel fluorescent nucleosides (**47–49**) with a uracil base and a fluorophore conjugated by rigid linkers to probe the microenvironment around specific sites of DNA. These sensors had unique fluorescence properties. Upon modification of the fluorophores with the uracil base, it was found that the sensor **48** obtained by the Suzuki coupling reaction was highly sensitive to solvent polarity with typical ICT characteristics. Furthermore, both the absorption and emission wavelengths of probe **49** were evidently longer than those of **47** because of the extension of the DNA conjugation system.

Cho and co-workers[69] developed a two-photon turn-on probe (**50**) for the lipid rafts imaging. In terms of structure, 2-amino-6-acetylnaphthalene was employed as a fluorescent moiety, a hydrophilic carboxylic group was tethered to an amino group,

and an aliphatic chain was attached to the acetyl end, which allowed the molecule to anchor into lipid rafts but not enter the cell. The probe emitted brighter two-photon fluorescence in lipid rafts than in non-raft regions and provided direct observation of the lipid rafts in living cells and a pyramidal neuron layer with a depth of 100–250 μm in biological tissues using the two-photon microscope.

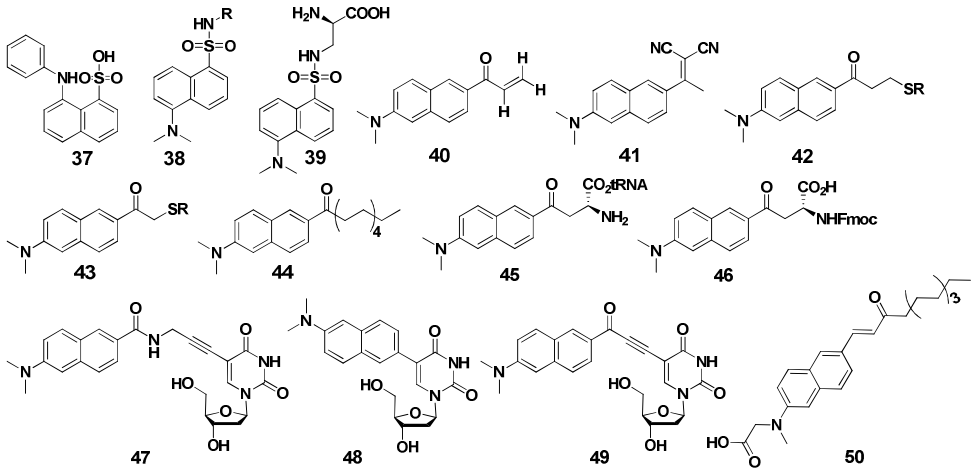

Fig. 13 Naphthalene-based solvent polarity sensors (**37–50**).

Taking into consideration the short emission wavelength of PRODAN, Twieg et al.[70] developed a novel fluorophore (**51**) (Fig. 14) with a longer emission wavelength. Compared with PRODAN, they used the longer conjugating system anthracene instead of naphthalene. It showed very wide fluorescence spectral response with emission spanning from 400 to almost 600 nm with variations in solvent polarity. The additional spectral red shift of anthracene can avoid the biological autofluorescence and allowed for more efficient excitation wavelengths for fluorescence applications.

Recently, Konishiwe and coworkers[71] synthesized a kind of pyrene analogue (**52**, **53**) with longer emission wavelengths than those of PRODAN through the Buchwald-Hartwig reaction. The fluorescence quantum yields (QYs) in various organic solvents demonstrated that they possessed outstanding fluorescence properties suitable for various applications, e.g. high QYs from hexane to methanol, large Stokes' shifts, and emission wavelength sensitive to polarity. These special properties arose from the chromophore changes from naphthalene to alkylpyrene, which barely affected the n–p* excited states.

Dimethylaminophenylimide, dimethylaminophthalimide, and dimethylamino anthralimide belong to another large family with solvatochromic effect. Their maximal emission wavelengths increase with the extension of the conjugation moiety. The fluorescence becomes brighter with a decrease in environmental polarity. First, Samanta et al.[72] investigated the spectral properties of 4-aminophthalimide (**54**) and its solvent effect. They provided this compound and its derivatives as potential fluorescence probes for organized media. The fluorescence response, including the maximum wavelength, fluorescence intensity, and lifetime, was well responsive to the medium polarity. All of these factors can be further increased with the involvement of the ICT emission state with hydrogen bonding interactions in solvent molecules containing hydroxyl groups. They further used this kind of fluorophore to monitor the local heterogeneous environments of solvent media such as cyclodextrins and micelles. The combination of hydrophobic interaction with the host media and the hydrogen bonding interaction with solvent molecules were found to determine the location of the fluorophore, which was observed to be the interfacial region between the separating nonpolar core of the micelle or the cyclodextrin cavity and the polar aqueous environment.

Imperiali et al.[73] synthesized a 4-(*N*,*N*-dimethylamino) phthalimide-based environment-responsive fluorescent Fmoc-protected amino acid **55** for solid-phase peptide synthesis. Peptides incorporating this residue showed great potential for biologically studying protein/protein interactions. These methods were applied in the synthesis of new fluorescent peptide sensors for 14-3-3 proteins, demonstrating the potential of this new fluorescent probe to monitor protein/protein interactions. Later, this group[74] developed another polarity-sensitive fluorophore, 6-*N*,*N*-dimethylamino-2,3-naphthalimide **(56)** with longer emission in the 500–600 nm region, which markedly responded to changes in the environmental polarity. Its maximal emission peak showed more than 100 nm red-shift in polar protic environments from 491 (in toluene) to 592 nm (in water). Additionally, the QYs was largely decreased from chloroform (Φ_f = 0.225) to water (Φ_f = 0.002). They further synthesized an Fmoc-

protected amino acid (**57**). Peptides combining the new residue can monitor protein-protein interactions (e.g. studying Src homology 2 (SH2) phosphotyrosine binding domains) due to the sensitivity of this residue to the microenvironment. Peptides containing **57** exhibited a substantial increase in the QYs at 596 nm upon binding to designated SH2 domains (e.g., Crk SH2, Abl SH2, and PI3K SH2). The peptides can work as ratiometric sensors (I_{596}/I_{460}), because the short wavelength band (460 nm) was almost invariable throughout the titrations.

In order to observe the immune response during the binding of antigens to major histocompatibility complex (MHC) proteins, Stern and coworkers[75] designed new fluorogenic probes (**58–60**) conjugating with environment-sensitive amino acids 6-*N*,*N*-dimethylamino-2,3-naphthalimidoalanine and 4-*N*,*N*-dimethylaminophthalimidoalanine. After binding to class II MHC proteins, the fluorophores showed great emission changes, QYs and fluorescence lifetime, respectively. Peptides modified with these fluorophores specifically interacted with class II MHC proteins on antigen-presenting cells and can follow peptide binding *in vivo*. By means of these probes, they tracked a developmentally regulated cell-surface peptide-binding activity in primary human monocyte-derived dendritic cells.

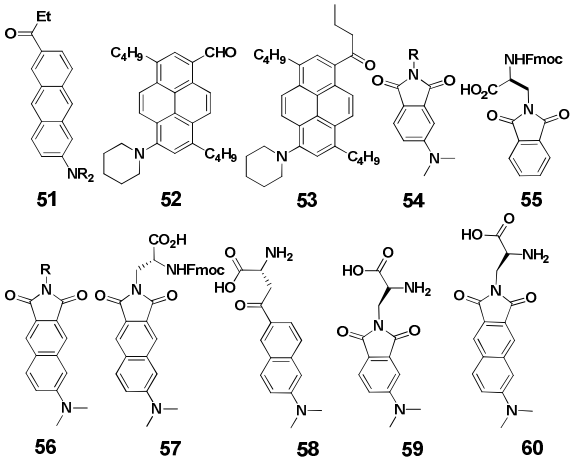

Fig. 14 Naphthalimide -based solvent polarity sensors (**51–60**).

As shown in Fig. 15, a 4-*N,N*-dimethylamino-1,8-naphthalimide (**61**) is a well-known solvatochromic fluorophore with special spectral properties, and its fluorescence is greatly enhanced in hydrophobic environments or non-polar solvents.

It displayed some advantages over related fluorophores with better chemical stability, a longer excitation wavelength (408 nm), and improved synthetic accessibility. Imperiali and coworkers[76] developed a **62** based amino acid incorporating into an Fmoc-protected amino acid *via* standard solid-phase peptide synthesis in the study of protein-protein interactions. The fluorescence QYs of this probe was highly responsive to the local environment. This resulting probe was considered as a potential tool for studying protein-protein interactions, as demonstrated by its introduction into a peptide that can be recognized by calcium-activated calmodulin. A greater than 900-fold fluorescence enhancement was observed after the binding between the two components.

Zhu et al.[77] reported a naphthalimide-based fluorescent probe **(63)** to specifically label cellular vicinal dithiol proteins (VDPs). In this probe, naphthalimide was employed as environment-sensitive reporter to show labeling of VDPs with the probe. It can act as a tool for the faster and specific detection and visualization of VDPs both *in vitro* and in living cells. This approach permitted the noninvasive study of VDPs both *in vitro* and in living cells.

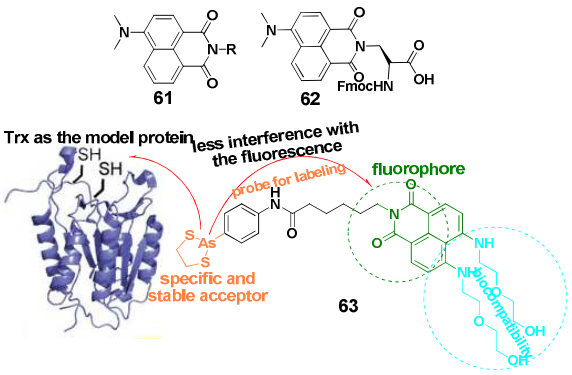

Fig. 15 Naphthalimide-based solvent polarity chemosensors (**61–63**). Adapted with permission from ref. 77 (**63**) ©2011 John Wiley and Sons.

Nile Red is a well-known uncharged hydrophobic fluorophore whose fluorescence markedly depends on the polarity of its surroundings. It has several advantages, e.g. photostability, broad working window of emission wavelength, easy removal from biomolecules, broad working pH range (4.5–8.5) and high fluorescence quantum yield, making it a suitable candidate for sensing hydrophobic sites on protein and for lipid

imaging.

Compared with previous polarity-sensitive fluorophores, Nile Red and its derivatives are highly sensitive to polarity with longer emission wavelengths, and exhibit large emission shifts with variations in their environment. Fowler et al.[78] reported that Nile Red (**64**) (Fig. 16) was an outstanding fluorescent dye for the imaging of cellular lipid droplets *via* fluorescence microscopy and fluorescence flow cytometry. They used Nile Red to specifically assess lipid distribution on aortic smooth muscle cells and on cultured peritoneal macrophages. It was found that Nile Red selectively localized at cytoplasmic lipid droplet regions and exhibited yellow-gold fluorescence (λ_{ex}: 450–500 nm; λ_{em} > 528 nm) (a), but not red fluorescence (λ_{ex}: 515–560 nm; λ_{em} > 590 nm) (b). Due to the difference in fluorescence emission from Nile Red, the above two cell types can be differentiated and analyzed through flow cytometry.

On the other hand, Nile Red is a good protein sensor as well, and its large spectral changes can be used to sense the hydrophobic cavities of many native proteins. Wolff and coworkers[79] investigated the interaction between Nile Red (**64**) and 3-lactoglobulin, K-casein, and albumin; upon the binding of ligand to calmodulin, it induced the formation of new hydrophobic surfaces, due to the oligomerization of melittin or the unfolding of ovalbumin during early denaturation.

Umezawa and colleagues[80] developed a new method based on Nile Red to image conformational changes of proteins in living cells. They used environment-sensitive Nile Red as fluorescent reporter, and two ethylenedithiol arsenates were covalently conjugated to Nile Red to provide the target sensor (**65**) (Fig. 16). This probe can covalently bind to proteins with four cysteine residues at positions *i*, *i* + 1, *i* + 4, and *i* + 5 of an α-helix. The specific recognition between the fluorescent probe and the 4Cys residue enables fluorescent marking inside cells. As the Nile Red moiety is highly sensitive to its micro-surroundings, conformational changes in proteins can be monitored in living cells as changes in fluorescence. As calmodulin (CaM) was known to expose its hydrophobic domains with variations of Ca^{2+} concentrations,

these researchers fused a helical peptide containing the 4Cys motif with the CaM protein as the protein model. The probe was then used to label the protein inside cells. Reversible changes in fluorescence intensity were observed in cells with changing intracellular Ca^{2+} concentrations, indicating conformational changes in CaM proteins in living cells.

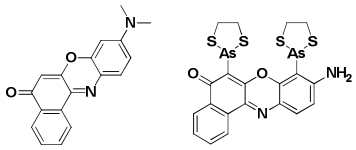

64 65

Fig. 16 Nile Red-based solvent polarity sensors (**64–65**).

L. Biczók et al.[81] investigated the micro-environmental effect on the fluorescence of 2-hydroxy-substituted Nile Red (**66**) and used it to sense micelles (Fig. 17). Based on measurements of the spectra in various solvents and micelles, they found two entirely distinct domains existing in the rate constant of the internal conversion. When it changed from apolar towards polar solvents, a decrease in non-radiative deactivation was observed because of the diminishing of intramolecular orbital coupling interactions. In alcohol solutions, a significant increase in the transition to ground states was observed due to efficient energy consumption through intermolecular hydrogen bonding interactions. Furthermore, they characterized the local environment of the sensor in micelles *via* the correlation of fluorescence lifetime, absorption, excited-state energy and fluorescent emission maxima with the solvent polarity. Further evidence for the differences in the binding site of the sensor in various micelles was provided by means of fluorescence quenching.

In order to study the local polarity and dynamics in biological system, Okamoto[82] synthesized a novel Nile Red-based solvatochromic sensor (**67**), consisting of Nile Red covalently linked to β-C-2′-deoxyriboside. It could be incorporated selectively into an oligodeoxynucleotide. When the microenvironment around the sensor changed, it exhibited large absorption and fluorescence responses. The same group[83] reported another nucleoside modified with Nile Red (**68**) to examine polarity changes of local environment around DNA. This nucleotide was constructed by coupling a 2-

hydroxylated Nile Red derivative with 1, 2-dideoxyglycan. It demonstrated high solvatofluorochromicity. The maximal fluorescence wavelength of **68** linked to DNA exhibited an obvious blue shift upon the addition of β-cyclodextrin, making it an ideal optical reporter for detecting local polarity changes at a specific location on the target sequence involved in the interaction between DNA and its binding molecules.

Pitner et al.[84] synthesized a kind of thiol-reactive 2-iodoacetyl-terminated Nile Red derivative **(69–70)** to continuously monitor galactose/glucose binding proteins (GGBP) with the fluorometer. The sensor could be conjugated to GGBP proteins containing cysteine mutations, which were designed to provide optimal site-specific binding of the fluorescent sensor. These binding sites provided the maximal local environment change for the attached sensor between the bound and unbound conformations. Marked fluorescence enhancement (ca. 50% increase in fluorescence intensity) of the sensor was observed at the selected cysteine sites of GGBP binding to glucose, which could be used to transfer the signal from the skin to an external monitor.

Thomas et al.[85] used the same probes to specifically label the S337C maltose binding protein (MBP) mutant with various sensitivities. The sensors showed a 3-fold (+200%) fluorescence enhancement upon binding to S337C MBP with an associating constant (K_d) of 435 μM, whereas the fluorescence change was only 20% with a K_d of 1.4 mM. Conformational analysis of the sensors by molecular modeling revealed that different conformational freedom was conferred on the dye upon the binding of the sensors, resulted in various fluorescence responses.

Moerner et al.[86] developed a Nile Red-based polarity-sensitive probe (**71**), containing a maleimidyl unit as the covalent labeling moiety. It was capable of exploring local conformational changes in the sequence caused by the bacterial chaperinin GroEL and its cofactor GroES to assist in protein folding. The probe was able to label a special single-cysteine mutant of GroEL (Cys261), containing a cysteine in the central cavity at the apical region of the protein. The fluorescence spectra of Cys261-NR were measured after the probe reacted with various proteins in the local environment. The fluorescence intensity was increased by 32 ± 7% after

interacting with denatured proteins and decreased by 13 ± 3% in the present of ATP, demonstrating the changes in local polarity of the protein. They further measured the fluorescence intensity changes of the probe upon the addition of the substrate, GroES and different nucleotides in various orders, and the differences in fluorescence intensity change provided an insight into the conformational changes in the protein during GroEL-mediated protein folding.

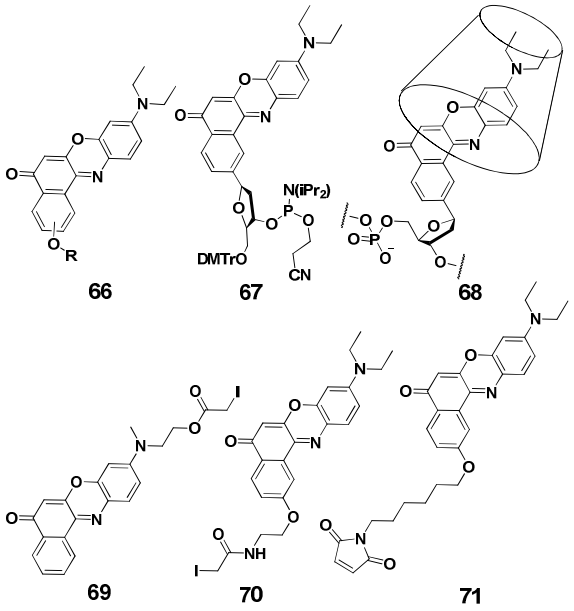

Fig. 17 Nile Red-based solvent polarity sensors (**66–71**).

Sapre et al.[87] also investigated the solvent effect on the spectral properties of Neutral Red (**72**) (Fig. 18) and their biological importance in various neat and mixed solvents. The fluorophore exhibited dual solvatochromic behaviors, indicating two closely spaced electronic excited states. In low-polarity solvents, it mainly emitted local fluorescence (LE emission); while in polar solvents, its emission was dominated by the ICT state. The dipole moment changes between the ground state and excited state, fluorescence QYs, and fluorescence lifetime correlated with the solvatochromic shifts of Neutral Red.

Ma et al.[88] constructed a phenazine-based polarity-sensitive probe to detect the local polarity of specific proteins such as the N-terminal domain of proteins (**73**). In this molecule, an *s*-triazine ring was selected as the backbone, Neutral Red as the signal reporter, and hydrazine as the labeling unit. The probe was stable in different

solvents, the emission wavelength was longer than 550 nm, and the emission wavelength maxima was responsive to polarity only and independent of pH and temperature. The hydrazine subunit reacted readily with activated carbonyl groups, leading to *N*-terminal-specific linking of the probe and facilitating the measurement of the local polarity around the protein molecule. The probe was used to label both native and heat-denatured α-lactalbumin protein to obtain a dielectric constant of ca. 16. These authors proposed that the strategy would offer a general method for studying local environmental changes around a protein molecule under various denaturation conditions.

Another polarity-sensitive fluorescent sensor (**74**) was reported by the same group[89], which was capable of detecting the local polarity and structures, e.g. thiol-containing domains, in a protein. The sensor consisted of a polarity-dependent Neutral Red moiety and a thiol-specific labeling group (maleimidyl unit). Neutral Red demonstrated a marked fluorescence spectra shift and was sensitive to variations in polarity but not to pH and temperature variations, making this probe an ideal candidate to determine local polarity changes in a denatured protein caused by pH or temperature. It was further used to detect the polarity of the Cys123 domain of β-lactoglobulin, corresponding to a dielectric constant of 17.3 that showed almost no change upon heat treatment. The authors demonstrated that the combination of a polarity-reponsive fluorescent probe with site-specific labeling might serve as a powerful tool for understanding the structures and functions of proteins.

Taking into consideration the advantages of longer emission wavelengths, the authors[90] devised another Nile Red-based polarity-sensitive fluorescence probe (**75**) for selectively modifying tyrosine residues to get insights into the local environment of tyrosine domains in proteins. It was composed of Nile Red moiety and an active allyl group, which was able to form allylpalladium complexes to covalently label proteins with tyrosine residues. After linking to proteins containing the Tyr108 domain, this probe displayed different fluorescent responses to acid-denatured and heat-denatured proteins; this was the first measurement of the polarity and

microenviromental changes of the Tyr108 domain in native and acid-/heat-denatured bovine Cu/Zn superoxide dismutase.

Jan and co-workers[91] developed a compact and neutral Cys-reactive probe, aminophenoxazone maleimide (**76**). There was a very short linker between the sensor and the protein, which ensured close tracking of the motions of the side chain to the location of attachment. It displayed marked polarity-dependent variations in Stokes' shift and significant red shifts in both the excitation maxima (521 nm in toluene and 598 nm in water) and the emission maxima (580 and 633 nm), respectively, which provided a potent correlation of fluorescence to local structure and motions.

Klymchenko and colleagues[92] developed a probe by modifying Nile Red with an amphiphilic anchor moiety (**77**) to monitor lipid order in the membrane and to evaluate the flip-flop properties of lipids. They designed a method to control the reversible redox switching of the fluorescence of the probe in one membrane leaflet through sodium dithionite, resulting in the probe exclusively binding to the outer leaflet of model lipid vesicles and live cells without considerations of flip-flop at the same time, compared with its parent Nile Red. After its incorporation into the ordered phase (sphingomyelin-cholesterol), it exhibited an evident blue shift in the emission maximum. Furthermore, it could be used to differentiate between the two phases *via* fluorescence ratiometric imaging. The authors also used the sensor to monitor the cholesterol depletion process, as the emission of sensor correlated well with the cholesterol content in the plasma membranes of cells.

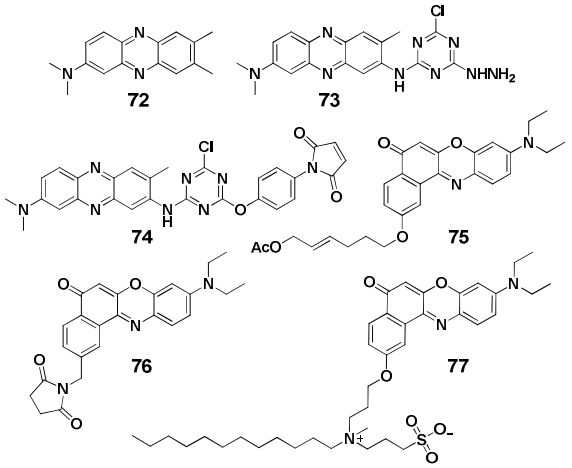

Fig. 18 Nile Red-based solvent polarity sensors (**72–77**).

Hahn et al.[93] developed a series of merocyanine dyes (**78–81**) that were very sensitive to the microenvironment with long emission wavelengths (> 590 nm), good photostability, and high extinction coefficients. As seen from the structures in Fig. 19, these dyes are composed of two different ends linked by a conjugated chain, maintaining sufficient hydrophobicity to interact with proteins. They were found to be aqueous soluble and did not aggregate at high concentrations. The fluorescence QYs of these dyes showed great changes with variations in solvent polarities or viscosities, allowing the measurement of microenvironmental variations in protein labeling and further in quantifying protein activities in living cells. They were able to selectively and covalently label the proteins through reactive iodoacetamide and succinimidyl ester side chains to study protein conformational changes, ligand binding, or posttranslational modifications. When used as biosensors to activate the GTPase protein Cdc42, these dyes exhibited 3-fold fluorescence intensity enhancement upon GTP binding.

Additionally, some new polarity-sensitive fluorophores have also been recently developed. Chang et al.[94] reported a new fluorescence sensor for solvent polarity based on 8-aminoquinoline-benzothiazole (**82**) (Fig. 19). The probe showed distinctive emission wavelength changes depending on the solvent polarity, which occurred over a wide span in the visible region from 486 nm to 598 nm; this fluorescence color change could be detected with the naked eye. Because the compound interacted specifically with water molecules through hydrogen bonding, the sensor showed significant spectral shifts when applied in binary solvent systems. This probe could be used to assess the polarity of the microenvironment and the water composition in biological systems.

Ohwada developed a coumarin derivative (**83**) with unusual fluorescence properties.[95] It was almost non-fluorescent in aprotic solvents (e.g. $\Phi_f < 0.0003$ in n-hexane), but showed very strong fluorescence at longer wavelengths (> 450 nm) in protic solvent (e.g. $\Phi_f = 0.21$ in methanol). The fluorophore was highly stable with a

long emission wavelength and a large Stokes' shift, and allowed facile structural modification to develop new fluorogenic (fluorescent "off-on") sensors.

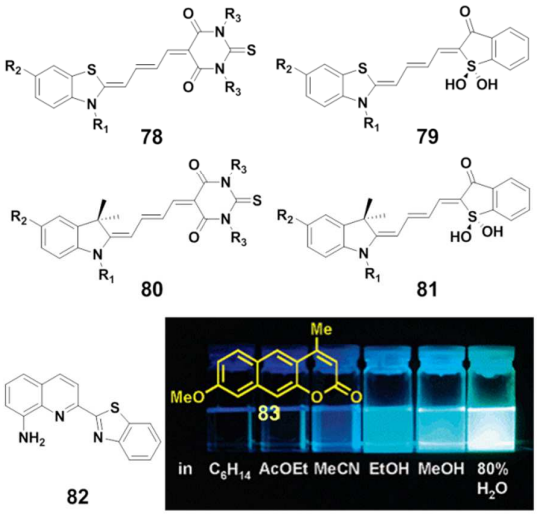

Fig. 19 Merocyanine dye-based solvent polarity sensors (**78–83**) and the fluorescence of **83** in different solvents. Adapted with permission from ref. 95 (**83**) ©2006 American Chemical Society.

Nagano and coworkers[96] synthesized a library of BODIPY derivatives with different benzene moieties substituted at position 8 (**84**), as seen in Fig. 20. The fluorescence OFF/ON (PeT process) of these fluorophores was strictly controlled by the solvent polarity. At lower solvent polarities, more positive oxidation potentials of the benzene units and more negative reduction potentials of the BODIPY moiety could be observed, which provided an even larger driving force for the PeT process from benzene units to the BODIPY moiety. When these fluorescent BODIPY dyes were further utilized to measure the microenvironment of bovine serum albumin (BSA) and in live cells, it was demonstrated that the polarity at the BSA surface was similar to that of acetone solvent, and that of the internal membranes of HeLa cells was similar to that of methylene chloride.

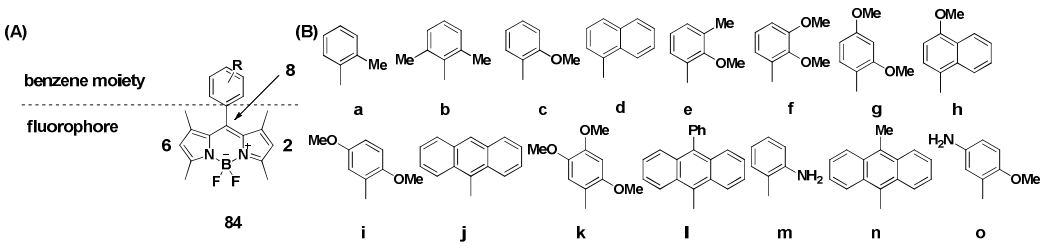

Fig. 20 BODIPY derivatives as solvent polarity probes (**84**).

Zhao and coworkers reported a series of fluorescent dyes based on 1, 10-fused ring phenothiazines and their derivatives (**85**, **86**)[97], which exhibited stronger fluorescence in protic solvents than in aprotic solvents. They were observed to exhibit higher fluorescence quantum yields and longer fluorescence emission wavelength in protic solvents, e.g. for **85**, $\Phi_f = 0.075$ in diethyl ether and $\Phi_f = 0.517$ in methanol; for **86**, $\Phi_f = 0.739$ in methanol. This was interpreted as indicating a transition from the C-C double bond to C-C single bond in the fused ring responsible for modulating photophysical properties. On comparing various methods on the analysis of the solvatochromic effect, it was concluded that Kamlet–Taft scale was a more suitable method than other solvent scales to describe the solvatofluorochromism of these compounds (Fig. 21).

In 2009, Bizzarri et al.[98] developed a polarity-sensitive probe **87**, whose structure was based on a "push-pull" system, including an electron-donating naphtyl ring and an electron-withdrawing benzothiazene group, conjugated to a coumarin fluorophore. The sensor was nonfluorescent in water but showed enhanced fluorescence in isopropanol, the sensor showed a polarity-dependent signal that changed nearly linearly with decreasing polarity of the medium. After modified with a versatile sulfonyl chloride group, the fluorophore was covalently linked to proteins, and the solvatochromic properties were nearly unchanged. There was a big difference between the fluorescent signal of probe-labeled streptavidin before and after the addition of BSA-labeled biotin.

In order to investigate the different polarity microenvironments in cells, this group[99] developed a series of coumarin derivatives (**88–89**). These compounds included a donor-coumarin core-acceptor system, where alkylether or naphthyl groups acted as the electron donor, and benzothiazene and cyano groups played the role of electron acceptor. These compounds displayed strong solvatochromism: they were almost nonfluorescent in water but highly fluorescent in less polar media (up to 780-fold enhancement). When they were tested in cultured cells, the results demonstrated

that the developed coumarins were unchanged compared to free solution. Because of their solvatochromic properties, the fluorescence of these probes was detected only in the most lipophilic environments of the cell.

Arai et al.[100] synthesized a full-color solvatochromic compound **90** to estimate protein (BSA) binding site polarity. As show in Fig. 22, it was composed of a pyrrole donor and a quinoxaline acceptor. The emission maxima of the compounds covered the visible light region with variations in solvent polarity, e.g. from n-hexane to water. There was a linear relationship between the maximum emission wavelength and the normalized solvent polarity. The polarity of BSA binding site could be measured from the solvatochromic plot. Therefore, compound **90** could be considered a promising candidate for a full-colored microenvironment-sensitive fluorescent sensor to estimate polarity of binding sites in proteins or other host molecules in aqueous solution.

Arai and co-workers[101] additionally synthesized another quinoxaline-based polarity-sensitive probe, 2-[(1*E*)-2-(1-*N*-methyl-pyrrol-2-yl)ethenyl]quinoxaline (**91**) and tested both probes in *in vivo* imaging applications. The two compounds were proven to be non-cytotoxic to Hep-2 cells at a concentration of 10 μM. When incubated with living cells, the compound (**90**) first penetrated into plasma membrane and then dispersed through the entire cell, showing site-dependent fluorescence spectra. In the case of **91**, it was also able to pass through the cell membrane, and was distributed throughout the whole cells, but did not exhibit site-dependent fluorescence, which suggested that it was a potential tool for mapping the local environmental polarity inside cells after conjugating to biomolecules.

Tobita et al.[102] synthesized a kind of 2, 1, 3-benzoxadiazole-based environment-sensitive fluorophore (**92–95**). Obvious solvachromism of probe **92** was observed in various solvents: it was highly fluorescent in n-hexane (Φ_f = 0.91, λ_{em} = 520 nm), excited at 449 nm, and almost non-fluorescent in water (Φ_f = 0.027, λ_{em} = 616 nm). When the oxygen was replaced with sulfur (**93**) and selenium (**94**), respectively, an obvious red shift was observed. The fluorophore **93** was fluorescent in *n*-hexane (Φ_f = 0.81, λ_{em} = 537 nm) and excited at 449 nm, but was quenched in water (Φ_f = 0.037, λ_{em}

= 616 nm); A similar fluorescence change was also obtained for **94** (Φ_f = 0.24, λ_{em} = 591 nm in *n*-hexane; Φ_f = 0.0046, λ_{em} = 672 nm in water). The authors of this study proposed that both the polarity effect and hydrogen bonding interaction between dye molecules and solvent promoted the non-radiative relaxation of the excited state of the fluorophores. With regard to **93** and **94**, internal conversion and intersystem crossing processes also contributed to non-radiative relaxation, verified by the results of time-resolved optoacoustic and phosphorescence measurements. Additionally, compound **93** exhibited a 10-fold enhanced photostability in water environments than **92**, suggesting that this compound could potentially be applied as a molecular nanogel thermometer **95**.

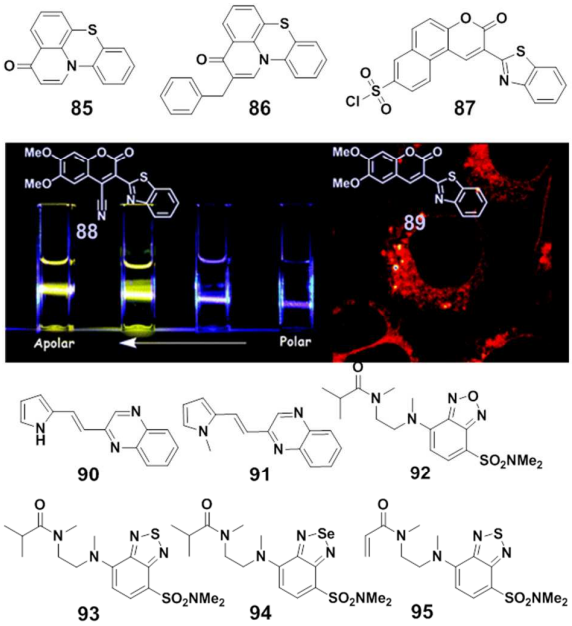

Fig. 21 Solvent polarity probes (**85–95**) and fluorescence imaging of **88–89** in living cells. Adapted with permission from ref. 99 (**88–89**) ©2010 American Chemical Society.

Recently, Konishi and coworkers[103] synthesized a series of nitrophenyl or nitrophenylethynyl oligothiophene derivatives (**96–97**) with unique environment-responsive fluorescence. With the increase in thiophene units, they are highly fluorescent (**96**, Φ_f = 0.43 in $CHCl_3$) and the fluorescence spectra display multicolored changes with moderate fluorescence quantum yields (Fig. 22). Furthermore, **96** showed solvatochromic fluorescence in various solvents (Em: 500–

700 nm) and a large fluorescence quantum yield, even though nitro groups were present in the compounds without a strong electronic donor, suggesting the potential of these compounds in the detection of nitro-reduction *in vivo*.

Qu [104] developed very sensitive solvatochromic two-photon fluorescent probes with small sizes derived from 4-methyl-2, 5-dicyano-4′-aminostilbene (**98–99**) (Fig. 22). They found that such probes exhibited marked viscosity-, polarity- and temperature-dependence of fluorescence. With variations in solvent polarity (e.g. from cyclohexane to DMSO), obvious shifts of the emission maxima (> 150 nm) and large changes of two-photon absorption cross sections have been observed.

Li et al.[105] synthesized a series of ICT type molecules (**100–102**) by the condensation of triphenylamine and malonitrile with good yields. It was observed that the fluorescence of these dyes were highly sensitive to polarities of various solvents with marked emission spectral shifts, producing blue to yellow and even red fluorescence in different organic solvents. According to the Reichardt–Dimroth equation, both the fluorescence intensity and the Stokes' shifts of the dyes showed linear changes with the orientation polarizability and empirical polarity parameter.

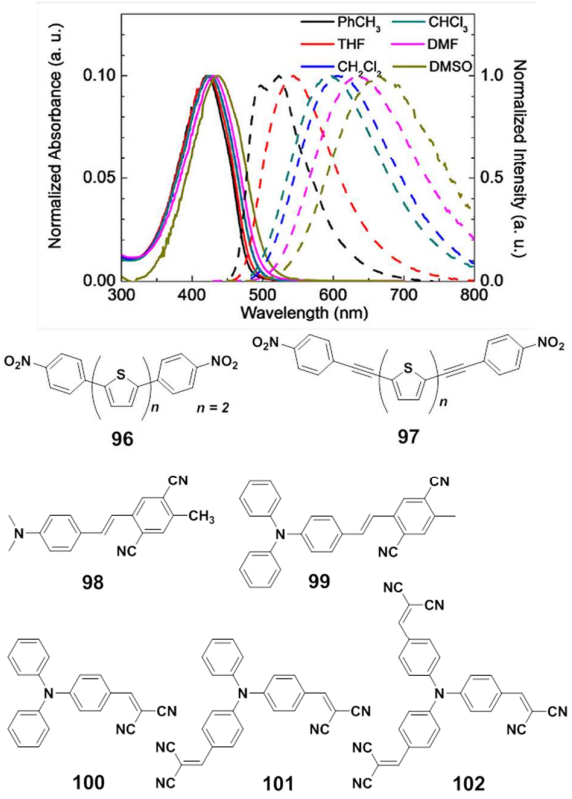

Fig. 22 Solvent polarity probes (**96–97**) and ICT-type probes (**98–102**). Adapted with permission from ref. 103 (**96–97**) ©2013 Elsevier.

4. Temperature-responsive fluorescent chemosensors and biological imaging

Temperature plays a key role in various physical and chemical processes, and fluorescent sensing of temperature has recently attracted much research interest from different fields. A variety of smart fluorescent materials have been designed and synthesized to sense temperature or to map intracellular temperature distribution. Thermoresponsive polymer is an outstanding organic material that has been increasingly applied in temperature sensing and imaging, due to its thermo-reversible phase transition at lower critical solution temperature (LCST) in aqueous solutions. Other materials have also been developed to work as a thermometer for biological imaging, such as molecular beacons, homogeneous and heterogeneous inorganic

quantum dots (QDs), as well as rare earth metal-doped nanomaterials etc.

4.1. Organic polymer-based thermosensitive nanomaterials

In 2004, Uchiyama and Iwai et al.[106] designed the first polymer material (**103**) working as an AND logic gate responding to near physiological temperature and pH at the same time as the input signals. This polymer material was composed of three moieties: *N,N*-dimethylaminopropylacrylamide (DMAPAM) and *N*-*tert*-butylacrylamide (NTBAM) (Fig. 23) were employed as the component *N*-alkylacrylamide monomers responding to temperature in aqueous solution. DMAPAM possessed dimethylamino groups in its structure and was sensitive to pH, as the ionization of these groups can inhibit the aggregation of the polymer and control its hydrophobicity and hydrophilicity balance. A benzofurazan fluorophore was tethered to the polymer as a polarity-sensitive group. The polymer was responsive to temperature by swelling or shrinking to change the internal polarity, which caused the successive fluorescence changes. It predominantly determined the thermosensitivity of the polymer towards a change in temperature at high pH conditions.

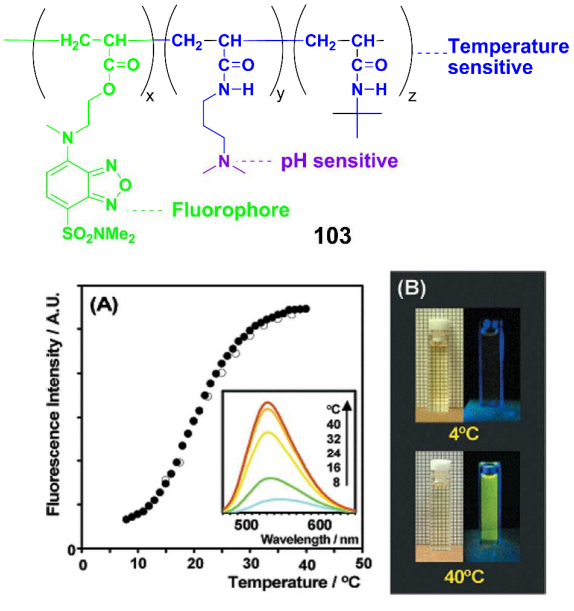

Fig. 23 Polymer material as temperature sensor (**103**). Adapted with permission from ref. 106 ©2004 American Chemical Society.

Later, Iwai et al.[107] synthesized a series of thermosensitive water-soluble

microgels (**104**), such as poly(*N*-isopropylacrylamide)(PNIPAM) (Fig. 24), labeled with the polarity-sensitive benzofuran, by emulsion polymerization. The fluorescence of the cross-linked polymer gel in water clearly increased when the temperature exceeded the LCST. These benzofuran-labeled microgels in water covered temperature sensitivity ranging from 18 to 47°C, demonstrating that they are ideal candidates for fluorescent thermometers.

Another thermosensitive polymer microgel particle was prepared by Matsumura and Iwai et al.[108] They prepared the sensor by 3-(2-propenyl)-9-(4-*N,N*-dimethylaminophenyl)phenanthrene (VDP)-labeling the poly(*N*-isopropylacrylamide) (PNIPAM) microgel (**105**) in Fig. 24 by emulsion polymerization. Upon studying the thermo-responsiveness of the microgel in water by turbidimetric and fluorescence analysis, the transition temperature of the microgel was determined to be ca. 32.5°C. The maximal emission wavelength of these microgels markedly blue-shifted around the transition temperature or even below the transition temperature, indicating an enhancement in hydrophobicity around the VDP units that can sense the de-swelling behavior of the microgel particles and report on the microenvironment caused by temperature change. Gradual shrinking of the microgel particles of **105** was seen with the increase of temperature from 26 to 31°C, and subsequent obvious shrinking occurred around 32°C.

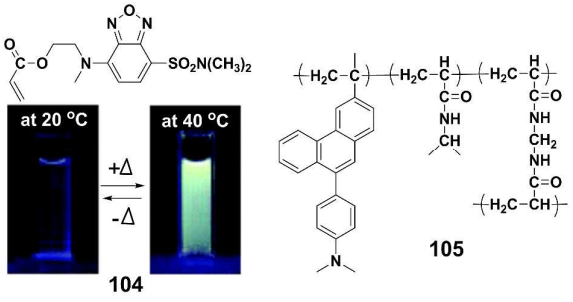

Fig. 24 Polymer microgel particle-based temperature sensors (**104–105**). Adapted with permission from ref. 108 (**104**) ©2010 Springer

Fluorescent polymeric thermometer-based *N*-alkylacrylamide and fluorophores demonstrate low temperature resolution in their working window, ranging from 15 to 50°C, due to their intermolecular aggregation, resulting in hysteresis in the fluorescent

response. To overcome this, Uchiyama et al.[109] modified the structure of the polymer **106** by adding some ionic components, e.g. sulfate propylacrylate (SPA) and 3-acrylamidopropyl)trimethylammonium (APTMA) to prevent the aggregation of the resulting polymer due to electrostatic repulsion, in Fig. 25. The obtained thermometers containing an ionic SPA component showed rare intermolecular aggregation with a significant improvement in their temperature resolution (＜0.2°C) over a wider temperature response range.

Considering the advantages of fluorescence lifetime-based imaging and detection, Uchiyama and coworkers[110] synthesized thermosensitive polymeric materials (**107**) using fluorescence lifetime imaging to map temperature. The organic material was composed of a random copolymer of *N*-isopropylacrylamide (NIPAM) and a polarity-sensitive monomer containing a 4-sulfomonyl-7-aminobenzofuran derivative. The obtained thermosensor exhibited dramatic sensitivity to temperature with a very sharp fluorescence lifetime change, which was increased from 4.2 to 14.1 ns when the temperature was raised from 30 to 35°C. Furthermore, fluorescence lifetime-based temperature measurement has the major advantage of being independent of the concentration of the sensor.

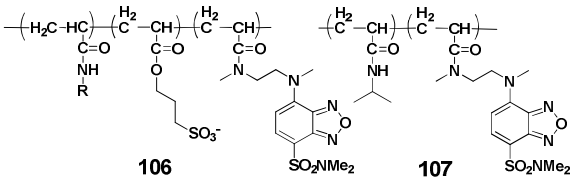

Fig. 25 Polymeric materials as temperature sensors (**106–107**).

In 2009, this group[111] developed another highly hydrophilic fluorescent nanogel thermometer for intracellular temperature imaging (**108**) (Fig. 26); this was the first case capable of measuring the intracellular temperature. The nanogel was composed of the thermosensitive polyNIPAM unit and a water-soluble fluorophore (such as the NBD-AA moiety). Its fluorescence in the cytoplasm markedly increased with increasing temperature. The temperature resolution was as high as 0.5°C, suggesting that this is a promising candidate to monitor intracellular temperature variations associated with biological processes.

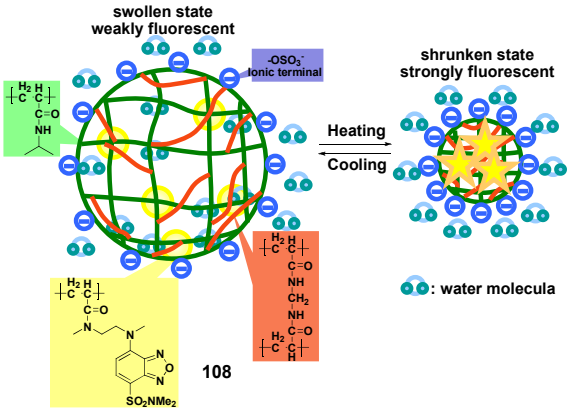

Fig. 26 A hydrophilic fluorescent nanogel thermometer (**108**). Adapted with permission from ref. 111 ©2009 American Chemical Society.

As demonstrated in Fig. 27, Ritter and coworkers[112] synthesized a switchable hydrogel (**109**) composed of a lower LCST copolymer bearing covalently linked polarity-responsive dyes, which exhibited solvatochromism in the presence of randomly methylated β-cyclodextrin (CD). It was demonstrated that the thermosensitive polymer was also strongly pH-sensitive because of its phenolic group. The polymer also exhibited an apparent red shift from orange to dark red at basic pH when the polymer was heated above the LCST value (ca. 31°C) in the aqueous solution; this temperature-dependent color change was completely reversible. Additionally, upon investigating the interaction between the polymer-linked dye and β-CD, it was found that the color change of the dye due to CD threading was almost identical compared to that caused by phase transition.

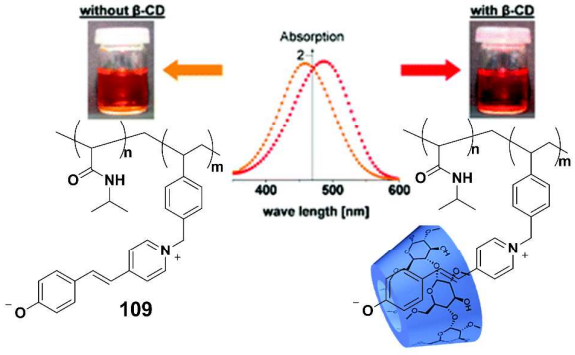

Fig. 27 Switchable hydrogel thermosensitive sensor (**109**). Adapted with permission from ref. 112 ©2007 American Chemical Society.

A rhodamine-based fluorescent thermometer (**110**) in Fig. 28 was developed by Shiraishi et al.[113] It was synthesized by the copolymerization of *N*-isopropylacrylamide (NIPAM) monomer and rhodamine (RD) units, the fluorescence of which was selectively enhanced in a specific temperature window. It showed very weak fluorescence at temperatures of 10–25 °C, but exhibited obviously enhanced fluorescence at temperatures > 25°C. The strongest fluorescence was observed at 33 °C. When the temperature exceeded 33°C, it gradually became weak in emission intensity and was almost quenched at > 40 °C. The changes in the fluorescence of RD at temperatures > 33°C were caused by strong polymer aggregation, which decreased absorption of incident light. The emission intensity decreased significantly, due to a decrease in the incident light absorption of the RD unit by robust polymer aggregation, which was driven by the heat-induced self-assembly of the polymer.

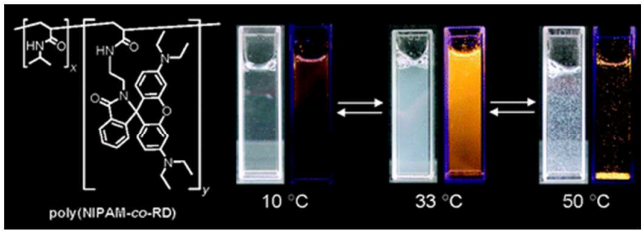

110

Fig. 28 Rhodamine B-labeled polymer responds as a temperature sensor (**110**). Adapted with permission from ref. 113 ©2007 American Chemical Society.

Shiraishi et al.[114] reported another thermosensitve copolymer (**111**) composed of *N*-isopropylacrylamide and 4-(4-dimethylaminostyryl) pyridine (hemicyanine HC) (Fig. 29). It displayed markedly heat-induced fluorescence enhancement caused by the phase transition. The fluorescence of the copolymer was very weak when the temperature was below 25°C, but was gradually enhanced at > 25°C and saturated at > 40°C. The fluorescence increase of **111** with the temperature change between 25 and 40°C was also driven by the heat-induced phase transition of the polymer from coiled to globular state. The heat-driven aggregation of the polymer resulted in fewer polar domains inside the polymer. The HC units conjugated to the polymer could transform from the benzenoid to the highly fluorescent quinoid form in these less polar domains. This was a promising candidate for use as a fluorescent thermometer with high

sensitivity, reversibility, and reusability.

Tang and coworkers[115] developed a new fluorescent thermometer (**112**) composed of PNIPAM labeled by tetraphenylethylene (TPE), which functioned by the mechanism of aggregation-induced emission (AIE) under neutral conditions. The TPE derivative was conjugated into the PNIPAM scaffold *via* a radical polymerization reaction of the corresponding monomer. The working mode was controlled by changing the degree of labeling of TPE. The intramolecular rotation of TPE quenched the fluorescence of the polymer, and with increasing temperature, the polymer gradually shrank to shorten the distance between the TPE molecules, resulting in the formation of an aggregate of TPE molecules to switch on fluorescence.

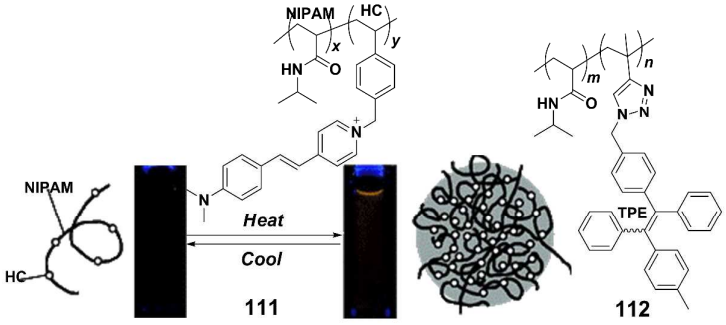

Fig. 29 Hemicyanine dye and aggregation-induced emission (AIE) involved in polymer as fluorescent thermometers (**111–112**). Adapted with permission from ref. 114 (**111**) ©2008 American Chemical Society.

A soluble dual responsive sensor (**113**) for both temperature and pH value was reported by Hoogenboom et al.[116] It was capable of responding sensitively to both temperature and pH, with a working window of 10–20°C for temperature and 1–7 for pH. The two different monomers (ethyleneglycol methacrylate and 4-nitro-4′-(*N*-ethylamino)azobenzene methacrylate (disperse red)) were employed to copolymerize through a reversible addition fragmentation chain transfer (RAFT) to provide target copolymer **113**. It exhibited a high cloud point at 92.1°C, above which it did not show color changes of disperse red at pH values varying from 1 to 13, which made the polymer unsuitable as a dual sensor. However, these results were able to demonstrate the potential of solvatochromic dyes incorporated into thermosensitive polymers to

obtain a good insight into hydration-dehydration processes during solubility transitions.

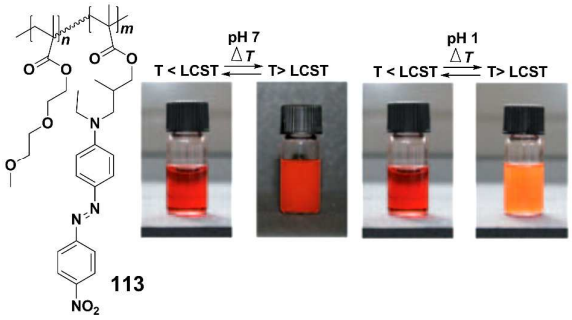

Fig. 30 Azo-benzene-based polymer fluorescent temperature probe (**113**). Adapted with permission from ref. 116 ©2009 John Wiley and Sons.

Subsequently, these authors developed different optical temperature sensors (**114**) in ethanol solution with a broad temperature-sensing range obtained by RAFT polymerization [117]. Some polarity-sensitive dyes (non-fluorescent or fluorescent) (e.g. disperse red and pyrene) were tethered to the poly(methylmethacrylate) (Fig. 31). Upon investigation of the optical response to temperature, the copolymers showed rare solvatochromic change because of the small polarity difference between ethanol/water and the polymer. The temperature-controlled UV/Vis and fluorescence spectroscopy changes revealed that the sensing capability of these copolymers was related to the scattering effects of disperse red, or excimer formation of the pyrene copolymer, respectively.

A smart fluorescent thermosensor (poly(methoxy diethylene glycol methacrylate)) (**115**) with pyrene functionalization obtained through RAFT polymerization was reported by the same group.[118] This polymer underwent a solubility transition with a transition from hydrophilic to hydrophobic state, when the environmental temperature was increased. At temperatures below the polymer LCST, the polymer was hydrated and the pyrene molecules were exposed to the polar environment, favoring excimer formation. Above the LCST phase transition, it was dehydrated and demixed from the aqueous solution, indicating a less polar environment for the pyrene capsulated inside the polymer aggregates. Therefore, it caused subsequent fluorescent responses of

pyrenes with variations in temperature.

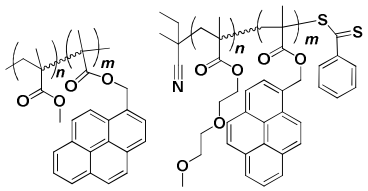

114 115

Fig. 31 Pyrene-functionalized polymers as fluorescent temperature sensors (**114–115**).

Liras et al.[119] synthesized a fluorescent thermo-sensitive terpolymer (**116**) composed of 2-(2-methoxy)ethyl methacrylate (MEO_2MA), oligo(ethylene glycol) methyl ether methacrylate ($OEG_{8\text{-}9}MA$), and a BODIPY methacrylate (Fig. 32). The terpolymer showed very low LCST, which could be easily tuned by controlling the composition of the monomers. The hydrophobicity of the BODIPY block promoted the formation of micelles below the LCST. Nevertheless, the polymer in the aqueous solution became turbid above the LCST, due to the π-π stacking interaction between the BODIPY fluorophores. When temperatures were higher than the LCST (ca. 26°C), the equilibrium swelling of the polymer was decreased and the solution became opaque, after which the fluorescence was largely enhanced.

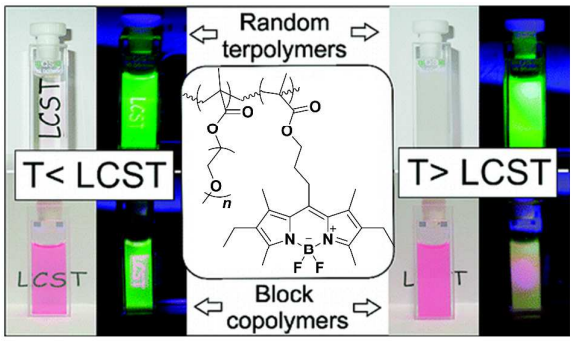

116

Fig. 32 BODIPY-functionalized polymers as fluorescent temperature sensors (**116**). Adapted with permission from ref. 119 ©2010 American Chemical Society.

Lin et al.[120] reported reversible thermo-responsive AuNPs (**117**) decorated with BODIPY-terminated water-soluble polymer on the surface. The polymer was prepared by RAFT polymerization of NIPAM attached with BODIPY, with absorption at 526 nm and emission at 558 nm. Then it was employed to stabilize AuNPs to construct a FRET system in the modulation of the fluorescence. PNIPAM

exhibited strong green fluorescence and exhibited increasing emission with rising temperature (from 20 to 40°C), while AuNPs showed inverse changes in fluorescence (Fig. 33). With the increase of the temperature, the distance between the AuNP core and BODIPY moiety was decreased to cause the quenching of both AuNP and BODIPY. On the contrary, this process could occur reversibly and efficiently, with heating or cooling.

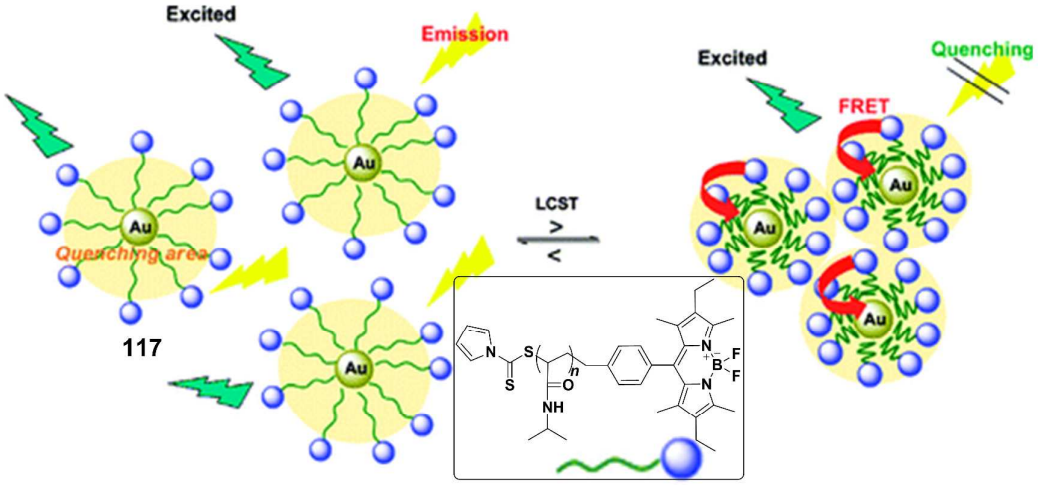

Fig. 33 Gold nanoparticle-based fluorescent temperature sensors (**117**). Adapted with permission from ref. 120 ©2010 American Chemical Society.

Chen and coworkers designed the first molecular thermometer (**118**) with ratiometric fluorescence changes (Fig. 34)[121]. It was composed of the PNIPAM nanogel labeled with 3-hydroxyflavones, which exhibited dual emission bands with normal excited state intramolecular charge transfer (ESICT) and tautomer excited state intramolecular proton transfer (ESIPT). With increasing temperature, the nanogel showed a fluorescence change from blue to green with good sensitivity and reversibility. The polymer displayed ratiometric changes when heating from 22 to 52°C, demonstrating a decline of the ESICT state instead of an ascent of the ESIPT state. The maximum emission of the two band shifts proved that the fluorescent ratiometric transition originated from the microenvironmental hydrophilic/hydrophobic conversion. Furthermore, the fluorescence of the nanogel showed a remarkable ratiometric change with an 8.7-fold leap, when the local temperature was increased from 33 to 41°C, and during this temperature window, it

revealed good linearity, suggesting potential applications in intracellular imaging.

Chiu and co-workers[122] developed another ratiometric temperature sensing system with semiconducting polymer dots (**119**) functionalized with rhodamine B (RhB) to construct the FRET system**.** The fluorescence intensity of RhB decreased with increasing temperature inside the matrix of polymer dots (Pdots). The obtained polymer nanoparticle showed high FRET efficiency from Pdot to RhB and exhibited good temperature sensitivity and strong fluorescence intensity because of the excellent light harvesting and energy transfer capability of Pdots. It displayed ratiometric fluorescent change with temperature with a single excitation wavelength. The ratio values showed good linear changes at physiological temperatures. The emission peak of RhB at 573 nm was temperature-dependent, while the emission peak of the semiconducting polymer at 510 nm was temperature-insensitive. Furthermore, the highly bright Pdot-RhB nanoparticle also showed its potential as a fluorescent probe in cell imaging.

Very recently, a novel fluorescent polymeric thermometer **(120)** working on intracellular temperature imaging and measuring using fluorescence lifetime imaging was reported by Uchiyama and colleagues.[123] They prepared the copolymer through copolymerization of *N*-n-propylacrylamide (NNPAM), 3-sulfopropylacrylate (SPA) and the environment-sensitive N-{2-[(7-*N,N*-dimethylaminosulfonyl)-2, 1, 3 - benzoxadiazol-4-yl](methyl)amino}ethyl-*N*-methylacrylate (DBD-AA). It was capable of intracellular temperature imaging with spatial and temperature resolution of 200 nm and 0.18–0.58°C, respectively. The copolymer was microinjected into COS7 cells, the heat generation process was observed by external chemical stimuli to show higher temperature in both the nucleus and centrosome than the cytoplasm; and the temperature difference between the nucleus and the cytoplasm varied during the cell cycle. Heat generation from mitochondria by surplus energy release was also visualized as a temperature increase.

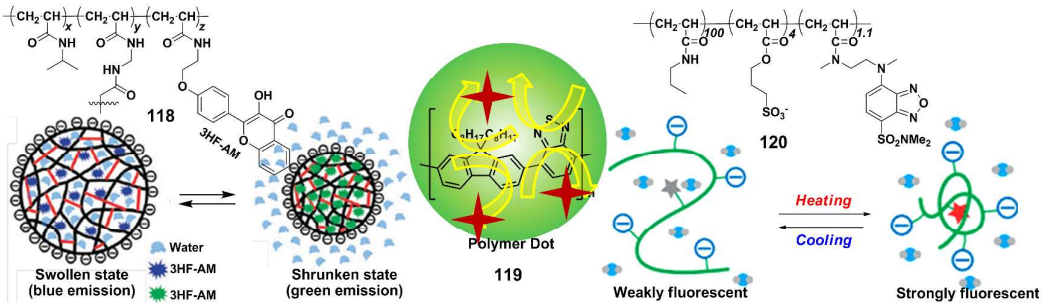

Fig. 34 fluorescent polymeric temperature sensors (**118–120**). Adapted with permission from ref. 122 (**119**) ©2011 American Chemical Society; from ref. 123 (**120**) ©2012 Nature publishing group.

Yang et al.[124] designed a FRET-based molecular beacon, L-MB (**121**), for temperature detection in living cells due to their inherent feature. It consisted of a non-natural L-DNA base, which formed a stable and accurate nano-thermometer in complicated cellular surroundings. This non-natural configuration ensured that L-MBs were not bound or degraded by cellular nucleic acids, proteins, or digesting enzymes. The sensor was small in size (less than 10 nm), and showed excellent response reversibility and a tunable working window, making it a promising candidate for potential applications in various situations. Furthermore, it was capable of intracellular temperature measurement during a photothermal study in living cells when the cells were exposed to near infrared light irradiation in the presence of palladium, as shown in Fig. 35.

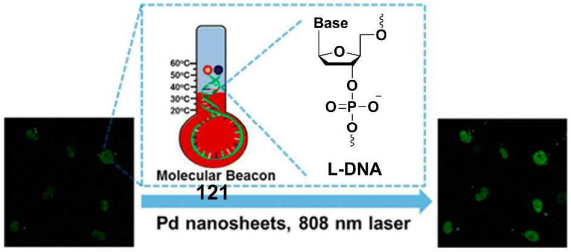

Fig. 35 Molecular beacon temperature sensors (**121**). Adapted with permission from ref. 124 ©2012 American Chemical Society.

4.2. Thermosensitive Inorganic Quantum Dots

Chen and coworkers[125] first developed the concept that luminescent nanoparticles were capable of measuring temperature. They compared the luminescence changes of

different types of nanoparticles with variations of environmental temperature. It was found that the luminescence of some nanoparticles exhibited a linear response to temperature; these were potential candidates for use as temperature sensors. Both pure CdTe- and ZnS-doped Mn^{2+} nanoparticles showed a linearly reversible response in the physiological temperature range, thus demonstrating a promising biomedical thermometry. With regard to double-doped ZnS: Mn^{2+}: Eu^{3+} nanoparticles, they responded differently for each dopant, and the ratio of luminescence intensity suggested a facile method for temperature measurement. For some other nanoparticles, the luminescent response to the temperature change was irreversible, which may be ascribed to the thermal instability of nanoparticle stabilizers or surface defects.

Individual QDs (**122**) were capable of measuring temperature changes as first reported by Yang et al.[126] They found that the steady emission spectrum of individual QDs was dependent on the environmental temperature, e.g. the biological temperature. Local temperature measurement can be achieved by a shift in the emission wavelength of QDs under various temperature conditions, which provided a method of non-contact, local temperature measurement.

Furthermore, this group developed another CdSe QD (**123**)-based two-photon nanothermometer.[127] CdSe QDs was employed as fluorescent nanothermometers for two-photon fluorescence microscopy, exhibiting marked enhancement in inherent spatial resolution. The fluorescence intensity caused by two-photon (near-infrared) excitation provided higher temperature sensitivity than that of one-photon (visible) excitation. In addition, it also demonstrated a dependence of maximum emission wavelength on temperature variations, offering another approach for thermal imaging, which was suitable for inhomogeneous disperse environments. The thermo-sensitive CdSe QDs system with two-photon excitation was successfully used to fluorescently image a biocompatible solution (PBS buffer) with an artificial temperature gradient and to measure temperature changes in single living cell.

Capobianco and coworkers[128] firstly evaluated the fluorescence response of CdSe-QDs (**124**) to temperature using both one-photon and two-photon excitation. The

systematical record of their emission spectra showed a function of temperature in the physiological temperature range. Two-photon (near-infrared) excitation caused much higher temperature sensitivity of the emission intensity than that achieved under one-photon (visible) excitation. The temperature dependence of the two-photon excited emission was determined by thermally induced changes of both the fluorescence QYs and the two-photon absorption cross-section, which enhanced thermal sensitivity together with the increased spatial resolution of two-photon excited fluorescence made these CdSe-QDs nanoprobes suitable for high-resolution nanothermometry. These properties provided the possibility to capture a high-quality thermal gradient image in a fluid (PBS) and to measure internal temperature changes in single HeLa cell.

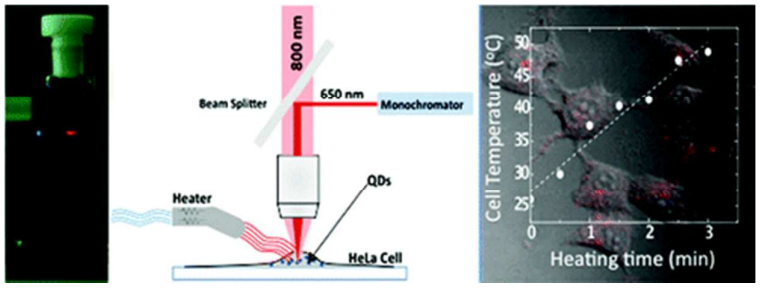

Fig. 36 Quantum dots-based thermosensitive probe (**124**). Adapted with permission from ref. 128 ©2010 American Chemical Society.

Another dual emission-based luminescent nanocrystal (**125**) was developed by Gamelin and coworkers.[129] The nanocrystal was composed of manganese-doped ZnSe QDs. Distinct dual emissive bands of the nanocrystal were observed, displaying intrinsic high temperature dependence. The emission intensities of the photo-exciting nanocystral exhibited ratiometric changes with changes of temperature, the ratio of which was independent of non-radiative effects. The temperature window controlling the ratiometric changes can be modulated by variations in the energy gap of the nanocrystal. This may open a new avenue to ratiometrically measure temperature (Fig. 37).

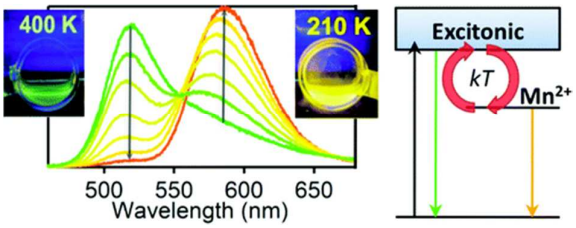

Fig. 37 Quantum dot-doped nanocrystals as temperature sensors (**125**). Adapted with permission from ref. 129 ©2010 American Chemical Society.

Yang and Lin et al.[130] further investigated intracellular thermogenesis (NIH/3T3 cells) by the optical response of QDs upon the trigger of extracellular Ca^{2+} stress. The spectral shift of QDs (**126**) correlating to temperature was found to be 0.057 nm/°C in the living cells, which was the basis of cellular temperature determination. In the presence of high concentrations of extracellular Ca^{2+} ions, the intracellular temperature was increased by ca. 1.5°C. Direct observation of the heterogeneous temperature progression inside living cells was possible, providing a potential means to investigate subcellular temperature changes for signaling and regulation.

Jaque and coworkers[131] developed multi-photon excitation CdTe QDs (**127**) with the particularly small sizes close to 1 nm, which demonstrated thermosensitivity as high as 0.2°C, more than 5 times larger than that reported for CdSe QDs. The two-photon emission band of the nanomaterials showed an unexpected thermally induced spectral red shift from 23 to 75°C.

Gamelin et al.[132] synthesized a thermosensitive multishell semiconductor nanocrystal (**128**) exhibiting inherent dual photoluminescence with high photo- and thermo-stability. It was composed of Mn^{2+}-doped ZnSe QDs as the core structure and ZnS/CdS/ZnS as multishell materials. The dual emission can be observed upon the phase transfer of the QDs into aqueous solution.

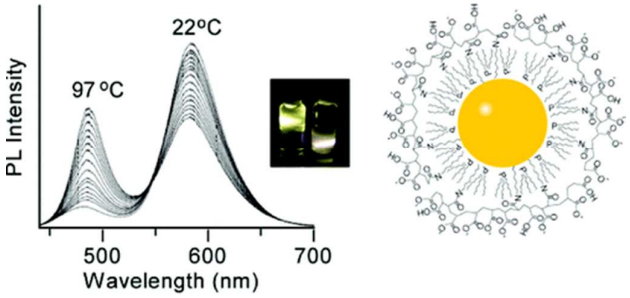

Fig. 38 Semiconductor nanocrystals function as temperature-sensitive probes (**128**). Adapted with permission from ref. 132 ©2011 American Chemical Society.

Cohen and Helms et al.[133] devised a FRET system comprised of CdSe-CdS quantum dot-quantum rods (QD-QRs) as the energy donor and a cyanine dye (Cy5) as the energy acceptor (**129**). The nano-complex was coated with an amphiphilic polymer. The whole system was temperature-responsive with ratiometric changes. A 2.4% ratio change/°C was obtained over the physiological temperature range in an aqueous environment, demonstrating a temperature determination precision of at least 0.2°C, enabling the nanoparticles to sense subtle cellular temperature changes. After delivery through a pH-sensitive cationic polymer colloid into living cells, the nanoparticles were released from endosomes. A large increase in the temperature response and sensitivity were observed. This system was suitable for explorations of microenvironmental thermometry and thermogenesis inside cells (Fig. 39).

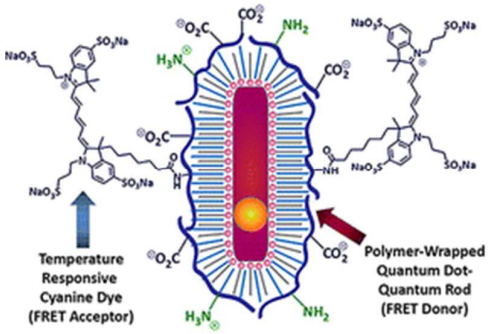

Fig. 39 Quantum dots-based FRET as the temperature sensor (**129**). Adapted with permission from ref. 133 ©2012 American Chemical Society.

4.3. Thermosensitive rare earth metal ion-doped nanoparticles and organic complexes

Luminescent materials with multi-photon (Near Infrared (NIR)) excitation wavelength utilized in biological imaging have demonstrated outstanding advantages over single-photon fluorescence imaging. Capobianco and co-workers[134] devised a lanthanide (Ln^{3+})-doped upconversion nanoparticle (**130**) as a versatile fluorescent nanothermometer used to accurately determine the temperature in both solution and living cells for the first time. When excited at 920 nm, the nanothermometer,

consisting of different contents of rare earth metal (Er^{3+}, Yb^{3+})-doped $NaYF_4$ nanoparticles, exhibited luminescent intensity ratio changes of the green emission bands of Er^{3+} dopant ions ($^2H_{11/2}\rightarrow{}^4I_{15/2}$ and $^4S_{3/2}\rightarrow{}^4I_{15/2}$) with variations in temperature. When an aqueous colloidal solution containing $NaYF_4$:Er^{3+}, Yb^{3+} nanoparticles was heated, thermal-responsive profiles were obtained from the emission of nanoparticles. Furthermore, it was demonstrated that the material was capable of measuring the intracellular temperature from 25 to 45°C, at which temperature death was thermally induced.

Europium (III)-β-diketonate complexes were also designed as optical sensors of temperature due to their high photostability and strong luminescence. Wolfbeis et al.[135] developed a dual sensor (**131**) to detect temperature and oxygen simultaneously. The sensor was composed of an europium (III)-β-diketonate complex encapsulated in poly(vinyl methyl ketone) or poly(*tert*-butyl styrene) microparticles as the temperature sensor and a palladium porphyrin as the oxygen indicator. The two materials were combined in a thin layer of hydrogel that could be excited by a single light source. This sensor was highly temperature-dependent at temperatures ranging from 0 to 70°C. This design showed potential uses in temperature-compensated oxygen sensing and related fields.

It is reported that organic europium (III) and terbium (III) complexes displayed excellent photo-luminescence, such as rather bright emission, short bandwidth, and long luminescence lifetime. Therefore, such materials-based chemosensors have also been developed to sense environmental temperature. Yu and coworkers[136] synthesized europium- and terbium-based temperature probes (**132–133**), which were the most sensitive to temperature among the lanthanide complexes. The complexes were incorporated into different polymer matrices to provide film-sensing materials as temperature-sensitive paints (TSPs). All materials displayed good sensitivity to temperature; in particular, TSP-based complexes (**133)** were even sensitive to environmental temperature with a high resolution of -13.8 and -9.2 μs per °C, respectively (Fig. 40).

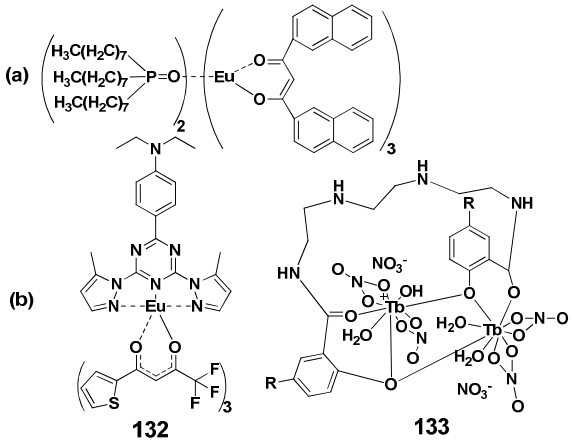

Fig. 40 Europium- and terbium-based temperature probes (**132–133**).

Peng et al.[137] synthesized a silica nanoparticle (**134**) with ratiometric fluorescence to sense the environmental temperature by the method of encapsulation and reprecipitation. The silica material was prepared by the introduction of alkoxysilanized 1, 8-naphthalimide as internal reference and a europium-based complex as the sensitive moiety, which can be excited at a single wavelength. The obtained nanoparticles had high resolution (small size, 20–30 nm) and good biocompatibility (outer silica layer). The whole silica-based nanomaterial was highly temperature-dependent between 25 and 45°C, making this a promising nanosensor for intracellular temperature imaging and measurement (Fig. 41).

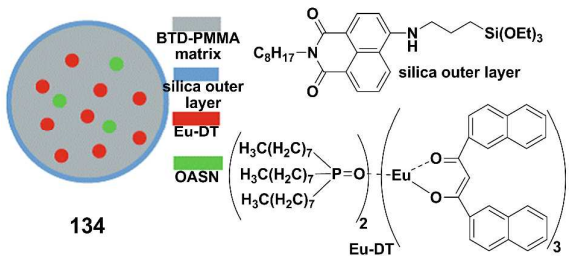

Fig. 41 Silica nanoparticle-based temperature probes (**134**). Adapted with permission from ref. 137 ©2010 Springer.

Aida et al.[138] synthesized a series of zinc-(3-pyridyl)porphyrin derivatives (**135**) to show supramoleular thermochromism, with changes in temperature ranging from 0 to 100°C. It can form a cyclic tetramer in toluene solvent. When the compounds contained an alkynyl side arm, it demonstrated very sharp color changes from red to green with changes in temperatures, as thermal-induced self-assembly caused the

differential extension of the π-conjugation of the porphyrin moiety. In contrast, both compounds without an alkynyl unit and a compound with two alkynyl units displayed less marked color changes with the variation in temperatures. It provided a potential to design a novel molecular thermometer based on thermal-induced self-assembly (Fig. 42).

Nienhaus et al.[139] synthesized ultrasmall fluorescent gold nanoclusters (AuNCs) (**136**) to sense intracellular temperature changes using fluorescence lifetime imaging to show high spatial and temperature resolution. AuNCs were explored to function as a nanothermometer with near-IR emission and excellent stability in the physiological temperature range. They showed very sensitive responses to temperature with respect to both fluorescence intensity and lifetime, ensuring the precise measurement of temperature under physiological conditions (0.1–0.3°C resolution in PBS solution and 0.3–0.5°C in HeLa living cells).

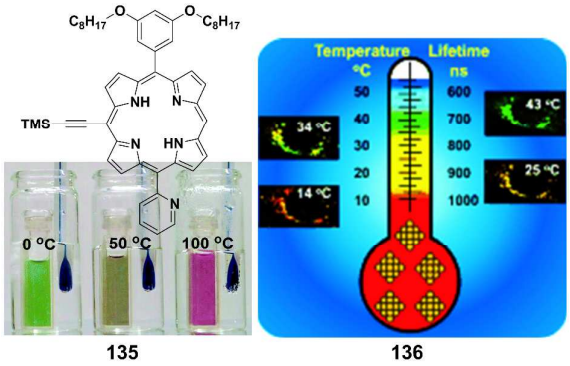

135 136

Fig. 42 Supramolecular thermometer (**135**) and gold nanocluster-based temperature probe (**136**). Adapted with permission from ref. 138 (**135**) ©2003 American Chemical Society; from ref. 139 (**136**) ©2013 John Wiley and Sons.

5. Hypoxia-based fluorescent chemosensing and imaging

A hypoxic environment within tumors can cause bioreductive reactions of small molecules with a hypoxia-sensitive moiety, such as a nitro group, quinone group, azo group, and N-oxide. This feature has been exploited to construct fluorescent probes for hypoxia imaging. Under hypoxic conditions, reductases within cells are capable of

catalyzing one-electron reduction of the above groups involved in specific functional compounds, which is a very typical pathophysiological feature of solid tumors. Enzyme-catalyzed one-electron reduction has been utilized as a powerful reaction to design a hypoxia target and image tool. For example, nitro-containing aromatic compounds are well characterized as general substrates for nitroreductase with the reduced nicotinamide adenine dinucleotide (NADH), and are ready to be stepwise reduced by cellular nitroreductase under hypoxic condition during cellular metabolic processes. Thus, such nitroaromatic compounds have been widely used to design bioreductive prodrugs and fluorescent sensors for nitroreductase and tumor hypoxia.

In 1991, Hodgkiss et al. synthesized some heteroaromatic nitro-compounds,[140] (**137–138**) (Fig. 43), the fluorescence of which was very weak because it was quenched by the nitro group; when they were incubated with hypoxic mammalian cell suspensions, the bioreduction of the nitro group gave rise to a fluorescent product. The two compounds could be used as a potential fluorescent sensor for hypoxia in tumors.

Next, they prepared coumarin compounds containing 2-nitroimidazole as potential fluorescent sensors for hypoxic cells (**139–140**).[141] The side chain 2-nitroimidazole was efficiently attached to cellular constituents. The fluorophores were selectively bound to cellular constituents of hypoxia because of bioreductive metabolism of the nitroimidazole. These two compounds showed more than 5-fold hypoxic-oxic differences in the *in vitro* test system. The fluorescence efficiencies and hydrophilicity were obviously improved by selecting bicyclic fluorophores with low molecular weights, and the transfer efficiency to the tumor was clearly enhanced. The time dependence of accumulation of tumor cells with **140** demonstrated that the fluorescence of cells under hypoxic conditions exhibited a 17-fold increase.[142]

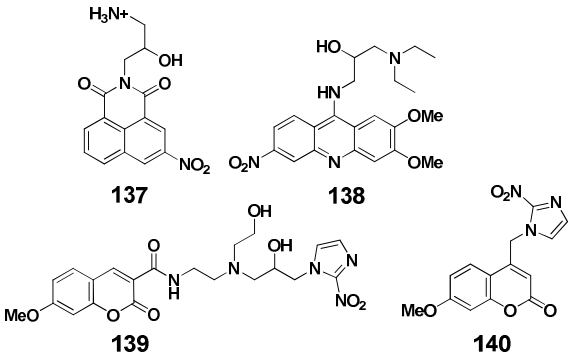

Fig. 43 Structures of fluorescent hypoxia markers (**137–140**).

Generally, the nitro group is known as a fluorescence quencher. Upon the bioreduction of the nitro group under hypoxia, the compound becomes highly fluorescent, which is usually employed to design fluorescence imaging for tumor hypoxia. Regarding this concept, Qian et al. synthesized bioreductive markers (**141**, **142** in Fig. 44) for hypoxia in solid tumors, with the emission wavelength at 590 nm. They consisted of 8-Oxo-8*H*-cyclophenta[*a*]acenaphthylene-7-carbonitrile as the fluorescent reporter and 2-nitroimidazole as the sensing targeting moiety.[143] The nitro moieties in hypoxia were reduced by nitroreductase enzymes by two electron steps under an oxygen insensitive process, resulting in high fluorescence enhancement. The obvious emission between hypoxic and normoxic cells was observed through the fluorescence scan ascent of these compounds. The hypoxic-oxic differential of fluorescence incubated with the compounds for 3 hours was up to 11- and 15-fold increase, respectively. Later, the same group introduced two heterocyclic side chains to the naphthalimide fluorophore to construct fluorescent markers for hypoxic cells. The increased bioreductive moieties were able to fix the fluorescent reaction products in the hypoxic cells. The hypoxic-oxic fluorescence differential of compound **143** (20-fold) was higher than the value of **144** (15-fold) upon incubation with cancer cells.[144] This could be potentially used as fluorescent sensors for hypoxia imaging *in vivo*. Qian et al. designed a series of nitroheterocyclic-based fluorescent sensors as potent hypoxic markers. A group of nitro unit-substituted acenaphtho[1,2-b]quinoxalines (**145**–**147**) were synthesized to target hypoxia environments[145] and exhibited marked fluorescence changes when the nitro group was reduced under hypoxic conditions.

The strongly yellow fluorescence from the quinoxaline could be easily distinguished from the weak background fluorescence of the tumor. The hypoxic–oxic fluorescence differential after the probes were incubated with V79 cells could be increased by 6-, 9-, and 11-fold, respectively.

Later, this group designed several fluorescent probes for hypoxia cells with a nitro group conjugating to the fluorophore 7H-benzimidazole [2, 1-a]benz[de]isoquinolin-7-one (**148**–**151**), instead of the 2-nitroimidazole moiety.[146] The nitro group in compound **148** was mainly used as electron withdrawing group and an amino group was attached to the fluorophore, undergoing a strong ICT process to emit strong fluorescence. While for compound **151**, the nitro group was conjugated to the naphthalene part of the fluorophore, resulting in a weak ICT system, the nitro group acted as a normal fluorescent quencher. Therefore, the compounds showed significantly different fluorescence changes, fluorescence quenching (**148**, **149**), or enhancement (**150**, **151**).

In hypoxic cells, tertiary amine N-oxides based on the PET or ICT mechanism could be bioreduced to produce the corresponding tertiary aliphatic amines, causing significant fluorescence changes. In 2011, Qian et al. introduced the N-O group into an amino unit side chain to the planar naphthalimide chromophore (**152**).[147] Together with above ideas, both active sites for bioreduction (the nitro group and the NO group) was conjugated to a naphthalimide fluorophore. In hypoxic cells, the nitro group could be reduced to the corresponding product to result in the chromophore changing from a pull-pull system to pull-push one, and the fluorescence exhibited large changes with 17-fold enhancement. This proved an ideal candidate for a hypoxia marker in living cells.

Additionally, the first ratiometric fluorescent probe (**153)** was also developed by Qian and coworkers in 2011.[148] It was composed of a *p*-nitrobenzyl unit connected to naphthalimide through a carbamate group for hypoxia monitor. It was also a prodrug derivative with a *p*-nitrobenzyl unit, which was activated by nitro reduction as a hypoxia-selective leaving group. In this compound, the carbamate group was

employed as the electron-withdrawing group to weaken the ICT system and result in a fluorescence wavelength blue shift. After reduction, the amino group would be released and the fluorescence recovered; it showed an obvious blue (475 nm) to green (550 nm) emission wavelength change in solution and cell lines. Cell imaging results demonstrated good capability for the probe to distinguish between aerobic and hypoxic cells.

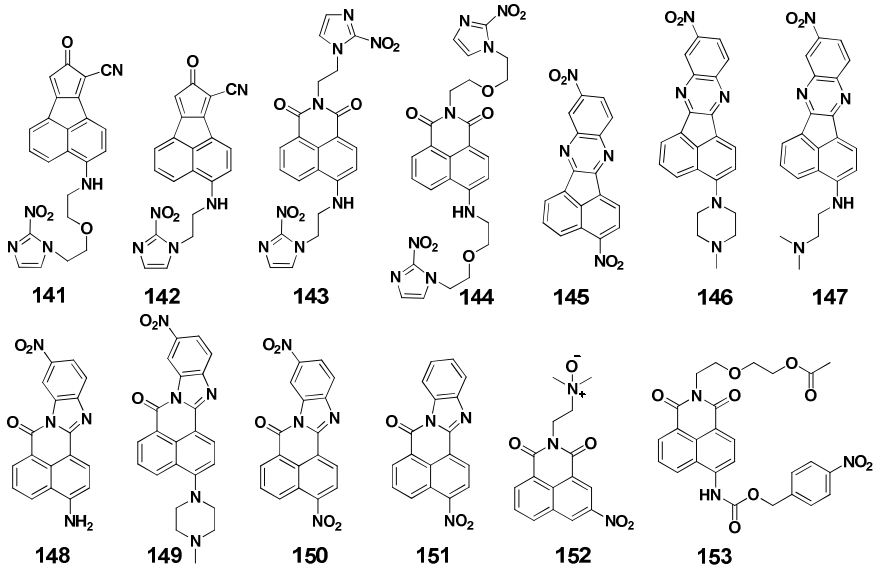

Fig. 44 structures of fluorescent hypoxia sensors (**141–153**).

A dual-response fluorescent probe **154** was designed by Hori et al.[149] It was composed of a *p*-nitro benzyl moiety directly linked to seminaphthorhodafluors (SNARF). The *p*-nitro moiety acted as a potential hypoxia-selective leaving group activated by nitro-reduction. The sensor **154** was initially colorless and nonfluorescent because of the presence of the lactone form and the nitro quencher. Nitro reduction triggered the release of SNARF, which had long wavelength absorption (544 nm) and fluorescence (583 nm) that was sensitive to pH. This probe was biologically reduced under hypoxic conditions and SNARF was produced to selectively image the tumor acidic environment with a reduced background signal. This sensor system was able to clearly reveal the differences between hypoxic and aerobic situations in liver microsomes and inside cells. (Fig. 45)

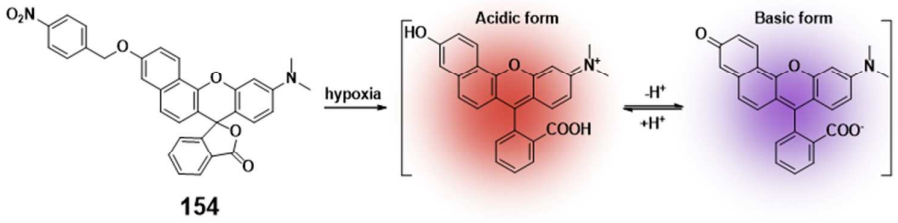

Fig. 45 the mechanism of **154** sensing hypoxia.

However, the maximum absorption/fluorescence peaks of these fluorescent probes are located in the UV/Vis region, which was inadequate for *in vivo* imaging. In 2012, Nagasawa et al.[150] developed a novel tricarbocyanine dye (Cy7)-based near-infrared (NIR) fluorescent probe **155** with longer Ex/Em wavelengths (753/778 nm), favoring *in vivo* imaging in tumor. It comprised a Cy7 dye and two 2-nitroimidazole parts as the hypoxia-targeting parts. After treatment with the probe, significantly higher fluorescence were observed in hypoxic conditions than in normoxia, because of the decrease in the nitro quenching effect. Nevertheless, the fluorescence intensity of the probe showed high background fluorescence even under normoxia due to the possible nonspecific noncovalent binding of the probe to intracellular constituents and/or persisting as a released form in cells owing to its electronic and lipophilic characters. In addition, *in vivo* fluorescence image revealed specific accumulation of **155** in tumors. *Ex vivo* analysis showed a strong correlation of fluorescence intensity with hypoxia inducible factor (HIF)-1 in active hypoxia regions. This probe is a promising fluorescence imaging sensor for tumor hypoxia *in vivo.* (Fig. 46)

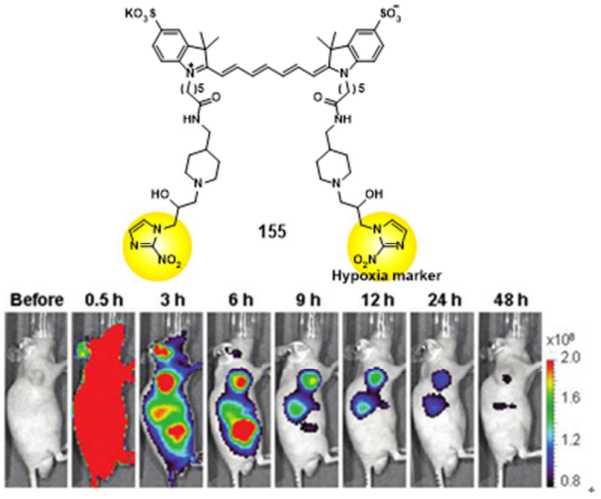

Fig. 46 Cy7-based hypoxia probe (**155**) and *in vivo* imaging. Adapted with permission

from ref. 150 ©2012 American Chemical Society.

Low sensitivity to hypoxia is a disadvantage for hypoxia sensors, as they could then be responsive only under severely hypoxic conditions. Taking this into consideration, Tang and his co-workers developed a highly selective and sensitive NIR fluorescence probe **156**, which consisted of a nitroimidazole conjugated to a Cy7 dye at the meso-position of the polymethine chain[151]. The nitroimidazole moiety worked as both a reporter for nitroreductase (NTR) and as an excellent fluorescence quencher. The probe showed a large Stokes' shift of ca. 55 nm with excitation and emission wavelengths of 695/750 nm, which probably improved detection sensitivity. After treatment with by nitroreductase, the fluorescence intensity of the sensor was gradually increased. The probe was able to monitor the degree of hypoxia in HepG2 cells via the detection of endogenous nitroreductase. Furthermore, it was successfully used in investigating the relationship between epithelial-mesenchymal transitions (EMTs) in tumor progression and intracellular hypoxic levels, which demonstrated the potential for studying hypoxia-dependent molecular events (Fig. 47).

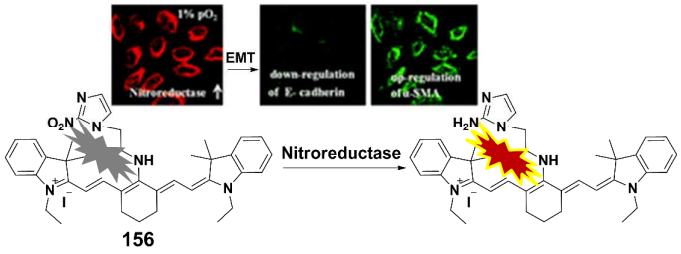

Fig. 47 Proposed mechanism of Cy7 (**156**) fluorescence switch-on in the presence of nitroreductase and their cell imaging.

Another highly selective and sensitive fluorescence probe (**157)** was reported by Ma and coworkers.[152] It was composed of 5-nitrofuran as a hypoxia-sensitive unit and resorufin as the fluorescent reporter, respectively, and showed long analytical wavelengths of excitation and emission (550/585 nm), better water solubility, and extremely low background fluorescence. Upon the treatment of **157** by nitroreductase, 5-nitrofuran was reduced to cause the 1, 6-rearrangment-elimination reaction releasing active resorufin, and obvious changes in both the color and fluorescence of resorufin were observed. The detection limit for nitroreductase was 0.27 ng/mL,

which was the lowest detection limit. It was capable of differentiating HeLa and A549 cells under hypoxic and normoxic conditions by measuring the hypoxia status through the monitor of endogenous nitroreductase (Fig. 48).

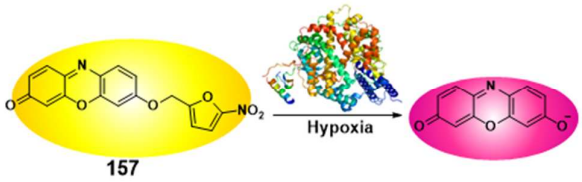

Fig. 48 Nitrofuran-based hypoxia probe (**157**). Adapted with permission from ref. 152 ©2013 American Chemical Society.

Most reported hypoxia-targeted fluorescent probes possessed a nitroaromatic or quinone moiety in structures, but they were inadequate for *in vivo* imaging because of the low sensitivity response to hypoxia and/or short absorption/emission wavelengths. As an alternative to a nitroaromatic or quinone moiety as the hypoxia-sensitive moieties, Nagano et al. developed a series of near-infrared fluorescent probes (**158–160**) (Fig. 49) possessing an azo functional group that displayed excellent response to hypoxic conditions. These probes consisted of a NIR dicarbocyanine dye and a quencher (Black Hole Quencher; BHQ) linked by an azo-functional group[153]. Under normoxic conditions, the azo group cannot be reduced and the cyanine dyes remained in the dark state owing to FRET quenching of the fluorescence. Under hypoxic conditions, the quencher dye (BHQ-3) was readily reduced and lost its absorption covering the emission band of cyanine dyes, so the FRET process between the cyanine dyes and BHQ-3 was blocked, resulting in a large enhancement of fluorescence. The probes were able to distinguish hypoxia *in vivo*, and were the first ones used for real-time fluorescence imaging of acute ischemic hypoxia in living animals with rapid response and high imaging quality.

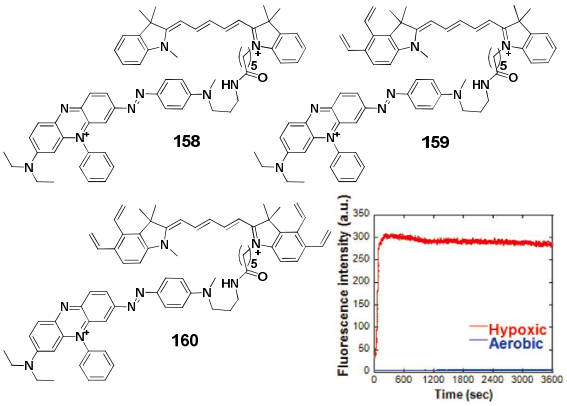

Fig. 49 Azo group-based hypoxia probe (**158–160**). Adapted with permission from ref. 153 ©2010 American Chemical Society.

Building on the sensitivity of compound **158–160** to hypoxic conditions, the same group made a further improvement to azo-based hypoxia sensors. They conjugated an azo group directly to a rhodamine fluorophore analogue to afford the probes **161–162**. These fluorophores were initially non-fluorescent because of the ultrafast conformational variation around the N=N double bond upon excitation.[154] When the azo bond was reductively cleaved, fluorescence was restored by producing the original fluorescent rhodamine derivatives. They analyzed an *in vitro* assay in rat liver microsomes; under hypoxic conditions, the fluorescence increased by 630- and 20-fold, respectively. When the probes were applied to monitor cellular hypoxic conditions in living cells, a markedly time-dependent enhance in fluorescence was detected in cells, and almost no fluorescence enhancement within cells was observed in normoxia. **161** featured even higher sensitivity and were able to detect mild hypoxia. Multicolor imaging with both probes achieved the visualization of the oxygen concentration gradient in live cells. Moreover, probe **161** was capable of checking retinal hypoxia in a rat retinal artery occlusion, indicating that it is a powerful tool for hypoxia detection *in vivo* (Fig. 50).

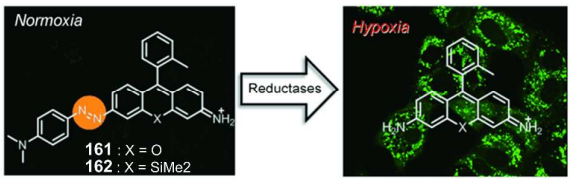

Fig. 50 Azo group-based rhodamine hypoxia fluorescent probes (**161–162**). Adapted

with permission from ref. 154 ©2013 John Wiley and Sons.

Generally, hypoxia-responsive fluorescence probes were designed based on irreversible bioreduction of the conjugating units of the probes (e.g. nitro, quinone, and azo groups) to produce fluorescence signal changes under hypoxic conditions. When the sensors were reduced in a hypoxic region to obtain a fluorescent product, they remained brightly fluorescent even after the region returned to normoxia. Therefore, Hanaoka and his co-workers designed the first reversible off-on fluorescence probe **163** for hypoxia imaging, as shown in Fig. 51.[155] The probe was designed to undergo FRET between a Cy5 dye energy donor and a rhodamine derivative (QSY-21) as the FRET acceptor. When QSY-21 experienced one-electron reduction under hypoxia to yield the corresponding radical product, the absorption at 660 nm gradually disappeared to block the FRET process, and Cy5 concomitantly became highly fluorescent. However, upon the recovery of the normoxic state, the radical was rapidly reoxidized to QSY-21 to decrease the fluorescence of Cy5 to the initial level, thereby allowing this probe to reversibly detect repeated cycles of hypoxia-normoxia in living cell imaging.

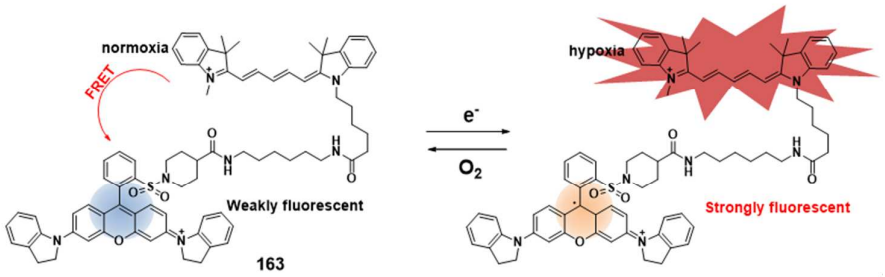

Fig. 51 Reversible changes in fluorescent probe **163** under hypoxic and normoxic conditions. Adapted with permission from ref. 155 ©2012 American Chemical Society.

Bioreductive reactions were also employed to construct "turn-on" fluorescent probes for hypoxia imaging. Indolequinone derivatives were identified as a new series of hypoxia-specific prodrugs that could be activated by radiolytic reduction or bioreduction under hypoxic conditions. Nishimoto and co-workers[156] developed a fluorescent probe **164** consisting of hypoxia-sensitive oxidizing indolequinone

skeleton, two coumarin fluorophores, and a 2, 6-bis(hydroxymethyl)-*p*-cresol linker. The indolequinone unit performed a fluorescence quenching function as well as hypoxia-sensitive reduction reactivity. The probe itself initially showed very weak fluorescence due to the fluorescence quenching of the coumarin unit by the neighboring indolequinone. Under hypoxia conditions, the indolequinone experienced a one-electron reducing process, and the coumarin fluorophores were released from the sensing package, causing fluorescence enhancement at 420 nm.

Later, this group developed another fluorescent probe **165** consisting of an indolequinone unit and a rhodol fluorophore with better aqueous solubility and longer absorption and emission wavelengths, compared with **164**, which was the first case to image hypoxic cells through the enzymatic reduction characteristics of indolequinone derivatives (Fig. 52).[157] The fluorescence (emission, 550 nm) of rhodol was quenched by the intramolecular indolequinone unit. It could be restored to its fluorescent state under hypoxic conditions through enzymatic reduction to release nonconjugated free rhodol. After incubation with A549 cells, it was preferentially activated by endogenous reductase under hypoxic conditions, and hypoxic cancer cells were visualized by robust fluorescence.

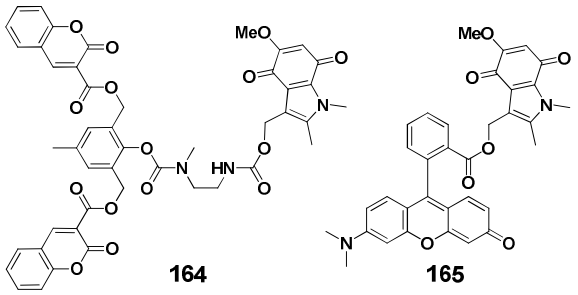

Fig. 52 Indolequinone-based fluorescent hypoxia probes (**164–165**).

Triplet oxygen is well known as a powerful quencher for oxygen-sensitive phosphorescent probes. Therefore, various phosphorescent probes have been recently developed for hypoxia imaging. Lack of oxygen in the tumor area can significantly increase the brightness of these probes, making them good candidates to target hypoxia *in vitro/in vivo*. Recently, Takeuchi et al. reported a red light-emitting phosphorescent iridium complex $Ir(btp)_2(acac)$ **(166)** for sensing hypoxia (Fig. 53).[158]

The red phosphorescence was favorable for deep tissue penetration and its long lifetime (5.8 μs) was advantageous for oxygen-induced quenching. When it was injected into mice bearing transplanted tumors, the red fluorescence was visible in 5 minutes. The sensor and its analogues were distributed through the whole body and emitted strong phosphorescence in hypoxic regions with insufficient oxygen supply. Furthermore, this compound was readily modified to emit fluorescence at a longer wavelength and exhibit appropriate water solubility; e.g. compound **167** depicted a clearly luminescent image of tumors transplanted 6~7 mm deep from the skin.

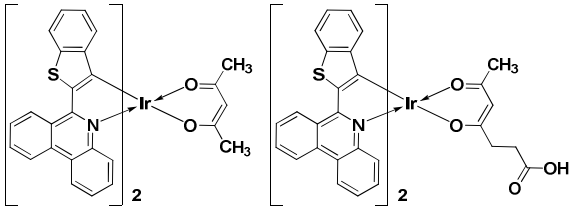

Fig. 53 Chemical structures of iridium complexes as phosphorescent hypoxia probes (**166–167**).

Tanabe et al. reported a polypyridine ruthenium complex **168** targeting ischemia-based hypoxia *in vivo*.[159] It was constructed by linking a hydrophobic pyrene unit to form an energy transfer system. The phosphorescence of the ruthenium complex was in dark state under aerobic situations by the collisional quenching function of oxygen. While under hypoxic conditions, the phosphorescence (around 600 nm) was greatly increased and accompanied by the prolonged lifetime of the triplet excited state, providing high sensitivity to hypoxia. Furthermore, the employ of hydrophobic pyrene enhanced the lipophilicity of the probe to improve cellular uptake when **168** was utilized to optical imaging in living mice (Fig. 54).

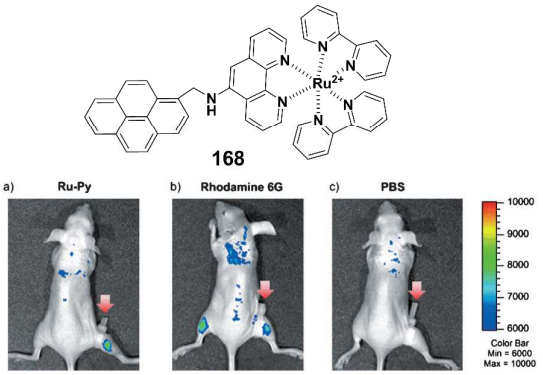

Fig. 54 Ruthenium complex-based phosphorescent hypoxia probes (**168**). Adapted with permission from ref. 159 ©2013 John Wiley and Sons.

Polystyrene nanoparticle **169** (Fig. 55) was developed with a near-infrared oxygen-sensitive emission palladium *meso*-tetraphenylporphyrin (PdTPTBP) and oxygen-insensitive inert cyanine as the reference dye.[160] The nanomaterial was prepared by coating the nanoparticle with nontoxic maleimide-modified polyethylene glycol, and the surface was functionalized with the targeting group monoclonal antibody herceptin. This nanosensor was excited at 635 nm for both components and provided NIR emissions separated by optical filters. The phosphorescence of PdTPTBP was strongly quenched in an oxygen-saturated solution; and the reference signals were not affected. In addition, the phosphorescence lifetime of PdTPTBP was strongly dependent on oxygen. Thus, the compound was employed as a ratiometric lifetime-based and dual-wavelength photoluminescent hypoxia sensor. It was efficiently taken up by incubated murine alveolar macrophages, generating a reversible and characteristic change in ratiometric response with oxygen concentration variation, which related to cellular hypoxic condition by the monitor of hypoxia inducible factor-1α accumulation. Furthermore, experiments on tumor-transplanted mice showed an obvious ratiometric response in the tumor in hypoxic conditions.

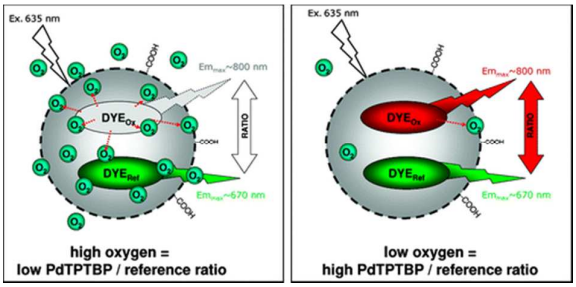

Fig. 55 Polystyrene nanoparticles as ratiometric hypoxia sensor (**169**). Adapted with permission from ref. 160 ©2011 American Chemical Society.

Another ratiometric probe **170** for hypoxia imaging *in vivo* was reported by Fraser et al.[161], which consisted of iodide-substituted difluoroboron dibenzoylmethane-poly (lactic acid). It showed weak fluorescence as an internal reference and strong phosphorescence as a "turn-on" sensor, which was switched on in anaerobic or low-oxygen content environments. The ratiometric change was calculated based on relative changes in fluorescence and phosphorescence intensity, modulated by variations in oxygen content. The signal ratio of the probe was found to be consistent with oxygen concentrations *in vitro* and *in vivo*. It was successfully used to image hypoxia in tissue (Fig. 56).

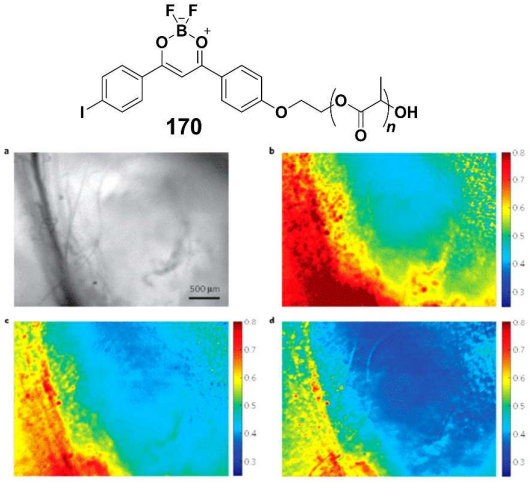

Fig. 56 Polymer as a ratiometric hypoxia sensor (**170**) and used in tissue. Adapted with permission from ref. 161 ©2009 Nature publishing group.

6. pH-targeted fluorescence sensing and imaging

Acidic-basic environment-targeted fluorescent chemosensors (pH probes) work as a predominant factor in controlling environmental conditions. The acid-base environment is responsible for determining reaction rates and mediating biological processes in living cells. A large number of pH-targeted fluorescence chemosensors have been developed in the past several years. Most of the work before 2011 has been summarized by Burgess.[162] Therefore, in the present section, we will cover research progress on pH chemosensing and cell imaging in the period spanning 2011–2013.

6.1. Single molecule used as a fluorescent pH sensor

In 2011, Nagano and co-workers reported a ratiometric, reversible, NIR fluorescent pH probe **171** based on aminocyanine (Cy7) bearing a diamine moiety.[163] Under acidic conditions, the probe showed a 61-nm red shift in its absorption maximum. Fluorescence cellular imaging results demonstrated that it could be used to monitor intracellular pH changes (Fig. 57).

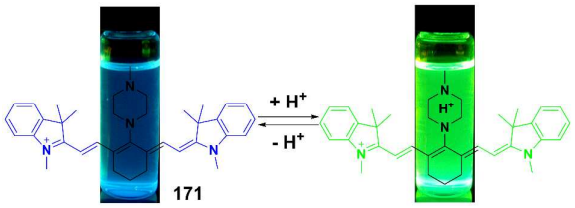

Fig. 57 Cy7-based ratiometric pH sensor (**171**). Adapted with permission from ref. 163 ©2011 American Chemical Society.

Subsequently, a tumor-selective NIR pH-activatable sensor **172** was developed by Achilefu and coworkers, which was based on a pH-sensitive cyanine dye conjugated to a cyclic arginine-glycine-aspartic acid (cRGD) peptide.[164] The probe was reversibly protonated or deprotonated at the N-position of indolenium, exhibiting high spectral sensitivity to pH variations with a pK_a of 4.7. Above pH 6.0, it displayed negligible fluorescence but became highly fluorescent below pH 5, which was ideal for imaging acidic cellular organelles, for instance tumor lysosomes or late endosomes. Moreover, it could be used as an integrin-targeted pH-sensitive sensor to monitor primary and metastatic cancer (Fig. 58).

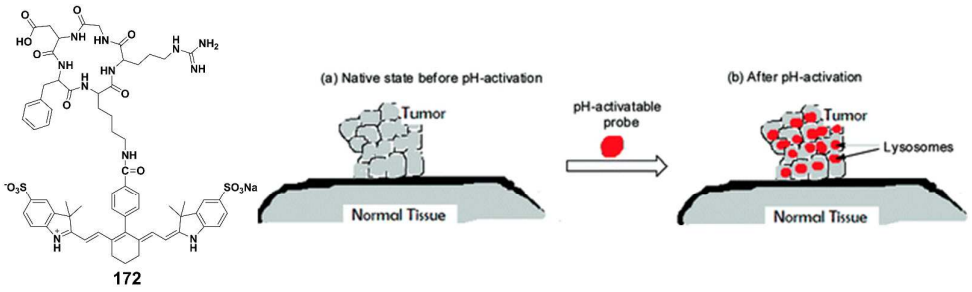

Fig. 58 Cy7-based fluorescent pH sensing (**172**). Adapted with permission from ref. 164 ©2011 American Chemical Society.

In 2010, Guo and co-workers reported a charge transfer pH fluorescent sensor **173** which was constructed through ethylene linking of benzothiazole and pyridine.[165] This sensor showed a particular fluorescent response to pH with a low pK_a of 4.22 and a large Stokes' shift. When the pH was gradually raised from 3.2 to 5.2, the fluorescence intensity was enhanced about 22-fold. Additionally, the probe was applied to image intracellular pH in macrophage cells targeting acidic microenvironments (Fig. 59).

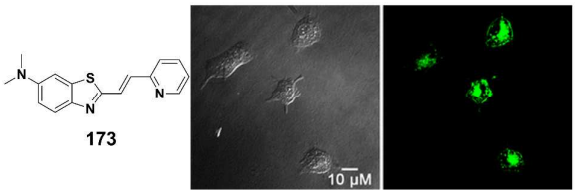

Fig. 59 Chemical structure of a turn-on pH fluorescent sensor (**173**) and fluorescent imaging in living cells.

A cell-permeable pH indicator **174** (Fig. 60) was developed by Hori et al., which was derived from a seminaphthorhodafluor (SNARF).[166] The target compound was non-fluorescent because of the formation of non-fluorescent aggregates in the aqueous matrix before acetate ester hydrolysis. The low background fluorescence was an advantage for accurate pH monitoring compared to SNARF. The probe readily penetrated the cell membrane, and then the acetate ester was hydrolyzed in the presence of certain enzymes inside cells, which released the highly fluorescent SNARF to sense local pH values.

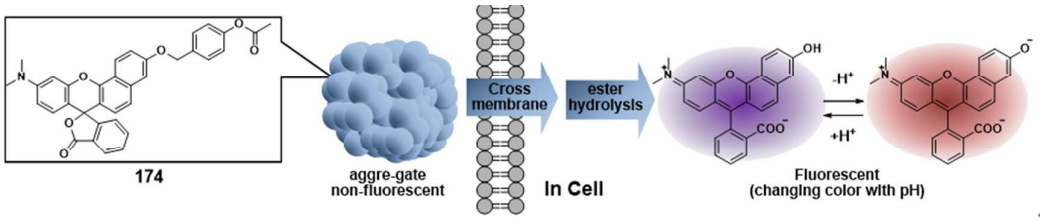

Fig. 60 Proposed mechanism of **174** passing through cell membrane and functioning as a pH fluorescent sensor inside cells.

In 2011, Chattopadhyay et al. reported a highly selective fluorescent pH probe **175** based on a half-condensed Schiff base with the maximum emission at ca. 540 nm (Fig. 61).[167] It showed a 250-fold fluorescence increase in the pH range of 4.2 and 8.3, with a pK_a of 6.63. Furthermore, it could be used as a candidate to monitor intracellular pH change under biological condition.

Two imidazo[1,5-a]pyridinium ion pH sensors **176–177** were synthesized by Aron and coworkers,[168] In structure, the only difference between the two compounds was in the positions of the diethylamino and methylxoy groups. However, it caused two distinct de-excitation pathways of the sensors. For **176**, when the solution pH was increased from 2.5 to 7.5, it evidently displayed ratiometric responses to the emission wavelength red-shifting from 400 nm to 580 nm because of the ICT process, which was an advantage for the precise determination of local pH values. While, for **177**, it exhibited a fluorescence turn-off response with fluorescence quantum yields decreasing from 0.42 to 0.0006 at 450 nm due to the PeT process, it was ideal for acidic cellular environments because of minimal interference from background fluorescence.

In 2012, Freccero et al. reported fluorescent reporters capable of sensing pH in aqueous solution based on naphthalene diimide fused to 1, 4-dihydropyrazine-2,3-dione (**178**).[169] This probe demonstrated on-off fluorescence with the pH changing from 5.0 to 8.5, which was suitable for physiological applications. The monocationic form of **178** acted as a fluorescent weak acid with a pK_a of 6.9, but its conjugate base was a non-fluorescent orange dye. The compound and its various forms tended to band with G-4 folded DNA to exhibit their fluorescent property, and were also

responsive to pH. The resulting cell images indicated that the compound mainly localized in the nucleus to exert cytotoxicity towards the colon cell line HY29, suggesting that it was also a potential drug in addition to being a fluorescent probe.

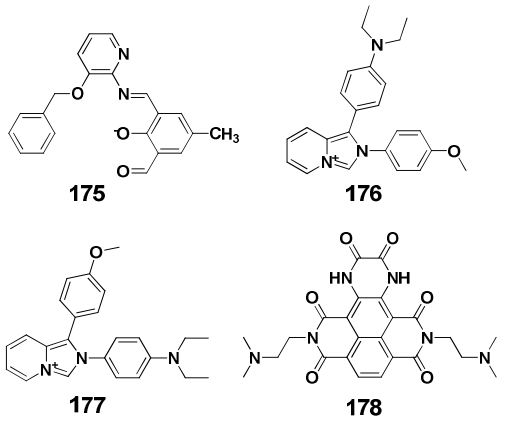

Fig. 61 Structures of pH fluorescent sensors (**175–178**).

Avarez-Pez and coworkers designed ratiometric fluorescent pH sensors consisting of a methyl ester **179** and a sodium salt **180** based on BODIPY with a pH-sensitive ligand imidazole linked *via* an ethenyl linker[170] These dual-emission pH probes emitted strong green-yellow fluorescence in lower pH and intense orange fluorescence in higher pH. They could be used as aratiometric fluorescent sensor for pH monitor in the near-neutral pH range of 5 to 7 (Fig. 62).

A 8-hydroxyquinoline-substitued at the *meso*-position of BODIPY **181** was reported by Jiang and coworkers with special off-on-off pH sensing performance[171] The fluorescence behavior of the BODIPY moiety was observed to gradually decrease with either increasing or decreasing pH values, respectively, because the PeT process occurred either from excited BODIPY part to 8-hydroxyquinoline unit (d-PeT) or through the opposite process (a-PeT), which was responsible for fluorescence quenching in either acidic or basic environments. These compounds were the first off-on-off type pH fluorescent probes.

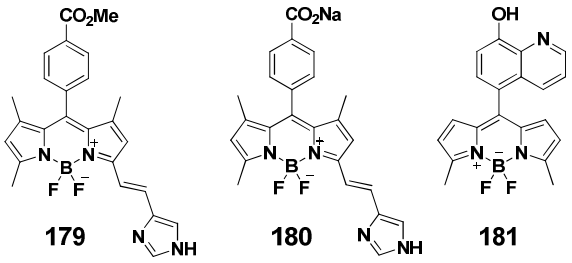

Fig. 62 Structures of BODIPY-based pH fluorescent sensors (**179–181**).

A series of FRET-based dual-excitation fluorescent ratiometric pH probes (**182–185**) (Fig. 63) was developed by Lin and coworkers, constructed with coumarin and rhodamine with piperazine as a spacer.[172] These molecular pairs were capable of independent excitation with separate excitation bands up to 172 nm apart. The excitation band difference was much larger than those in dual-excitation fluorescent sensors based on single dyes (less than 70 nm). The fluorescent ratio of **182–183** showed good linearity to the pH value in the range from 6.01 to 7.85, exhibiting their potential for the quantitative determination of pH. Furthermore, the photo-uncaged analogues (**184–185**) showed photo-controllable dual-excitation ratiometric response to pH change, making these the first ratiometric sensor utilizing the photo-cleavage mechanism for intracellular pH determination.

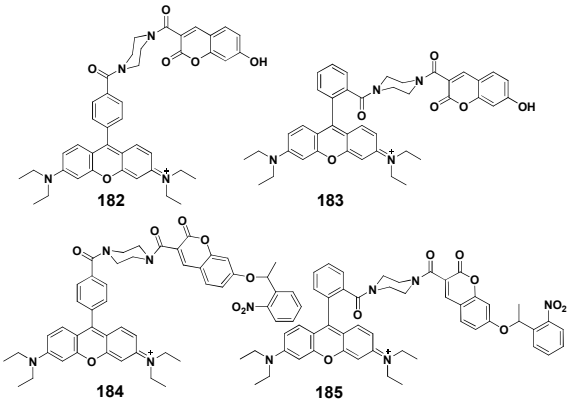

Fig. 63 Rhodamine- and coumarin-based pH ratiometric sensors (**182–185**).

Recently, Tang et al. reported a pH-sensitive ratiometric probe **186** (Fig. 64) based on a tetraphenyl-ethene-cyanine adduct for pH sensing and tracking within the total pH range.[173] It responded sensitively to intracellular pH with the emission color changing from red to blue with increasing solution pH values. This allowed the

visualization of the acidic and basic compartments with strong red and blue fluorescence, respectively. The ratiometric signal could serve as an indicator for local proton concentration, and was applied for intracellular pH imaging and monitoring by ratiometric analysis.

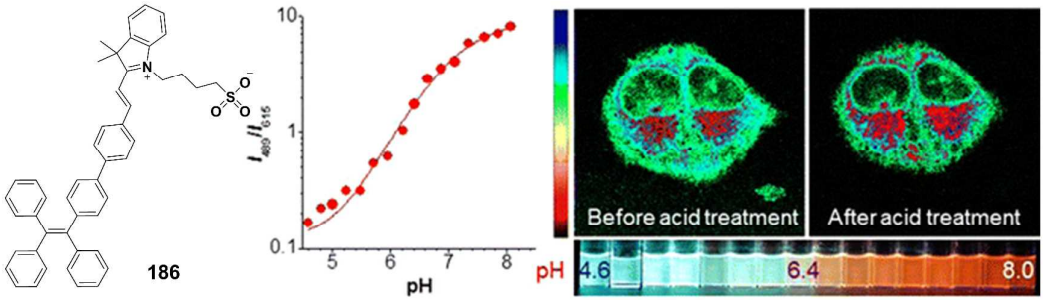

Fig. 64 An AIE-based pH ratiometric sensor (**186**) and the cell test. Adapted with permission from ref. 173 ©2013 American Chemical Society.

A pH-sensitive fluorescent probe **187** based on an acridine-containing cyanine dye was developed by Ladame and co-workers.[174] It showed a colorimetric response to pH varying between 4 and 9 because of the protonation and deprotonation of the non-alkylated acridine moiety. Under acidic conditions, it was dark blue and gradually turned orange when the pH was increased above 7.4. With an enhancement in pH from 5 to 8, the emission of **187** became even weaker, accompanied by a blue fluorescence shift. Therefore, it could serve as an indicator through colorimetric change or fluorescent variation for pH sensing.

Another ratiometric fluorescent pH sensor **188** with dual emission color alternation was reported by Kim et al.[175]; this consisted of a fluorescein and a rhodamine tethered by a diethylenetriamine spacer. The rhodamine and fluorescein moieties showed their red to green fluorescence with increasing pH from acidic to basic conditions. The ratio of the two emissions revealed good linearity in the pH range 4–8. The sharp change in the fluorescence ratio over a wide pH range was utilized to visualize the acidic environment within cellular organelles with different pH values, which could be used as a promising diagnostic method for monitoring pH fluctuations in pathogenic cells (Fig. 65).

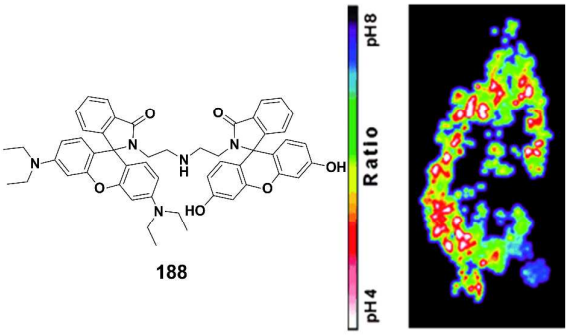

Fig. 65 Rhodamine- and fluorescein-based pH ratiometric sensor (**188**) and cell imaging. Adapted with permission from ref. 175 ©2013 John Wiley and Sons.

6.2. Nanoprobe-based pH chemosensing and cell imaging

In 2010, Mohr and co-workers designed a ratiometric pH nanosensor (**189**) (Fig. 66) based on poly(acrylamide) nanogels. This polymer was used to covalently fix a naphthalimide as a pH-sensitive reporter in the shell structure and a rhodamine as a pH-insensitive reference dye in the core layer.[176] The two kinds of fluorophores constructed a FRET system from the shell to core. When the surrounding pH was gradually increased, it exhibited two marked emission color changes, enabling the ratiometric determination of pH in living cells.

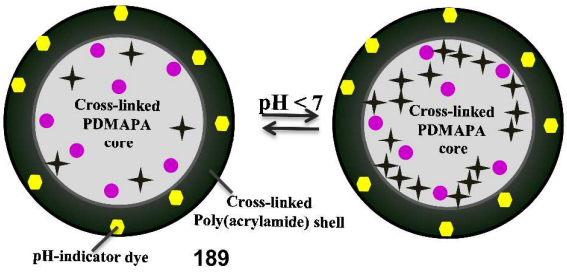

Fig. 66 Nanogels-based pH ratiometric sensor (**189**).

A dendrimer-based ratiometric fluorescent biosensor **190** was developed by Albertazzi et al.[177] It was conjugated with pH-sensitive and pH-insensitive fluorophores to control the energy transfer behavior. The dendrimer scaffold was able to target specific sub-orgnelles by tuning physicochemical properties through appropriate selection of the pH-sensitive dye, which allowed selective pH determination in various organelles in living cells.

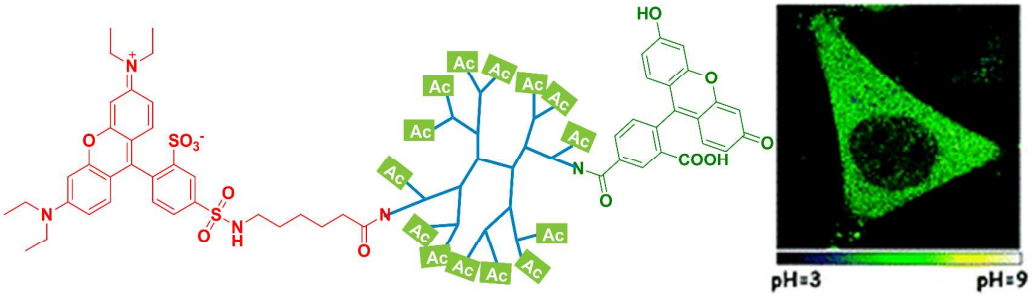

190

Fig. 67 A dendrimer-based ratiometric fluorescent pH sensor (**190**). Adapted with permission from ref. 177 ©2010 American Chemical Society.

Wolfbeis et al. reported the first ratiometric fluorescent nanogel (**191**) to sense intracellular pH in the range 6–8.[178] The nanogel was composed of polyurethane, bromothymol blue (BTB), Nile Red (NR), and coumarin 6 (C6) (Fig. 68). The polyurethane was suitable for used as a matrix material in nanogels because it has both hydrophobic and hydrophilic domains, and its volume hardly changed with pH variations. Efficient FRET occurred between C6 and NR inside the nanogel in an aqueous solution and showed a strong and inverse dual fluorescence change (increasing C6 and decreasing NR fluorescence) with pH variations.

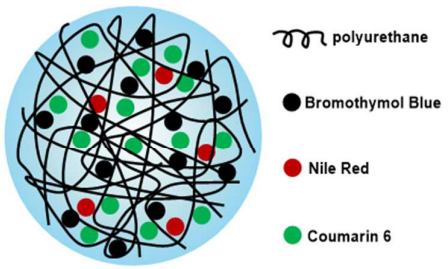

191

Fig. 68 Nanogel-based ratiometric fluorescent pH sensor (**191**). Adapted with permission from ref. 178 ©2010 John Wiley and Sons.

Sung and co-workers designed a dual-emission nanosensor **192** with a Cy3 dye as the donor and a Cy5 dye as the acceptor labeling a biocompatible polyelectrolyte (*N*-palmitoyl chitosan nanoparticle), which was able to sense environmental pH changes.[179] Environmental pH changes in the range of 4.5–7.5 induced the conformational transition of the nanosensor to change the FRET efficiency between Cy3 and Cy5. This pH-responsive ratiometric nanoprobe could be used to

discriminate and image pH changes in the biological environment at different length scales.

In 2011, Chiu reported the first ratiometric pH nanoprobe **193** (Fig. 69) based on semiconducting polymer dots, constructed by the attachment of fluorescein to a polyphenylalkyne moiety.[180] Rapid monitoring of pH was achieved based on ratiometric fluorescence changes with a single excitation wavelength and two different emission peaks. The polymer dots showed linear response to pH variations in the range 5–8, and demonstrated ultra-brightness, excellent reversibility, and stability when used to measure intracellular pH values.

Andresen and colleagues reported a ratiometric pH nanosensor **194** using a triple-labeled nanoparticle. Two pH-sensitive fluorophores, Oregon Green and fluorescein, with different pK_a values, and the reference fluorophore rhodamine B was incorporated into the nanoparticle to construct the FRET system.[181] The nanosensor demonstrated appealing time-resolved characteristics, and was capable of quantifying the physiologically relevant pH (3.2–7.0) of the endosome-lysosome system.

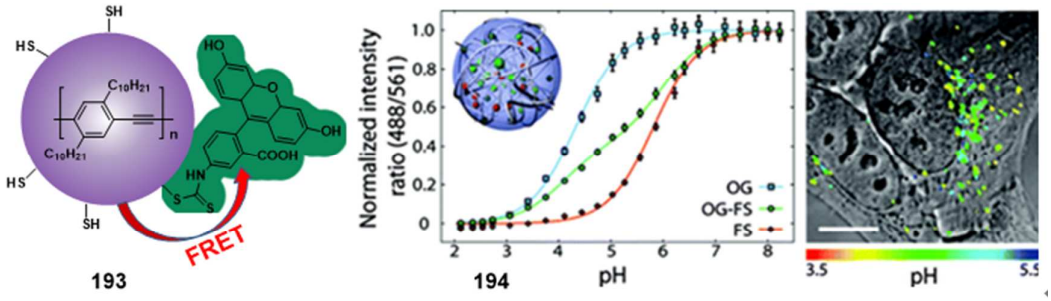

Fig. 69 Polymer dots as ratiometric fluorescent pH sensors (**193–194**). Adapted with permission from ref. 180 (**193**), ref. 181 (**194**) ©2011, 2011 American Chemical Society.

This group further developed a series of polyacrylamide-based nanoparticles containing similar components for use in pH sensing. The pH-sensitive Oregon (pK_a = 4.8) and fluorescein (pK_a = 6.4) dyes, and the pH-insensitive fluorophore rhodamine B were combined to afford nanosensor **195**,[182] which could measure the pH in the range 3.9 to 7.3. Another nanosensor (**196**) was obtained by changing the pH-sensitive component to a fluorescein derivative (pK_a = 7.0) and the pH-insensitive fluorophore

to Alexa 633. This enabled a shift in the pH response range to 3.9–7.9, demonstrating great potential for monitoring the pH in mammalian cells (Fig. 70).

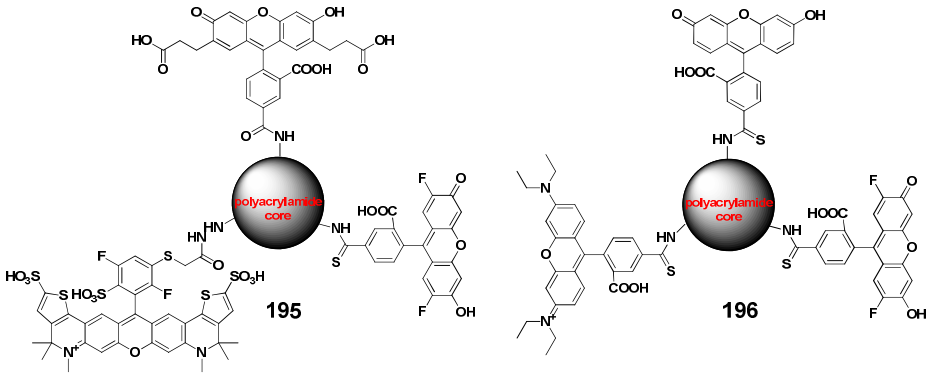

Fig. 70 Triple-labeled nanoparticles as ratiometric fluorescent pH sensors (**195–196**).

Gao et al. reported a pH-activatable micellar (pH_{AM}) material (**197)** (Fig. 71) with a tunable and highly sensitive response in specific endocytic organelles (e.g. endosome, lysosome) in live cells.[183] Different amines were used to control the water solubility of the material in different pH solutions. Under higher pH conditions, neutral tertiary amine-containing segments readily self-assembled in the hydrophobic cores, which drove the evident aggregation of the fluorophores (tetramethyl rhodamine, TMR) to quench fluorescence via homo-FRET between TMRs or PeT from amines to TMR. Under lower pH conditions, the protonated tertiary amines promoted the disassembly of the micelles to enhance the fluorescence of TMR. This self-assembly and disassembly allowed a fast temporal response (less than 5 ms) to the variable pH and controlled the fluorescence switch between the ON and OFF states with small pH changes of smaller than 0.25 pH units. Moreover, nanoprobes with alterations at pH 6.3 and 5.4 were selectively activated in different endocytic partitions, for instance lysosomes (pH 5.0–5.5) and early endosomes (pH 5.9–6.2).

To obtain new insights into complicated disease processes, in 2011, Babilas and co-workers developed an optical nanosensor **198** with 2D high resolution for pH imaging *in vivo*.[184] FITC and ruthenium(II)tris-(4,7-diphenyl-1,10-phenanthroline) were first employed to bind or incorporate into aminocellulose- and polyacrylonitrile-based microparticles. Ratiometric sensing was based on time-domain optical imaging of the two fluorophores immobilized in polyurethane hydrogel. A noninvasive method was

used for 2D and potential real-time imaging pH *in vivo*. The *in vitro* and *in vivo* experiments demonstrated that the target sensors were versatile, with high precision and validity in pH detection during chronic cutaneous wound healing in humans.

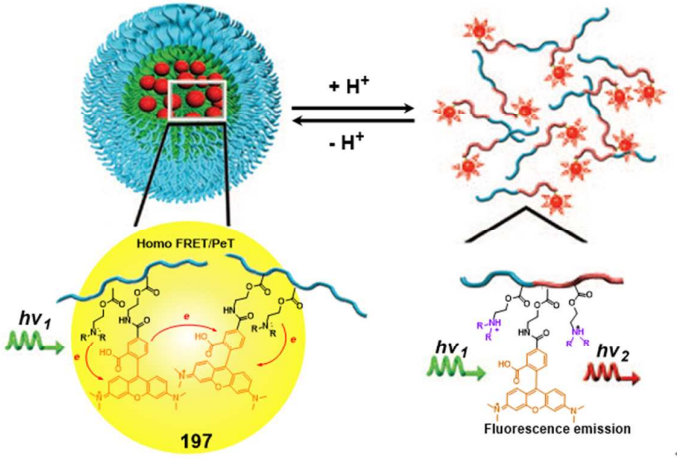

Fig. 71 Micellar material-based fluorescent pH sensor (**197**). Adapted with permission from ref. 183 ©2011 John Wiley and Sons.

Gao et al.[185] reported a general method to produce tunable, ultra-pH-responsive multicolored fluorescent nanoparticles **199** (Fig. 72). In these nanoprobes, amino groups were attached for use as the pH-sensitive units, and commonly available pH-insensitive fluorophores with emission ranging from green to the near IR region were introduced as fluorescent reporters. The pH change induced nanosensor micellization corresponding to fluorescence activation between the ON and OFF states within only 0.25 pH units.

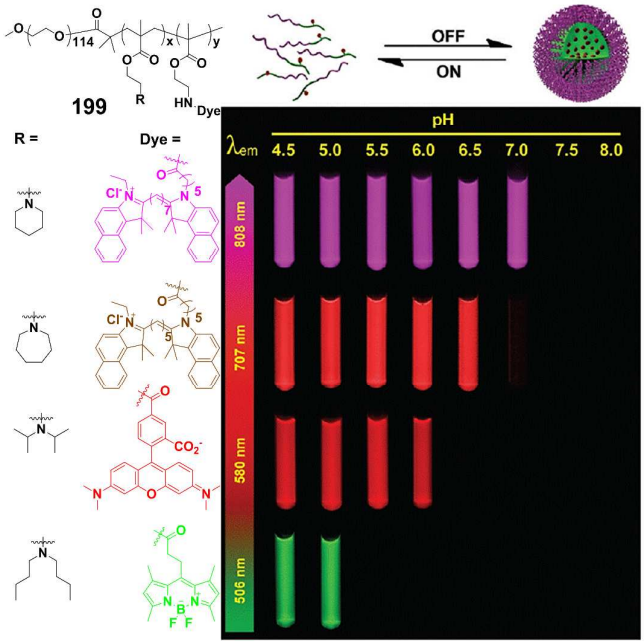

Fig. 72 Tunable and multicolored fluorescent pH nanosensors (**199**). Adapted with permission from ref. 185 ©2012 American Chemical Society.

Zhao et al.[186] designed a simple-structured copolymer as a temperature and pH fluorescent nanosensor **200** (Fig. 73). The nanoprobe showed an enhancement or decrease in absorbance with variations in pH value, while the fluorescence exhibited enhancement with rising temperature regardless of pH value in the range 4–10. Upon the addition of protons, it showed fluorescence suppression which could be applied as a convenient apparatus for the environmental detection of protons.

Ma and colleagues developed the first carbon nanodots-based tunable ratiometric fluorescent pH nanoprobe **201** decorated with a pH-sensitive fluorescein and a pH-insensitive rhodamine B to create the FRET system.[187] The obtained nanosystem was able to quantify the pH pattern in HeLa cells by fluorescent ratiometric methods. It was even available to study the intracellular pH fluctuation caused by various redox species. Cell imaging results demonstrated the biocompatibility and intracellular dispersibility of the nanosensors, which achieved quantitative measurement of intracellular pH fluctuations under different stimuli (e.g. oxidative stress).

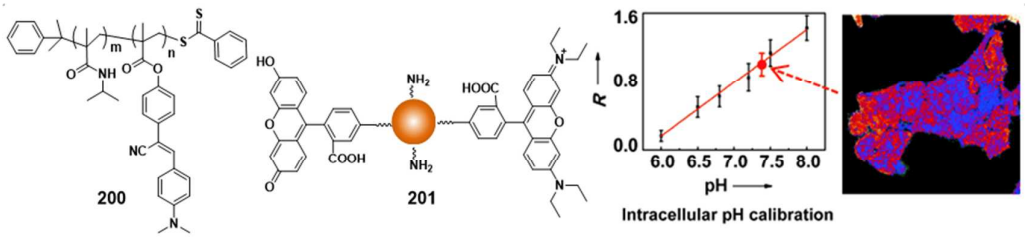

Fig. 73 Polymer- and carbon nanodots-based fluorescent pH nanosensors (**200–201**). Adapted with permission from ref. 187 (**201**) ©2012 John Wiley and Sons.

A gold nanoparticle-based ratiometric fluorescent pH sensor **202** (Fig. 74) was recently reported by Russell and co-workers. The sensor consisted of a thiolated anthracene as the fluorescent PeT-based pH compound and a rhodamine as the ratiometric pair.[188] This was the first to provide precise localized detection of pH in acidic organelles such as lysosomes by ratiometric intracellular measurements.

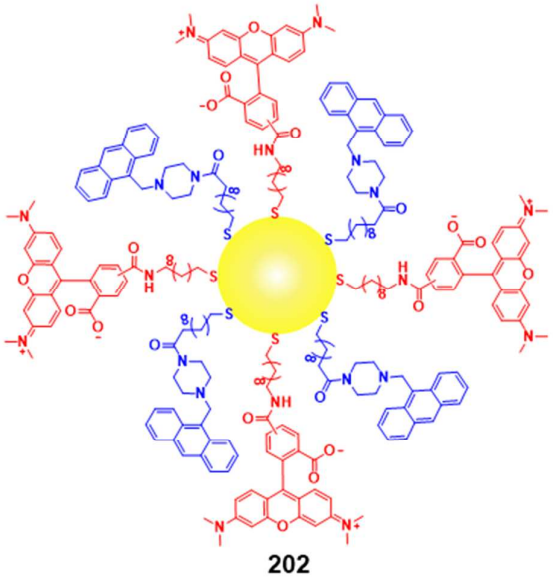

Fig. 74 Gold nanoparticle-based ratiometric pH sensors (**202**).

Zhang et al. designed a mesoporous silica nanoparticle **203** to ratiometrically sense cellular pH distribution.[189] The mesoporous silica nanoparticle was functionalized by a dual-FRET pair of fluorescein and rhodamine B. It exhibited high sensitivity and a tunable range with excellent reversibility to pH variations, which could be used for ratiometric measurement pH under a single-wavelength excitation.

In 2011, Han and co-workers reported dual-colored mesoporous silica nanoprobes **204** for the ratiometric detection of lysosomal pH in living cells (Fig. 75).[190] The

nanosensor was doped with acid-responsive rhodamine 6G lactam as the signal fluorophore and fluorescein as the reference dye, which exhibited an inverse decrease in fluorescence in acidic media. It was a good candidate for the ratiometric imaging of lysosome acidity with high sensitivity.

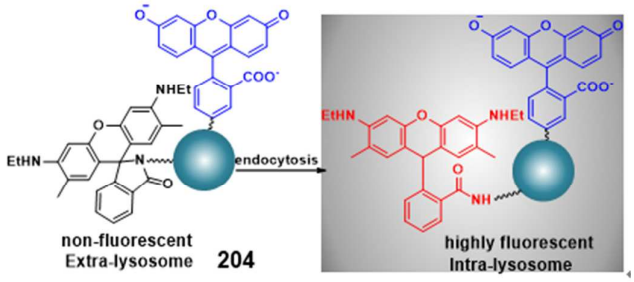

Fig. 75 Mesoporous silica nanoparticle-based ratiometric pH sensor (**204**).

Hall and coworkers developed a silica analytical nanosphere sensor **205** encapsulating quantum dots used to measure local pH in a ratiometric fashion (Fig. 76).[191] Two populations of quantum dots with different fluorescence were bound into a single sensing matrix that produced a self-calibrating sensor. The nanoprobe was photostable, robust, and capable of monitoring pH under physiological conditions.

In 2010, Medintz and co-workers[192] reported a conjugate of quantum dots decorated by dopamine peptide, used as a charge transfer-coupling pH nanosensor **206**. The dopamine functionalized two inherent redox properties: a Nernstian dependence of formal potential on pH and the oxidation of hydroquinone to quinone by oxygen at basic pH. In addition, the latter quinone could be used as an electron acceptor that quenches the photoluminescence of QDs in a directly pH-dependent manner. The probe also facilitated the measurement of pH changes in the cytoplasm of cells undergoing drug-induced alkalosis.

Jin et al. designed a quantum dot material **207** to ratiometrically sense pH in the range 6–8.[193] By tethering a pH-responsive fluorescent dye (fluorescein) to the surface of quantum dot nanocrystals, the dual emission of the pH nanosensor was used as a ratiometric pH monitor.

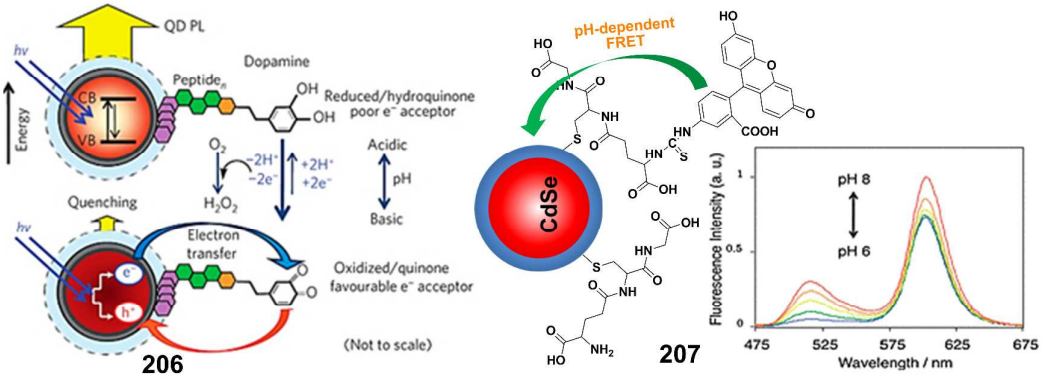

Fig. 76 quantum dots-based fluorescent pH nanosensors (**206–207**). Adapted with permission from ref. 192 (**206**) ©2010 Nature publishing group.

A color-distinctive and ratiometric pH nanosensor **208** was developed by Kim et al. It was mainly built by the organic modification of pyrene onto the surface of fluorescent quantum dots.[194] Red and blue fluorescence colors were observed from the quantum dot cores and pyrene shells, respectively. The FRET efficiency between these two chromophores was further controlled by the conformational changes in the polymer, which were responsive to the pH transition. The color of this nanoprobe in solution underwent a distinct change from blue to red corresponding to the pH change.

In 2012, Bao and co-workers reported a novel ratiometric nanosensor **209**, which was constructed through the fabrication of pH-sensitive proteins with brightly fluorescent quantum dots.[195] The FRET between the quantum dots and the fluorescent proteins modulated the emission ratio, resulting in a more than 12-fold variation between pH 6 and 8. This was well suited for a broad range of intracellular pH-dependent image applications that were not feasible with organic molecules or fluorescent proteins. **209** could be utilized for sensitive and multiplexed determination of intracellular pH.

In 2011, Yellen and colleagues reported the first ratiometric, single-protein **210** with red fluorescence that was responsible for cellular pH measurement.[196] It showed emission at 610 nm and dual excitation peaks at 440/585 nm that could be utilized for ratiometric image, and the ratio values responded to a pK_a of 6.6 and more than 10-fold dynamic range. Additionally, it had a pH-responsive fluorescence lifetime that changed by ~0.4 ns. It was used to analyze intracellular pH by imaging energy-

dependent transitions in mitochondrial and cytosolic pH.

Aylott et al. designed a ratiometric nanosensor **211,** which was constructed by combining the pH-sensitive fluorophore fluorescein dextran, Oregon Green dextran, and a reference dye (rhodamine dextran) together in a biocompatible polymer[197] This dual fluorophore with an extended dynamic range endowed the nanoprobe with the ability to simultaneously measure both cytoplasmic and endosomal pH in the range 4.0–7.5.

7. Concluding Remarks

Remarkable progress has been made in the design and synthesis of various environment-sensitive fluorescent chemosensors and their biological applications over the past several years. In the present review, we have covered recent exciting research developments of fluorescent chemosensor targeting for different biological environmental factors, e.g. viscosity, polarity, temperature, hypoxia, and pH, which play key roles in biological processes. Viscosity significantly controls diffusion-related events, such as transportation of nutrient and metabolic wastes, signal transduction, and interactions between macromolecules. Variations in local polarity reflect alterations in protein configuration at their active sites or the transfer of cell membranes. Temperature is a key factor influencing cellular metabolites or a hallmark that reflects cellular metabolic rates. Hypoxia represents the ischemic situation of local tissues, which creates a reducing milieu with the help of certain enzymes, such as nitroreductase and NADPH. The pH value as an acidic-basic indicator is considered an important factor that favors proteins or enzymes to exert biological functions in specific organelles. All of these factors independently or collectively determine the physical, chemical, or biological behaviors of the surrounding molecules; therefore, investigation of these factors would provide insight into biological processes that occur during cell proliferation, embryonic development, and occurrence of diseases.

Various fluorescent chemosensors have recently been developed to independently

detect or image the environment-related factors mentioned above. A viscosity-targeted molecular rotor based on fluorescence lifetime imaging and fluorescence ratiometric imaging was designed to measure microviscosity, and to map the viscosity distribution inside living cells and viscosity changes during cell dying. Various polarity-sensitive fluorophores were also developed to image the polarity in the membranes and to detect configuration changes in proteins at their active sites. A series of smart temperature-responsive materials fabricated with different fluorophores were synthesized to sense intracellular temperature. For example, polymethylacrylate amide and its derivatives are known to be thermo-sensitive materials, which will swell or shrink with variations in environmental temperature. After various environment-sensitive fluorophores are covalently doped into the polymers, they will respond to thermo-swelling or shrinking of the polymer. Additionally, various inorganic thermo-sensitive nanomaterials have also been developed to map the temperature distribution in living cells, e.g. fluorescence quantum dots, gold nanoparticles, and rare earth-doped nanomaterials. Hypoxia status has already been considered a typical indicator of the solid tumor environment. Many oxygen-sensitive chemosensors have been synthesized to facilitate the detection of hypoxia; for example, nitro-containing compounds are ideal hypoxia-targeting agents due to the triggering of the fluorescence by two-electron reduction under conditions in which oxygen is lacking. Some other compounds, such as transition metal complexes, which exhibit both fluorescence and phosphorescence emission switching with variations in hypoxia status, are utilized to visualize oxygen content *in vivo*. Intracellular pH plays a pivotal role in the modulation of cellular proliferation and apoptosis. Many fluorescence probes have been reported to target the pH distributions and fluctuations in living cells to facilitate the understanding of the complicated functions inside cells.

Much effort has been made to study the intracellular microenvironment by means of fluorescent sensing. Several chemosensors have been devised to target each environmental parameter *in vitro/in vivo*. However, the intracellular

microenvironment is always different in spatial and temporal distribution from locations with complexity. Furthermore, the physical and chemical behavior of the local target is not usually determined by only one environmental factor, but by the mutual influence of two or multiple factors together. Therefore, in order to better study the micro-environment within living cells, it should be necessary to develop multi-functional fluorescent sensors capable of simultaneously detecting more than one environmental parameter, and are able to respond to the local environment with multiple modalities, such as fluorescence intensity, fluorescence ratiometry, and fluorescence lifetime.

On the other hand, the microenvironment in the cellular organelles may play an even greater role in maintaining normal cellular functions. Sharp changes of such factors in sub-organelles would result in or from severe cell malfunction. Therefore, it would be more meaningful to develop various chemosensors that specifically measure or image the microenvironmental status in sub-organelles, although some fluorescence probes have already been reported to target specific sub-organelles, such as pH indicators for lysosomes, viscosity probes for mitochondria and so on. In this context, a number of researchers are still actively involved in this promising project; hence, more advanced molecular chemosensors with higher tempo-spatial resolution could be discovered in the near future. Therefore, we believe that the present review of macro-/micro-environment-sensitive chemosensing and biological imaging of parameters such as viscosity, polarity, temperature, hypoxia, and pH will have a great impact on the scientific community involved in multiple research fields such as analytical, organic, and biological chemistry.

8. Acknowledgement

This work was supported by the Creative Research Initiative program (No. 2009-0081566) of the National Research Foundation of Korea.

9. References

1. K. Luby-Phelps, *Int. Rev. Cytol.*, 2000, **192**, 189–221.
2. S. T. Ohnishi and T. Ohnishi, *Membrane Abnormalities in Sickle Cell Disease and in Other Red Blood Cell Disorders*, Eds., CRC Press, Boca Raton, Florida, 1994.
3. G. Deliconstantinos, V. Villiotou and J. C. Staverides, *Biochem. Pharmacol.*, 1995, **49**, 1589–1600.
4. M. Shinitzky, *Physiology of membrane fluidity*, Ed., CRC Press, Boca Raton, Florida, 1984, pp. 1–51.
5. S. J. Singer and G. L. Nicolson, *Science*, 1972, **175**, 720–731.
6. P. M. Moriarty and C. A. Gibson, *Cardiovasc. Rev. Rep.*, 2003, **24**, 321–325.
7. I. Uchimura and F. Numano, *Diabetes Frontier*, 1997, **8**, 33–37.
8. S. Alain, G. Jérôme, C. Gilles, M. Jean-Louis and L. Jaime, *J. Hypertens.*, 2002, **20**, 159–169.
9. M. J. Stutts, C. M. Canessa, J. C. Olsen, M. Hamrick, J. A. Cohn, B. C. Rossier and R. C. Boucher, *Science*, 1995, **269**, 847–850.
10. J. Harkness, *Biorheology*, 1971, **8**, 171–193.
11. H. R. Petty, *Microsc. Res. Tech.*, 2007, **70**, 687–709.
12. K. Simons and D. Toomre, *Nat. Rev. Mol. Cell Biol.*, 2000, **1**, 31–39.
13. S. Munro, *Cell*, 2003, **115**, 377–388.
14. R. G. W. Anderson and K. Jacobson, *Science*, 2002, **296**, 1821–1825.
15. S. Mukherjee and F. R. Maxfield, *Annu. Rev. Cell Dev. Biol.,* 2004, **20**, 839–866.
16. B. B. Lowell and B. M. Spiegelman, *Nature*, 2000, **404**, 652–660.
17. S. Prusiner and M. Poe, *Nature*, 1968, **220**, 235–237.
18. J. Himms-Hagen, *Annu. Rev. Physiol.*, 1976, **38**, 315–351.
19. W. Dröge, *Physiol. Rev.*, 2002, **82**, 47–95.
20. G. Kroemer, L. Galluzzi and C. Brenner, *Physiol. Rev.*, 2007, **87**, 99–163.
21. R. J. DeBerardinis, J. J. Lum, G. Hatzivassiliou and C. B. Thompson, *Cell Metab.*, 2008, **7**, 11–20.
22. M. Monti, L. Brandt, J. Ikomi-Kumm and H. Olsson, *Scand. J. Haematol.*, 1986, **36**, 353–357.
23. J. M. Brown and W. R. Wilson, *Nat. Rev. Cancer*, 2004, **4**, 437–447.
24. J. F. Garvey, C. T. Taylor and W. T. McNicholas, *Eur. Respir. J.*, 2009, **33**, 1195–1205.
25. Y. Tang, A. Lu, B. J. Aronow, K. R. Wagner and F. R. Sharp, *Eur. J. Neurosci.*, 2002, **15**, 1937–1952.
26. Wilson, W. R., and Hay, M. P., *Nat. Rev. Cancer*, 2011, **11**, 393–410.
27. A. Ishaque and M. Al-Rubeai, *J. Immunol. Methods*, 1998, **221**, 43–57.
28. R. A. Gottlieb, J. Nordberg, E. Skowronski and B. M. Babior, Proc. Natl. Acad. Sci. U. S. A., 1996, **93**, 654–658.
29. R. Martínez-Zaguilán, B. F. Chinnock, S. Wald-Hopkins, M. Bernas, D. Way, M. Weinand, M. H. Witte and R. J. Gillies, *Cell. Physiol. Biochem.*, 1996, **6**, 169–184.
30. R. A. Gottlieb and A. Dosanjh, Proc. Natl. Acad. Sci. U. S. A., 1996, **93**,

3587–3591.
31. S. Simon, D. Roy and M. Schindler, Proc. Natl. Acad. Sci. U. S. A., 1994, **91**, 1128–1132.
32. A. Varadi and G. A. Rutter, *Endocrinology*, 2004, **145**, 4540–4549.
33. M. Schindler, S. Grabski, E. Hoff and S. M. Simon, *Biochemistry*, 1996, **35**, 2811–2817.
34. S. Ohkuma and B. Poole, Proc. Natl. Acad. Sci. U. S. A., 1978, **75**, 3327–3331.
35. R. O. Loutfy and B. A. Arnold, *J. Phys. Chem.*, 1982, **86**, 4205–4211.
36. R. O. Loutfy, *Pure Appl. Chem.*, 1986, **58**, 1239–1248.
37. C. E. Kung and J. K. Reed, *Biochemistry*, 1986, **25**, 6114–6121.
38. B. D. Allen, A. C. Benniston, A. Harriman, S. A. Rostron and C. Yu, *Phys. Chem. Chem. Phys.*, 2005, **7**, 3035–3040.
39. M. A. Haidekker, T. Ling, M. Anglo, H. Y. Stevens, J. A. Frangos and E. A. Theodorakis, *Chem. Biol.*, 2001, **8**, 123–131.
40. M. A. Haidekker, T. Brady, K. Wen, C. Okada, H. Y. Stevens, J. M. Snell, J. A. Frangos and E. A. Theodorakis, *Bioorg. Med. Chem.*, 2002, **10**, 3627–3636.
41. J. Sutharsan, D. Lichlyter, N. E. Wright, M. Dakanali, M. A. Haidekker and E. A. Theodorakis, *Tetrahedron*, 2010, **66**, 2582–2588.
42. F. Zhou, J. Shao, Y. Yang, J. Zhao, H. Guo, X. Li, S. Ji and Z. Zhang, *Eur. J. Org. Chem.*, 2011, 4773–4787.
43. M. A. H. Alamiry, A. C. Benniston, G. Copley, K. J. Elliott, A. Harriman, B. Stewart and Y.-G. Zhi, *Chem. Mater.*, 2008, **20**, 4024–4032.
44. A. C. Benniston, A. Harriman, V. L. Whittle and M. Zelzer, *Eur. J. Org. Chem.*, 2010, 523–530.
45. X. Yin, Y. Li, Y. Zhu, X. Jing, Y. Li and D. Zhu, *Dalton Trans.*, 2010, **39**, 9929–9935.
46. K. Luby-Phelps, S. Mujumdar, R. B. Mujumdar, L. A. Ernst, W. Galbraith and A. S. Waggoner, *Biophys. J.*, 1993, **65**, 236–242.
47. B. Wandelt, P. Cywinski, G. D. Darling and B. R. Stranix, *Biosens. Bioelectron.*, 2005, **20**, 1728–1736.
48. M. A. Haidekker, T. P. Brady, D. Lichlyter and E. A. Theodorakis, *J. Am. Chem. Soc.*, 2006, **128**, 398–399.
49. D. Fischer, E. A. Theodorakis and M. A. Haidekker, *Nat. Protoc.*, 2007, **2**, 227–236.
50. M. E. Nipper, M. Dakanali, E. Theodorakis and M. A. Haidekker, *Biochimie*, 2011, **93**, 988–994.
51. M. K. Kuimova, S. W. Botchway, A. W. Parker, M. Balaz, H. A. Collins, H. L. Anderson, K. Suhling and P. R. Ogilby, *Nat. Chem.*, 2009, **1**, 69–73.
52. M. K. Kuimova, G. Yahioglu, J. A. Levitt and K. Suhling, *J. Am. Chem. Soc.*, 2008, **130**, 6672–6673.
53. J. A. Levitt, M. K. Kuimova, G. Yahioglu, P.-H. Chung, K. Suhling and D. Phillips, *J. Phys. Chem. C*, 2009, **113**, 11634–11642.
54. N. A. Hosny, G. Mohamedi, P. Rademeyer, J. Owen, Y. Wu, M.-X. Tang, R. J. Eckersley, E. Stride and M. K. Kuimova, Proc. Natl. Acad. Sci. U. S. A., 2013,

110, 9225–9230.
55. X. Peng, Z. Yang, J. Wang, J. Fan, Y. He, F. Song, B. Wang, S. Sun, J. Qu, J. Qi and M. Yan, *J. Am. Chem. Soc*., 2011, **133**, 6626–6635.
56. F. Liu, T. Wu, J. Cao, S. Cui, Z. Yang, X. Qiang, S. Sun, F. Song, J. Fan, J. Wang and X. Peng, *Chem. Eur. J*., 2013, **19**, 1548–1553.
57. E. Gatzogiannis, Z. Chen, L. Wei, R. Wombacher, Y.-T. Kao, G. Yefremov, V. W. Cornish and W. Min, *Chem. Commun*., 2012, **48**, 8694–8696.
58. L. Wang, Y. Xiao, W. Tian and L. Deng, *J. Am. Chem. Soc*., 2013, **135**, 2903–2906.
59. Z. Yang, Y. He, J.-H. Lee, N. Park, M. Suh, W.-S. Chae, J. Cao, X. Peng, H. Jung, C. Kang and J. S. Kim, *J. Am. Chem. Soc*., 2013, **135**, 9181–9185.
60. J. Slavík, *Biochim. Biophys. Acta*., 1982, **694**, 1–25.
61. D. Summerer, S. Chen, N. Wu, A. Deiters, J. W. Chin and P. G. Schultz, Proc. Natl. Acad. Sci. U. S. A., 2006, **103**, 9785–9789.
62. G. Weber and F. J. Farris, *Biochemistry*, 1979, **18**, 3075–3078.
63. F. G. Prendergast, M. Meyer, G. L. Carlson, S. Iida and J. D. Potter, *J. Biol. Chem*., 1983, **258**, 7541–7544.
64. A. Jacobson, A. Petric, D. Hogenkamp, A. Sinur and J. R. Barrio, *J. Am. Chem. Soc*., 1996, **118**, 5572–5579.
65. T. Hiratsuka, *J. Biol. Chem*., 1999, **274**, 29156–29163.
66. T. Parasassi, E. K. Krasnowska, L. Bagatolli and E. Gratton, *J. Fluoresc*., 1998, **8**, 365–373.
67. B. E. Cohen, T. B. McAnaney, E. S. Park, Y. N. Jan, S. G. Boxer and L. Y. Jan, *Science*, 2002, **296**, 170–1703.
68. A. Okamoto, K. Tainaka, T. Unzai and Isao Saito, *Tetrahedron*, 2007, **63**, 3465–3470.
69. H. M. Kim, B. H. Jeong, J.-Y. Hyon, M. J. An, M. S. Seo, J. H. Hong, K. J. Lee, C. H. Kim, T. Joo, S.-C. Hong and B. R. Cho, *J. Am. Chem. Soc*., 2008, **130**, 4246–4247.
70. Z. Lu, S. J. Lord, H. Wang, W. E. Moerner and R. J. Twieg, *J. Org. Chem*., 2006, **71**, 9651–9657.
71. Y. Niko, S. Kawauchi and G.-i. Konishi, *Chem. Eur. J*., 2013, **19**, 9760–9765.
72. G. Saroja, T. Soujanya, B. Ramachandram and A. Samanta, *J. Fluoresc*., 1998, **8**, 405–410.
73. M. E. Vázquez, D. M. Rothman and B. Imperiali, *Org. Biomol. Chem*., 2004, **2**, 1965–1966.
74. M. E. Vázquez, J. B. Blanco and B. Imperiali, *J. Am. Chem. Soc*., 2005, **127**, 1300–1306.
75. P. Venkatraman, T. T. Nguyen, M. Sainlos, O. Bilsel, S. Chitta, B. Imperiali and L. J. Stern, *Nat. Chem. Biol*., 2007, **3**, 222–228.
76. G. Loving and B. Imperiali, *J. Am. Chem. Soc*., 2008, **130**, 13630–13638.
77. C. Huang, Q. Yin, W. Zhu, Y. Yang, X. Wang, X. Qian and Y. Xu, *Angew. Chem. Int. Ed*., 2011, **50**, 7551–7556.
78. P. Greenspan, E. P. Mayer and S. D. Fowler, *J. Cell. Biol*., 1985, **100**, 965–

973.
79. D. L. Sackett and J. Wolff, *Anal. Biochem*., 1987, **167**, 228–234.
80. J. Nakanishi, T. Nakajima, M. Sato, T. Ozawa, K. Tohda and Y. Umezawa, *Anal. Chem*., 2001, **73**, 2920–2928.
81. K. Nagy, S. Göktürk and L. Biczók, *J. Phys. Chem. A*, 2003, **107**, 8784–8790.
82. A. Tainaka, Y. Fujiwara and A. Okamoto, *Nucleic Acids Symp. Ser*., 2005, **49**, 155–156.
83. A. Okamoto, K. Tainaka and Y. Fujiwara, *J. Org. Chem*., 2006, **71**, 3592–3598.
84. K. J. Thomas, D. B. Sherman, T. J. Amiss, S. A. Andaluz and J. B. Pitner, *Diabetes Technol. Ther*., 2006, **8**, 261–268.
85. D. B. Sherman, J. B. Pitner, A. Ambroise and K. J. Thomas, *Bioconj. Chem*., 2006, **17**, 387–392.
86. S. Y. Kim, A. N. Semyonov, R. J. Twieg, A. L. Horwich, J. Frydman and W. E. Moerner, *J. Phys. Chem. B*, 2005, **109**, 24517–24525.
87. M. K. Singh, H. Pal, A. C. Bhasikuttan and A. V. Sapre, *Photochem. Photobiol*., 1998, **68**, 32–38.
88. S.-Y. Dong, H.-M. Ma, X.-J. Duan, X.-Q. Chen and J. Li, *J. Proteome Res*., 2005, **4**, 161–166.
89. X. Wang, S. Wang and H. Ma, *Analyst*, 2008, **133**, 478–484.
90. S. Chen, X. Li and H. Ma, *Chem. Bio. Chem*., 2009, **10**, 1200–1207.
91. B. E. Cohen, A. Pralle, X. Yao, G. Swaminath, C. S. Gandhi, Y. N. Jan, B. K. Kobilka, E. Y. Isacoff and L. Y. Jan, *Proc. Natl. Acad. Sci. U. S. A*., 2005, **102**, 965–970.
92. O. A. Kucherak, S. Oncul, Z. Darwich, D. A. Yushchenko, Y. Arntz, P. Didier, Y. Mély and A. S. Klymchenko, *J. Am. Chem. Soc*., 2010, **132**, 4907–4916.
93. A. Toutchkine, V. Kraynov and K. Hahn, *J. Am. Chem. Soc*., 2003, **125**, 4132–4145.
94. Y.-H. Kim, J.-S. Youk, S. H. Kim and S.-K. Chang, *Bull. Kor. Chem. Soc*., 2005, **26**, 47–50.
95. S. Uchiyama, K. Takehira, T. Yoshihara, S. Tobita and T. Ohwada, *Org. Lett*., 2006, **8**, 5869–5872.
96. H. Sunahara, Y. Urano, H. Kojima and T. Nagano, *J. Am. Chem. Soc*., 2007, **129**, 5597–5604.
97. F. Han, L. Chi, W. Wu, X. Liang, M. Fu and J. Zhao, *J. Photochem. Photobiol., A*, 2008, **196**, 10–23.
98. G. Signore, R. Nifosì, L. Albertazzi and R. Bizzarri, *J. Biomed. Nanotechnol*., 2009, **5**, 722–729.
99. G. Signore, R. Nifosì, L. Albertazzi, B. Storti and R. Bizzarri, *J. Am. Chem. Soc*., 2010, **132**, 1276–1288.
100. K. Kudo, A. Momotake, Y. Kanna, Y. Nishimura and T. Arai, *Chem. Commun*., 2011, **47**, 3867–3869.
101. K. Kudo, A. Momotake, J. K. Tanaka, Y. Miwa and T. Arai, *Photochem. Photobiol. Sci*., 2012, **11**, 674–678.

102. S. Uchiyama, K. Kimura, C. Gota, K. Okabe, K. Kawamoto, N. Inada, T. Yoshihara and S. Tobita, *Chem. Eur. J*., 2012, **18**, 9552–9563.
103. S. Hachiya, K. Asai and G. Konishi, *Tetrahedron Lett*., 2013, **54**, 3317–3320.
104. C. Huang, X. Peng, D. Yi, J. Qu and H. Niu, *Sens. Actuators B*, 2013, **182**, 521–529.
105. Y. Yang, B. Li and L. Zhang, *Sens. Actuators B*, 2013, **183**, 46–51.
106. S. Uchiyama, N. Kawai, A. P. de Silva and K. Iwai, *J. Am. Chem. Soc*., 2004, **126**, 3032–3033.
107. K. Iwai, Y. Matsumura, S. Uchiyama and A. P. de Silva, *J. Mater. Chem*., 2005, **15**, 2796–2800.
108. Y. Matsumura and K. Iwai, *Polymer*, 2005, **46**, 10027–10034.
109. C. Gota, S. Uchiyama and T. Ohwada, *Analyst*, 2007, **132**, 121–126.
110. C. Gota, S. Uchiyama, T. Yoshihara, S. Tobita and T. Ohwada, *J. Phys. Chem. B*, 2008, **112**, 2829–2836.
111. C. Gota, K. Okabe, T. Funatsu, Y. Harada and S. Uchiyama, *J. Am. Chem. Soc*., 2009, **131**, 2766–2767.
112. C. Koopmans and H. Ritter, *J. Am. Chem. Soc*., 2007, **129**, 3502–3503.
113. Y. Shiraishi, R. Miyamoto, X. Zhang and T. Hirai, *Org. Lett*., 2007, **9**, 3921–3924.
114. Y. Shiraishi, R. Miyamoto and T. Hirai, *Langmuir*, 2008, **24**, 4273–4279.
115. L. Tang, J. K. Jin, A. Qin, W. Z. Yuan, Y. Mao, J. Mei, J. Z. Sun and B. Z. Tang, *Chem. Commun*., 2009, **33**, 4974–4976.
116. C. Pietsch, R. Hoogenboom and U. S. Schubert, *Angew. Chem. Int. Ed*., 2009, **48**, 5653–5656.
117. C. Pietsch, R. Hoogenboom and U. S. Schubert, *Polym. Chem*., 2010, **1**, 1005–1008.
118. C. Pietsch, A. Vollrath, R. Hoogenboom and U. S. Schubert, *Sensors*, 2010, **10**, 7979–7990.
119. R. París, I. Quijada-Garrido, O. García and M. Liras, *Macromolecules*, 2010, **44**, 80–86.
120. A. Nagai, R. Yoshii, T. Otsuka, K. Kokado and Y. Chujo, *Langmuir*, 2010, **26**, 15644–15649.
121. C.-Y. Chen and C.-T. Chen, *Chem. Commun*., 2011, **47**, 994–996.
122. F. Ye, C. Wu, Y. Jin, Y.-H. Chan, X. Zhang and D. T. Chiu, *J. Am. Chem. Soc*., 2011, **133**, 8146–8149.
123. K. Okabe, N. Inada, C. Gota, Y. Harada, T. Funatsu and S. Uchiyama, *Nat. Commun*., 2012, **3**, 705–713.
124. G. Ke, C. Wang, Y. Ge, N. Zheng, Z. Zhu and C. J. Yang, *J. Am. Chem. Soc*., 2012, **134**, 18908–18911.
125. S. Wang, S. Westcott and W. Chen, *J. Phys. Chem. B*, 2002, **106**, 11203–11209.
126. S. Li, K. Zhang, J.-M. Yang, L. Lin and H. Yang, *Nano Lett*., 2007, **7**, 3102–3105.
127. J.-M. Yang, H. Yang and L. Lin, *ACS Nano*, 2011, **5**, 5067–5071.

128. L. M. Maestro, E. M. Rodríguez, F. S. Rodríguez, M. C. Iglesias-de la Cruz, A. Juarranz, R. Naccache, F. Vetrone, D. Jaque, J. A. Capobianco and J. G. Solé, *Nano Lett*., 2010, **10**, 5109–5115.
129. V. A. Vlaskin, N. Janssen, J. van Rijssel, R. Beaulac and D. R. Gamelin, *Nano Lett*., 2010, **10**, 3670–3674.
130. J.-M. Yang, H. Yang and L. Lin, *ACS Nano*, 2011, **5**, 5067–5071.
131. L. M. Maestro, C. Jacinto, U. R. Silva, F. Vetrone, J. A. Capobianco, D. Jaque, and J. G. Solé, *Small*, 2011, **7**, 1774–1778.
132. E. J. McLaurin, V. A. Vlaskin and D. R. Gamelin, *J. Am. Chem. Soc*., 2011, **133**, 14978–14980.
133. A. E. Albers, E. M. Chan, P. M. McBride, C. M. Ajo-Franklin, B. E. Cohen and Brett A. Helms, *J. Am. Chem. Soc*., 2012, **134**, 9565–9568.
134. F. Vetrone, R. Naccache, A. Zamarrón, A. J. de la Fuente, F. Sanz-Rodríguez, L. M. Maestro, E. M. Rodriguez, D. Jaque, J. G. Solé and J. A. Capobianco, *ACS Nano*, 2010, **4**, 3254–3258.
135. S. M. Borisov and O. S. Wolfbeis, *Anal. Chem*., 2006, **78**, 5094–5101.
136. J. Yu, L. Sun, H. Peng and M. I. J. Stich, *J. Mater. Chem*., 2010, **20**, 6975–6981.
137. H.-S. Peng, S.-H. Huang and O. Wolfbeis, *J. Nanopart. Res*., 2010, **12**, 2729–2733.
138. A. Tsuda, S. Sakamoto, K. Yamaguchi and T. Aida, *J. Am. Chem. Soc*., 2003, **125**, 15722–15723.
139. L. Shang, F. Stockmar, N. Azadfar and G. U. Nienhaus, *Angew. Chem. Int. Ed*., 2013, **52**, 11154–11157.
140. R. Hodgkiss, A. Begg, R. Middleton, J. Parrick, M. Startford, P. Wardman and G. Wilson, *Biochem. Pharmacol*., 1991, **41**, 533–541.
141. R. Hodgkiss, G. Jones, A. Long, R. Middleton, J. Parrick, M. Stratford, P. Wardman and G. Wilson, *J. Med. Chem*., 1991, **34**, 2268–2274.
142. R. J. Hodgkiss, R. W. Middleton, J. Parrick, H. K. Rami, P. Wardman and G. D. Wilson, *J. Med. Chem*., 1992, **35**, 1920–1926.
143. Y. Liu, Y. Xu, X. Qian, Y. Xiao, J. Liu, L. Shen, J. Li and Y. Zhang, *Bioorg. Med. Chem. Lett*., 2006, **16**, 1562–1566.
144. Y. Liu, Y. Xu, X. Qian, J. Liu, L. Shen, J. Li and Y. Zhang, *Bioorg. Med. Chem*., 2006, **14**, 2935–2941.
145. W. Zhu, M. Dai, Y. Xu and X. Qian, *Bioorg. Med. Chem*., 2008, **16**, 3255–3260.
146. M. Dai, W. Zhu, Y. Xu, X. Qian, Y. Liu, Y. Xiao and Y. You, *J. Fluoresc*., 2008, **18**, 591–597.
147. H. Yin, W. Zhu, Y. Xu, M. Dai, X. Qian, Y. Li and J. Liu, *Eur. J. Med. Chem*., 2011, **46**, 3030–3037.
148. L. Cui, Y. Zhong, W. Zhu, Y. Xu, Q. Du, X. Wang, X. Qian and Y. Xiao, *Org. Lett*., 2011, **13**, 928–931.
149. E. Nakata, Y. Yukimachi, H. Kariyazono, S. Im, C. Abe, Y. Uto, H. Maezawa, T. Hashimoto, Y. Okamoto and H. Hori, *Bioorg. Med. Chem*., 2009, **17**, 6952–

6958.
150. K. Okuda, Y. Okabe, T. Kadonosono, T. Ueno, B. G. M. Youssif, S. Kizaka-Kondoh and H. Nagasawa, *Bioconj. Chem*., 2012, **23**, 324–329.
151. K. Xu, F. Wang, X. Pan, R. Liu, J. Ma, F. Kong and B. Tang, *Chem. Commun*., 2013, **49**, 2554–2556.
152. Z. Li, X. Li, X. Gao, Y. Zhang, W. Shi and H. Ma, *Anal. Chem*., 2013, **85**, 3926–3932.
153. K. Kiyose, K. Hanaoka, D. Oushiki, T. Nakamura, M. Kajimura, M. Suematsu, H. Nishimatsu, T. Yamane, T. Terai, Y. Hirata and T. Nagano, *J. Am. Chem. Soc*., 2010, **132**, 15846–15848.
154. W. Piao, S. Tsuda, Y. Tanaka, S. Maeda, F. Liu, S. Takahashi, Y. Kushida, T. Komatsu, T. Ueno, T. Terai, T. Nakazawa, M. Uchiyama, K. Morokuma, T. Nagano and K. Hanaoka, *Angew. Chem. Int. Ed*., 2013, **52**, 13028–13032.
155. S. Takahashi, W. Piao, Y. Matsumura, T. Komatsu, T. Ueno, T. Terai, T. Kamachi, M. Kohno T. Nagano and K. Hanaoka, *J. Am. Chem. Soc*., 2012, **134**, 19588–19591.
156. K. Tanabe, N. Hirata, H. Harada, M. Hiraoka and S. Nishimoto, *ChemBioChem*, 2008, **9**, 426–432.
157. H. Komatsu, H. Harada, K. Tanabe, M. Hiraokad and S. Nishimoto, *Med. Chem. Commun*., 2010, **1**, 50–53.
158. S. Zhang, M. Hosaka, T. Yoshihara, K. Negishi, Y. Iida, S. Tobita and T. Takeuchi, *Cancer Res*., 2010, **70**, 4490–4498.
159. H. Komatsu, K. Yoshihara, H. Yamada, Y. Kimura, A. Son, S. Nishimoto and K. Tanabe, *Chem. Eur. J*., 2013, **19**, 1971–1977.
160. J. Napp, T. Behnke, L. Fischer, C. Würth, M. Wottawa, D. M. Katschinski, F. Alves, U. Resch-Genger and M. Schäferling, *Anal. Chem*., 2011, **83**, 9039–9046.
161. G. Zhang, G. M. Palmer, M. W. Dewhirst and C. L. Fraser, *Nat. Mater.*, 2009, **8**, 747–751.
162. J. Han and K. Burgess, *Chem. Rev*., 2010, **110**, 2709–2728.
163. T. Myochin, K. Kiyose, K. Hanaoka, H. Kojima, T. Terai and T. Nagano, *J. Am. Chem. Soc*., 2011, **133**, 3401–3409.
164. H. Lee, W. Akers, K. Bhushan, S. Bloch, G. Sudlow, R. Tang and S. Achilefu, *Bioconj. Chem*., 2011, **22**, 777–784.
165. Z. Liu, C. Zhang, W. He, F. Qian, X. Yang, X. Gao and Z. Guo, *New J. Chem*., 2010, **34**, 656–660.
166. E. Nakata, Y. Yukimachi, Y. Nazumi, Y. Uto, H. Maezawa, T. Hashimoto, Y. Okamoto and H. Hori, *Chem. Commun*., 2010, **46**, 3526–3528.
167. U. C. Saha, K. Dhara, B. Chattopadhyay, S. K. Mandal, S. Mondal, S. Sen, M. Mukherjee, S. Van Smaalen and P. Chattopadhyay, *Org. Lett*., 2011, **13**, 4510–4513.
168. J. T. Hutt, J. Jo, A. Olasz, C.-H. Chen, D. Lee and Z. D. Aron, *Org. Lett*., 2012, **14**, 3162–3165.
169. F. Doria, M. Nadai, G. Sattin, L. Pasotti, S. N. Richter and M. Freccero, *Org*.

Biomol. Chem., 2012, **10**, 3830–3840.
170. N. Boens, W. Qin, M. Baruah, W. M. De Borggraeve, A. Filarowski, N. Smisdom, M. Ameloot, L. Crovetto, E. M. Talavera and J. M. Alvarez-Pez, *Chem. Eur. J.*, 2011, **17**, 10924–10934.
171. Y. Chen, H. Wang, L. Wan, Y. Bian and J. Jiang, *J. Org. Chem.*, 2011, **76**, 3774–3781.
172. L. Yuan, W. Lin, Z. Cao, J. Wang and B. Chen, *Chem. Eur. J.*, 2012, **18**, 1247–1255.
173. S. Chen, Y. Hong, Y. Liu, J. Liu, C. W. T. Leung, M. Li, R. T. K. Kwok, E. Zhao, J. W. Y. Lam, Y. Yu and B. Z. Tang, *J. Am. Chem. Soc.*, 2013, **135**, 4926–4929.
174. C. Percivalle, T. Mahmood and S. Ladame, *Med. Chem. Commun.*, 2013, **4**, 211–215.
175. M. H. Lee, J. H. Han, J. H. Lee, N. Park, R. Kumar, C. Kang and J. S. Kim, *Angew. Chem. Int. Ed.*, 2013, **52**, 6206–6209.
176. A. Schulz, J. Wotschadlo, T. Heinze and G. J. Mohr, *J. Mater. Chem.*, 2010, **20**, 1475–1482.
177. L. Albertazzi, B. Storti, L. Marchetti and F. Beltram, *J. Am. Chem. Soc.*, 2010, **132**, 18158–18167.
178. H.-S. Peng, J. A. Stolwijk, L.-N. Sun, J. Wegener and O. S. Wolfbeis, *Angew. Chem. Int. Ed.*, 2010, **49**, 4246–4249.
179. Y. Chiu, Show. Chen, J. Chen, K. Chen, H. Chen and H. Sung, *ACS Nano*, 2010, **4**, 7467–7474.
180. Y.-H. Chan, C. Wu, F. Ye, Y. Jin, P. B. Smith and D. T. Chiu, *Anal. Chem.*, 2011, **83**, 1448–1455.
181. R. V. Benjaminsen, H. Sun, J. R. Henriksen, N. M. Christensen, K. Almdal and T. L. Andresen, *ACS Nano*, 2011, **5**, 5864–5873.
182. H. Sun, K. Almdal and T. L. Andresen, *Chem. Commun.*, 2011, **47**, 5268–5270.
183. K. Zhou, Y. Wang, X. Huang, K. Luby-Phelps, B. D. Sumer and J. Gao, *Angew. Chem. Int. Ed.*, 2011, **50**, 6109–6114.
184. S. Schremla, R. J. Meierb, O. S. Wolfbeisb, M. Landthalera, R. Szeimiesa and P. Babilasa, Proc. Natl. Acad. Sci. U. S. A., 2011, **108**, 2432–2437.
185. K. Zhou, H. Liu, S. Zhang, X. Huang, Y. Wang, G. Huang, B. D. Sumer and J. Gao, *J. Am. Chem. Soc.*, 2012, **134**, 7803–7811.
186. G. Liu, W. Zhou, J. Zhang and P. Zhao, *J. Polym. Sci., Part A: Polym. Chem.*, 2012, **50**, 2219–2226.
187. W. Shi, X. Li and H. Ma, *Angew. Chem. Int. Ed.*, 2012, **51**, 6432–6435.
188. M. J. Marín, F. Galindo, P. Thomas and D. A. Russell, *Angew. Chem. Int. Ed.*, 2012, **51**, 9657–9661.
189. J. Lei, L. Wang and J. Zhang, *Chem. Commun.*, 2010, **46**, 8445–8447.
190. S. Wu, Z. Li, J. Han and S. Han, *Chem. Commun.*, 2011, **47**, 11276–11278.
191. X. Wang, C. Boschetti, M. J. Ruedas-Rama, A. Tunnacliffe and E. A. H. Hall, *Analyst*, 2010, **135**, 1585–1591.

192. I. L. Medintz, M. H. Stewart, S. A. Trammell, K. Susumu, J. B. Delehanty, B. C. Mei, J. S. Melinger, J. B. Blanco-Canosa, P. E. Dawson and H. Mattoussi, *Nat. Mater*., 2010, **9**, 676–684.
193. T. Jin, A. Sasaki, M. Kinjo and J. Miyazaki, *Chem. Commun*., 2010, **46**, 2408–2410.
194. K. Paek, S. Chung, C. Cho and B. J. Kim, *Chem. Commun*., 2011, **47**, 10272–10274.
195. A. M. Dennis, W. Rhee, D. Sotto, S. N. Dublin and G. Bao, *ACS Nano*, 2012, **4**, 2917–2924.
196. M. Tantama, Y. Hung and G. Yellen, *J. Am. Chem. Soc*., 2011, **133**, 10034–10037.
197. V. M. Chauhan, G. R. Burnett and J. W. Aylott, *Analyst*, 2011, **136**, 1799–1801.

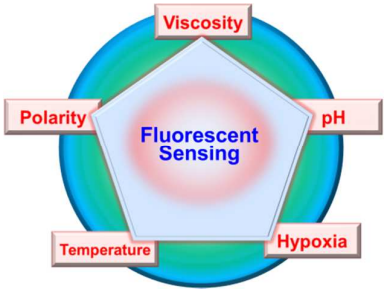

We summarized the research progress of fluorescent sensors responsive to environmental factors, including local viscosity, polarity, temperature, hypoxia and pH.

Jong Seung Kim was born in Daejon, Korea in 1963. He received Ph. D. from Department of Chemistry and Biochemistry at Texas Tech University. After one-year postdoctoral fellowship at University of Houston, he joined the faculty at Konyang University in 1994 and transferred to Dankook University in 2003. In 2007, he then moved to Department of Chemistry at Korea University in Seoul as a professor. To date, his research records 300 scientific publications and 50 domestic and international patents.

Xiaojun Peng received his Ph.D. in 1990 at Dalian University of Technology. After completing postdoctoral research in Nankai University (China), he has been working at the Dalian University of Technology in 1992. In 2001 and 2002, he has been a visiting scholar in Stockholm University and Northwestern University (USA). Currently he is a professor and the director of State Key Laboratory of Fine Chemicals of China in Dalian University of Technology. His research interests cover dyes for fluorescent bio-imaging/labeling and digital printing/recording.

Zhigang Yang was born in Hubei province, China in 1981. He received his Ph. D. in Applied Chemistry from Dalian University of Technology (China) in 2011 under the supervision of Prof. Xiaojun Peng. He is presently working as a postdoctoral fellow in the group of Prof. Jong Seung Kim at Korea University, Korea.

Jianfang Cao was born in Shandong Province, China in 1983. She received her M.S. of Chemical Physics in 2010 from Dalian University of Technology (China). She is now a Ph.D. candidate under the supervision of Prof. Xiaojun Peng in the Dalian University of Technology and Prof. Ke-Li Han at Dalian Institute of Chemical Physics.

Yanxia He was born in Henan Province, China 1983. She received her M.S. in Applied Chemistry from Dalian University of Technology (China) in 2009 under the supervision of Prof. Xiaojun Peng and Dr. Shiguo Sun; then she worked as a researcher in Shanghai ChemPartner Co. Ltd. for two years. She is presently working as a Master Researcher in the group of Prof. Jong Seung Kim at Korea University, Korea.

Jung Ho Yang was born in Korea in 1986. He received his Bachelor' degree from the department of Chemistry at Korea University in Korea. He entered the graduate school of Department of Chemistry at Korea University as a master student under the supervision from Prof. Jong Seung Kim in 2012.

Taeyoung Kim was born in Korea in 1985. He received his Bachelor' degree from the department of Chemistry at Kwang Woon University in Korea. He entered the graduate school of Department of Chemistry at Korea University as a master student under the supervision from Prof. Jong Seung Kim in 2012.

Group photo caption:
(From left to right; top row) Jong Seung Kim, Xiaojun Peng, Zhigang Yang, Jianfang Cao; (bottom row) Yanxia He, Jung Ho Yang, Taeyoung Kim